MULTI-CHANNAL ANALYSIS OF SURFACE WAVES OF A TRANSITION ZONE IN THE NEAR SURFACE OF THE INNER PIEDMONT: IMPLICATIONS FOR CONTAMINENT FLOW TRANSPORT

by

EMILY DAISY GALLAGHER

(Under the Direction of Robert B. Hawman)

Multi-channel analysis of surface waves (MASW) was used to provide constraints on the transition zone in the Inner Piedmont. The dispersion characteristics of shear waves are used to derive models of S-wave velocity as a function of depth. Data was acquired along two profiles in Watershed 2: 400-m, E-W profile recorded in 2007 using 30-Hz geophones; 170-m, NW-SE profile recorded in 2011 using 4.5-Hz geophones. Maximum depth of penetration was 12 m (former) and 15m (latter). Interpretations of S-velocities of material above bedrock were constrained by Well EPA6. Velocities of 200-250 m/s were interpreted as sandy saprolite. Velocities 250-400 m/s were interpreted as clay rich saprolite. Velocities 400 - 550 m/s were interpreted as highly degraded bedrock. Velocities exceeding 600 m/s were interpreted to be bedrock, based upon the correlations with exposures of bedrock. Shear-wave velocities within the transition zone (550 m/s) were higher than those within the saprolite.

INDEX WORDS: Transition zone, saprolite, surface waves, MASW

MULTI-CHANNEL ANALYSIS OF SURFACE WAVES OF A TRANSITION ZONE IN THE NEAR SURFACE OF THE INNER PIEDMONT:IMPLICATIONS FOR CONTAMIN

by

EMILY DAISY GALLAGHER

B.S., Northern Illinois University, 2005

A Thesis Submitted to the Graduate Faculty of The University of Georgia in Partial Fulfillment of the Requirements for the Degree

MASTER OF SCIENCE

ATHENS, GEORGIA

2013

MULTI-CHANNAL ANALYSIS OF SURFACE WAVES OF A TRANSITION ZONE IN THE NEAR SURFACE OF THE INNER PIEDMONT: IMPLICATIONS FOR CONTAMINENT FLOW TRANSPORT

by

EMILY DAISY GALLAGHER

Major Professor: Robert B. Hawman

Committee: John Dowd
Paul Schroeder

Electronic Version Approved:

Maureen Grasso
Dean of the Graduate School
The University of Georgia
May 2013

DEDICATION

I would like to dedicate this to my Dad and Mom, James and Noreen Gallagher, I love you. To my boyfriend, Daniel Zimmer and our puppy dog Cooper, for their outstanding support. To the magical unicorns.

ACKNOWLEDGEMENTS

I am very grateful to Rob Hawman for taking me on as his graduate student and investing his time into my education. His direction, insight, and motivation is a major contribution to this project.

I would also like to thank my committee Paul Schroeder and John Dowd for their interest and enthusiasm.

I would also like to thank the following individuals for their contributions to the study: Horry Parker, Peter Hawman, Jason Jones, Hamilton Goodner, Joe Boreman, and Don Yezerski for their assistance at the field site site; Brian Price for his first hand knowledge of the USDA site; Mohammed O. Khalifa who generously provided access to the data set for the May 2007 excursion; Dr. Bob Carver for professional insight and brainstorming sessions; Financial support was provided by NSF Grant EAR-0844154 and The University of Georgia (UGA) provided teaching assistant support.

Lastly, I would like to thank my all bar patrons at Roadhouse Bar for not only financially contributing support over the last 4 years, but for being my new family away from Home. I would not have completed this project without them

TABLE OF CONTENTS

LIST OF TABLES

LIST OF FIGURES

CHAPTER 1

INTRODUCTION

Importance of saprolite transition zone

The Inner Piedmont of Georgia is comprised of localized watersheds with no regional subsurface-flow systems, with groundwater movement from ridge to stream (Feild and Dowd, 2001). In the near surface, fractured bedrock is overlain by saprolite and clay-rich soils. There is a transition zone that separates the bedrock and saprolite that is poorly understood and is of interest when looking at contaminant flow in the subsurface. Stewart and others (1964) presented drill core data that showed the transition zone has a higher permeability than the bedrock and saprolite. This transition zone can act as a conduit for contaminant that flows in the sub-surface.

The transition zone is formed by the partial weathering of bedrock *in situ*. This zone is comprised of a mixture of saprolite, weathered bedrock, and un-weathered bedrock, with the thickness of the transition zone dependent in part on the parent material (Harned and Daniel, 1989; LeGrand, 2004; Gonthier, 2009). Figure 1.1 shows a comparison of a well-defined transition zone associated with foliated metamorphic rock and a poorly-defined transition zone associated with massive igneous rock (Harned and Daniel, 1989). The permeability differences in the saprolite, bedrock, and transition zone have an impact on how a contaminant will flow (Feild and Dowd, 2001). Fractures, in part, control the depth of groundwater flow in the Inner Piedmont. Since the hydraulic conductivity within fractured bedrock is poorly defined it is unknown how far the contaminants may flow (Gonthier, 2009). The hydraulic conductivity can vary significantly from site to site. The extent of the transition zone is also unknown.

Understanding the size and impact of this zone on hydrologic features will be valuable in evaluating the potential for contamination.

Objectives of Study

The objectives of this study are to 1) better understand hydrologic parameters in the Inner Piedmont region, 2) image the transition zone and bedrock topography, and 3) relate the transition zone to the hydrogeology of the area. We use the multi-channel analysis of surface waves (MASW) method to image the transition zone between bedrock and saprolite and to resolve the depth to bedrock in the near surface. We also focus on the use of mutes, a processing technique applied to the seismic record, to improve the clarity of the fundamental mode Rayleigh wave phase-velocity-frequency spectra. Inversion parameters are also varied to improve resolution of the models.

The results of this study will be used to map near-surface variations in rigidity in the Inner Piedmont by analyzing the propagation of surface waves. This will provide information on how contaminants could flow in the localized watersheds of the Inner Piedmont. The geophysical results will be used to extend the subsurface coverage provided by well data. Mapping the thickness of the transition zone and topography of the bedrock surface will shed light on how contaminants may flow within the Inner Piedmont and how localized watersheds are recharged. In the long run, this will assist in evaluating what kind of remediation may be needed in contaminated areas, which at the moment is poorly understood in the Piedmont Region.

Spectral Analysis of Surface Waves (SASW)

Nazerian and others (1983) introduced the first method to take advantage of the dispersive nature of Rayleigh waves ("ground roll") to image the near surface (uppermost 10-30 m). It is non-invasive and simple to deploy; it involves using two receivers and one source. Previously, ground roll data had been treated as noise. The use of only two receivers requires multiple deployments with varying spacing and geometry to acquire enough information. Early studies showed that multiple modes (same phase velocities found at different frequencies) are created during the generation of Rayleigh waves. The higher modes exist at higher phase velocities and at higher frequencies.

Multi-Channel Analysis of Surface Waves (MASW)

Although the SASW method has been effective in characterizing geotechnical sites, it is time consuming and highly sensitive to noise (Park et al., 1999). Noise is more effectively handled by the Multichannel Analysis of Surface Waves (MASW) method, which uses arrays of multiple receivers (Park et al., 1999; Ivanov et al., 2001). Compared with seismic refraction and reflection methods, MASW deals with lower frequencies (Park et al., 1999). It is suitable for mapping bedrock and variations in rigidity within soil and saprolite. The use of multiple receivers, usually 12 or more, improves the signal to noise ratio and resolution of fundamental and higher modes. The use of multiple channels provides a redundancy in coverage that SASW lacks (*Figure 1.2*) (Park et al., 1997). The shear wave (S-wave) profiles generated provide insight into the rigidity of a material at the very near surface, which is an important parameter in engineering and environmental studies. The shear-wave velocity is related to the rigidity of a material as shown by the following equation:

$$\beta = (\mu/\rho)^{1/2}$$

(β= shear-wave velocity, μ = shear modulus, and ρ = density of the material).

As a general rule, the velocities of Rayleigh waves are approximately 90 to 92 percent of the shear wave velocities (Stokoe et al., 1994; Park et al., 1997). Rayleigh waves are characterized by relatively low propagation velocities, low frequencies, and high amplitudes. The Rayleigh wave has vertical and horizontal components and travels in a retrograde motion (*Figure 1.3*). Rayleigh waves can travel in a homogenous elastic half space as well as layered media (Lowrie, 1997). Rayleigh waves with lower frequencies (and longer wavelengths) can penetrate deeper into the material than waves with higher frequencies and shorter wavelengths (*Figure 1.4*). Because S-wave velocities generally increase with depth, longer-wavelength energy travels faster than shorter-wavelength energy, resulting in dispersion of the recorded waveforms. Attenuation of surface waves is also dependent on wavelength (Lowrie, 1997); shorter wavelengths attenuate more quickly than longer wavelengths. There is an inverse relationship between maximum depth of penetration and spatial resolution. To a first approximation, the maximum depth of penetration is half the length of the receiver spread, which is equivalent to half the maximum wavelength that can be measured. This is also the approximate width of the smallest variation in S-wave velocity that can be resolved. The following equation can be used to estimate the maximum depth of penetration (Park et al., 1999):

$$D = Vp / (2*f),$$

Where: D is depth of penetration, Vp is phase velocity, and f is frequency.

The way a material responds to Rayleigh waves is frequency dependent. Dispersion is the wavelength dependent property that is used in Vs (shear wave) profile analysis (Shearer, 1999). Dispersion shows the frequency dependence of phase velocity. Higher modes are generated when several phase velocities with different wavelengths occur at one specific frequency. Because of their high amplitudes, Rayleigh waves are particularly useful for imaging structure in areas characterized by high levels of cultural noise (Miller et al., 2001).

The analysis of Rayleigh waves generally is carried out under the assumption that the cylindrical wave fronts are approximately planar. This approximation improves with distance from the source (Park et al., 2002; Yoon and Rix, 2009). If the recording distances are too great, however, body waves and higher energy surface waves may dominate over the fundamental mode (Park et al., 2002). If the offset is too small, then the wave may not travel in a planar motion. Trial shots at various distances can provide the optimum offset distance (Park et al., 2002).

The MASW method involves three steps: data acquisition, generation of dispersion curves, and inversion of dispersion curves for 1D models of shear-wave velocity as a function of depth. (Park et al., 1999) (*Figure 1.5*) Extraction of the dispersion curve is the most important step in the MASW method. It is then inverted into 1D shear wave velocity models for each station. A pseudo-2D shear wave velocity model then is generated by combining the individual 1D models into a single plot. The software used for processing and inverting data for this study was Surfseis, a program developed by the Kansas Geological Society (KGS).

Passive versus Active Profiling

Two types of sources can be used with the MASW method: Passive and Active. Active source methods include artificial impulses created by sledgehammer, vibroseis, or shotgun blasts. Passive sources include traffic noise and distant earthquakes. Passive sources require one to determine the direction from which the energy originates (Park et al., 2007); this generally requires a 2D array of receivers. For active-source surveys, the source is generally deployed in-line with the linear receiver array. Active surveys using hammer sources can image structure to depths of 30 meters, while passive surveys use much lower frequencies that can penetrate to depths up to 100 meters (Park et al., 1999).

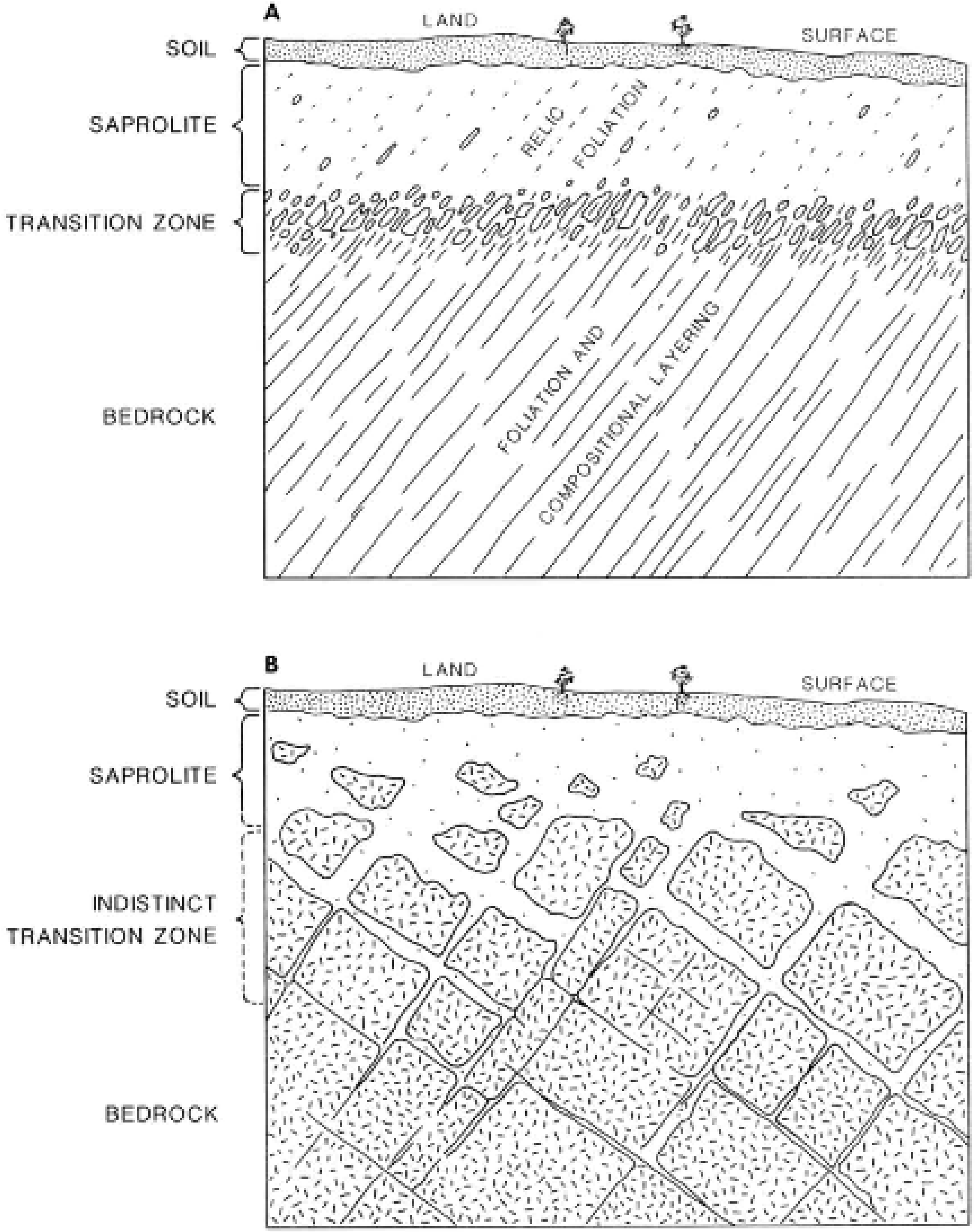

Figure 1.1

Cross section of transition zones in A) Foliated metamorphic bedrock (well defined transition zone) B) Massive Igneous bedrock (poorly-defined transition zone (Harned and Daniel, 1989).

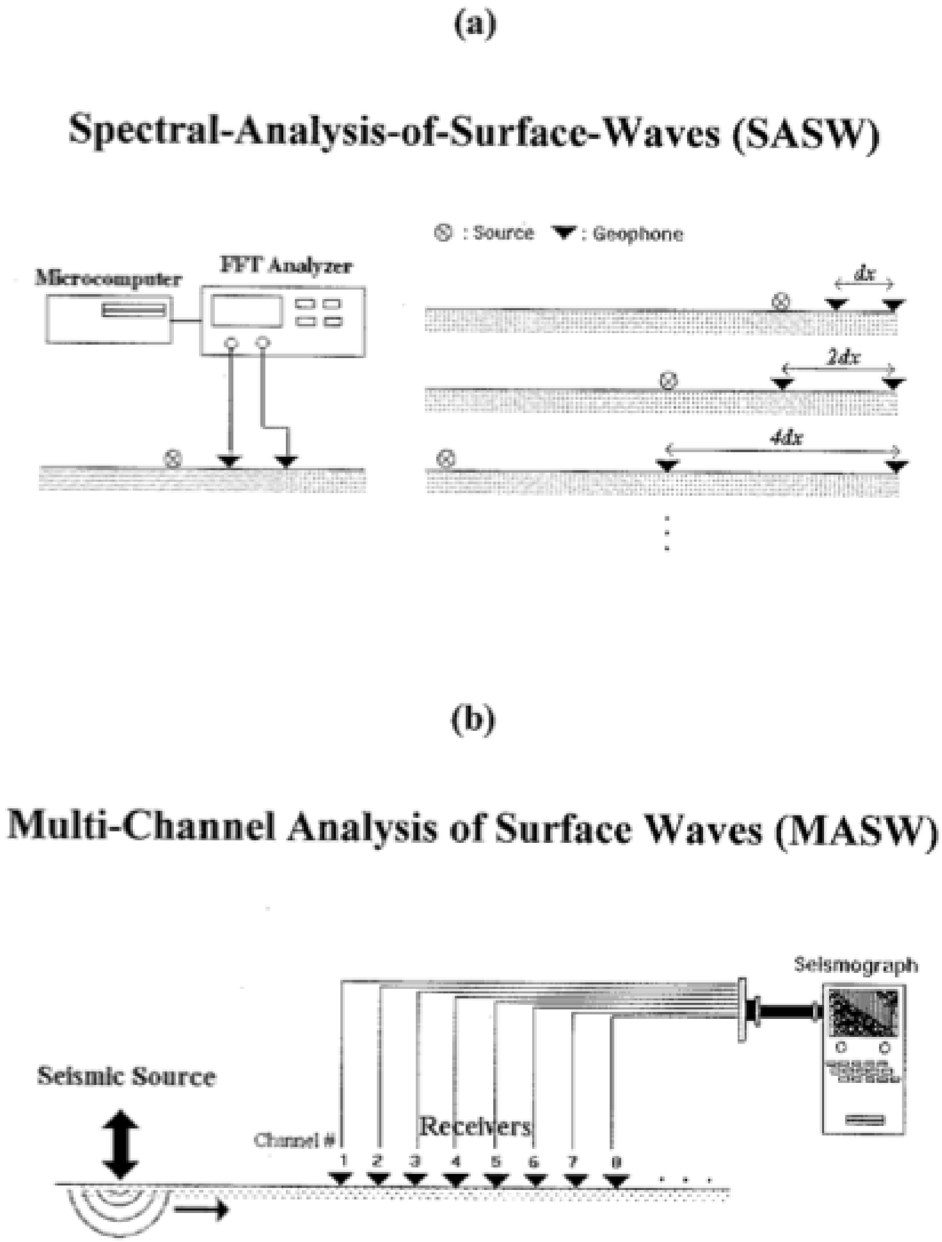

Figure 1.2

Comparison of A) Spectral Analysis of Surface Waves (SASW) and B) Multi-Channel Surface Wave (MASW) receiver deployments (Park et al., 1997).

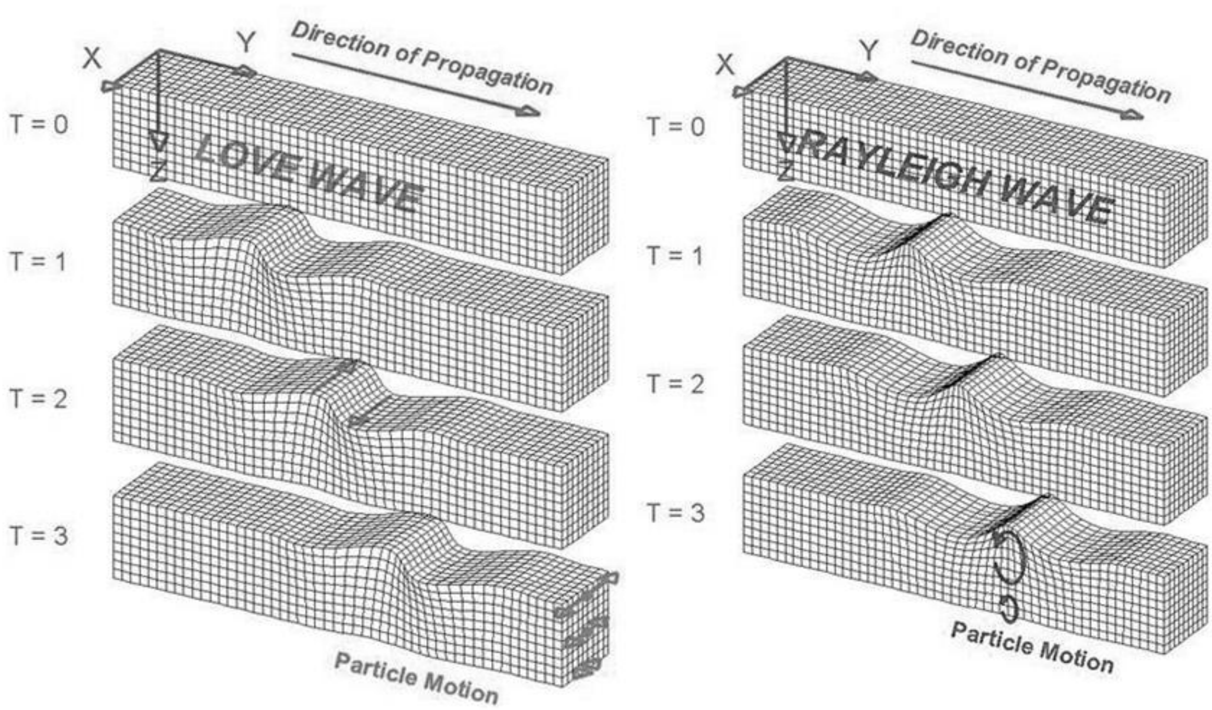

Figure 1.3

Surface waves and their propagation directions. Love waves (left image) have only horizontal motion. Rayleigh waves (right image) have horizontal and vertical motion, also referred to as retrograde particle motion.

Image source: http://www.geo.mtu.edu/UPSeis/waves.html

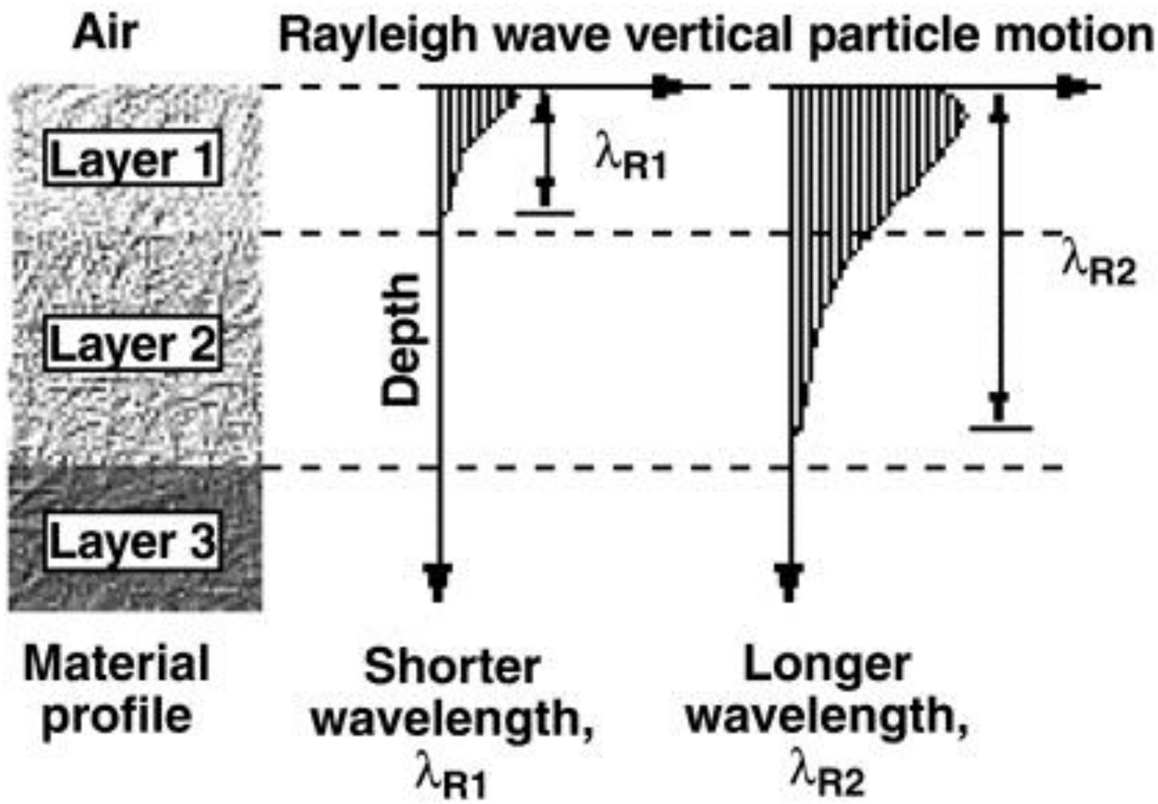

Figure 1.4

Short wavelength vs. long wavelength and respective depths of penetration

(Brown et al., 1999).

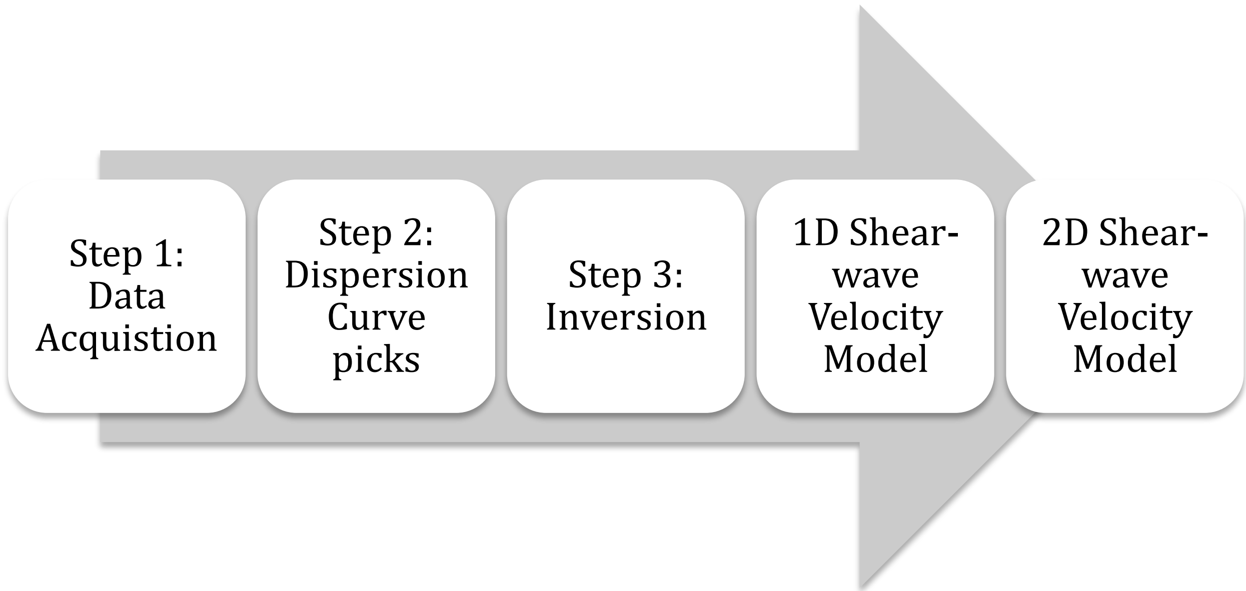

Figure 1.5

Step-by-Step flow chart for the MASW method.

CHAPTER 2

FIELD SITE

Geologic setting of Inner Piedmont and study area

The Appalachian Orogen consists of several distinct, roughly parallel belts representing various terranes (island arcs and continental fragments) that collided with North America from the Ordovician through the Permian (Hatcher, 1989; 2010). One of these belts, the Inner Piedmont, extends from Virginia to Alabama. It is bordered to the northwest by the Eastern Blue Ridge Terrane and to the southeast by the Carolina Terrane*(Figure 2.1)*. In Georgia and South Carolina, the Inner Piedmont and Carolina Terranes are separated by the Middleton-Lowndesville Fault Zone (MLFZ) (Stormer et al., 1980).

The Inner Piedmont region is comprised of fractured Precambrian to Paleozoic metamorphic rocks with Pre-Cambrian to late Paleozoic intrusive igneous rocks (Higgens et al., 1988; Gonthier, 2009). Chemically weathered bedrock, referred to as saprolite (Fetter, 1994), is separated from the bedrock by a transition zone. Due to incipient weathering of the bedrock, this transition zone contains less clay and has a relatively higher permeability than the soil-saprolite (Legrand, 2004). The thickness of the zone is not uniform and is comprised of rock fragments of varying size (Legrand, 2004). The transition zone separates the unweathered bedrock from the chemically altered saprolite- soil. At the study site, the soil that overlies the saprolite is comprised of a sandy loam and a sandy clay loam. These two soils are referred to as Pacolet and Cecil. Properties of the soils are very similar, but the Pacolet soil is much thinner due to erosion (Endale et al., 2006). Both soils have a higher concentration of clay particles then that of the saprolite**.** Thin lenses of sandy saprolite are occasionally found within the clay-rich saprolite. The variations in clay and sand are a result of the spatial variation of the mineralogy in the bedrock (i.e. foliations).

The field site was located at the United States Department of Agriculture, Agricultural Research Service, J. Phil Campbell Sr. Natural Resource Conservation Center in Watkinsville, GA *(Figure 2.2;* now under management by the UGA College of Agriculture and Environmental Services*)*. The study was conducted in Watershed #2 (W2) which was used originally in 1939 by farmers for terraced row cropping (Price, 2010). Cattle grazing began in the 1960's and today the grazing sites alternate between watersheds 1 and 2 (Price, 2010). The main flow of ground water occurs in the saprolite, which has a varying depth of 8 to 21 meters (Washington et al., 2006; Price, 2010). A north-west/south-east ridge runs parallel to the road cut and gently slopes to the west. Outcrops of bedrock are exposed at the top of the ridge. The parent material is the Athens gneiss (Railsback et al., 1996; Price 2010).

Spatial variations in composition of the bedrock result in varying soil at different sites. The soils form from gneiss and are referred to as the Cecil series. These soils are sandy loams with mixtures of quartzite (Callaghan, 1997). The A horizon is thinner than the Bt horizon due to erosion and comprises the top few cm. The Bt horizon is comprised of a sandy clay loam with a sub-angular, blocky structure (Callaghan, 1997). The quartzite fragments found in the series are a result of incomplete weathering of quartz veins in the saprolite (Callaghan, 1997). Due to variations in mineral composition, the amount of clay in the saprolite varies from area to area. The porosity of the soils ranged from 0.464 to 0.528 (Callaghan, 1997).

Hydrogeology of the Piedmont

Heath (1980) first described the hydro-geologic framework for the Piedmont and Blue Ridge. The system was broken down into 4 components that represented the structure of the near surface. These zones in the system are (from surface downward): unsaturated zone in regolith (saprolite), saturated zone in regolith, transition zone between regolith and bedrock, and fractured bedrock *(Figure 2.3)* (Harned and Daniel, 1989). The unsaturated and saturated regolith contains clay rich and silt rich soils (Heath, 1980). The transition zone is a mixture of saprolite and slightly weathered bedrock (Harned and Daniel, 1989). The greatest abundance of fractures in the bedrock occurs in the uppermost 120 m (Harned and Daniel, 1989). These structures play an important role in how the ground water may flow.

Two models have been proposed to describe groundwater flow in the Inner Piedmont. The first model, presented by LeGrand (1989), consists of 2 layers with the saprolite and bedrock acting as two layer aquifer *(Figure 2.3)*. In this model the saprolite acts as the recharge zone for the bedrock, with the hydraulic conductivity being greater in the vertical than the horizontal direction. The water table generally lies within the saprolite layer, which also stores water that is then fed to the fracture system in the bedrock. Nelson (1989) showed a relationship between the topography of the bedrock and direction of flow of water within this saprolite. His studies showed that the bedrock and regolith both discharge into a local river, thus supporting the 2 layer model system.

A second model presented by Schumak et al. (1989) combines both layers into a single aquifer with each layer having different horizontal conductivities. The saprolite has a higher conductivity than the granite bedrock. Flow within the saprolite and fractured bedrock is largely horizontal. Within this model the direction of groundwater flow is controlled by the gradient toward large rivers and leakage into the fractured bedrock below. The discharge into local streams was upward from the fractured bedrock and not from the saprolite-soil layer. This suggests that the saprolite feeds into the bedrock and acts as one system.

The watersheds in the Inner Piedmont are isolated. The hydraulic properties of the bedrock are controlled by fractures (Gonthier, 2009). Groundwater porosity is found mostly in the saprolite, which has a hydraulic conductivity (K) of 18.6 mm/day to 25.2 mm/day (Washington et al., 2004). Hydraulic conductivity for the soils varies with clay content. Shallower soils (Bt horizon) have higher clay content and higher K value than the deeper sandier soils (Abreu, 2005). The increased hydraulic conductivity is assumed to be a result of a higher degree of weathering. Fractures in the Inner Piedmont are known to extend to depths of at least 500ft (Stewart, 1962; Fetter 1994). It is unknown how much deeper these hydraulically conductive fractures extend, so constraints on the bedrock are undefined (Gonthier, 2009). The highly permeable transition zone that lies above the bedrock may create a zone of high contaminate flow in the ground water system of the Inner Piedmont (Harned and Daniel, 1989).

Field Acquisition

Line A was collected in November 2011 and orientated across the top of the ridge. It is 170m long and positioned 10m from the road cut. Stations 1-150 were utilized in this study. Line Z, collected by Khalifa and Hawman in 2007 (*unpublished data*), is oriented East-West at a high angle to Line A. It has a total length of 450m. Stations 1- 150 were utilized for this study. Line Z line cuts across well EPA6 , which was applied for ground truth. Locations of seismic lines are found in Figure 2.4.

Using a 24-channel Bison seismograph system, standard roll-along techniques were used to collect data along both lines. Both lines used a sledgehammer as a seismic source, a station spacing of 1 m, and source-receiver distances of 1-48 m. Line Z used 30-Hz geophones. To record lower frequencies for greater depth penetration, we used 4.5-Hz geophones for Line A. Recording parameters are summarized in Table 2.1.

Well data from boreholes

During the drilling of monitoring wells (January 2000 - February 2001), the EPA collected borehole data at W2. Figure 2.4 shows the locations of the 7 wells in W2. EPA6 was drilled to a total depth of 7.09 m and was drilled on Feb 6, 2001. No saturation was found during the drilling. The top 2.5 meters are comprised of red, silty loam to silty clay loam with no coarse fragments. From 2.5 m to 2.74m, there is a transition from a thin layer of silt to a silt-loam soil. At 2.74m is the first occurrence of saprolite, with moderately weathered coarse fragments found at 3.08 meters. At 4.3 meters, less than 5% of the material is composed of coarse fragments with muscovite chips. From 4.3-4.9 meters the drill core is saprolite comprised of quartz, feldspar, muscovite, and biotite with (fine coarse) fragments. Small sandy pockets in a silt matrix occur in this zone. At 5.5 m, is the first encounter with larger rocks with sub-angular to rounded coarse fragments with mixtures of yellowish/brownish saprolite. This extends to 6.4 meters where a high-gravel content is found. The gravel ranges in size from 0.5 to 3-cm. It is representative of the beginning of the transition zone. Gravel content increases at 6.7 m. Drilling was continued until refusal at 7.09 m. Coarse fragments indicated that bedrock is composed of grandioritic to granitic gneiss. See Appendix A for the drill log data.

EPA7, located approximately 85 meters south of Line Z, was drilled to a total depth of 11.9m and was drilled from Feb 6- Feb 7, 2001. Red, silty clay loam with no coarse fragments comprised the top 2.5m. From 2.5 m to 5.79 m, the material contained less than 5% coarse fragments. The soil consisted of brown silty clay loam to brown silt loam. The first encounter with saturation was at 4.88 m. At 5.79 m was the first contact with saprolite and extends to 7.93 m. The water table was found to be at 6.22 on the day of drilling. The saprolite is a yellowish brown color and contains muscovite chips. From 7.93 m to 10.4 m is a variable zone comprised of clay loam and a silty clay loam except at 8.84 m-9.45 m depth. This zone consists of pockets of quartzitic, weathered rock having sub-angular fragments, found within a layer of saprolite. From 9.45 m to 10.4 m the zone is yellowish-brownish saprolite. At 11m, fragments greater than 5% appear and the EPA noted that the drilling was meeting with resistance. Bedrock was encountered at 11.9 m. The coarse fragments indicate that the bedrock is grandioritic to granitic gneiss.

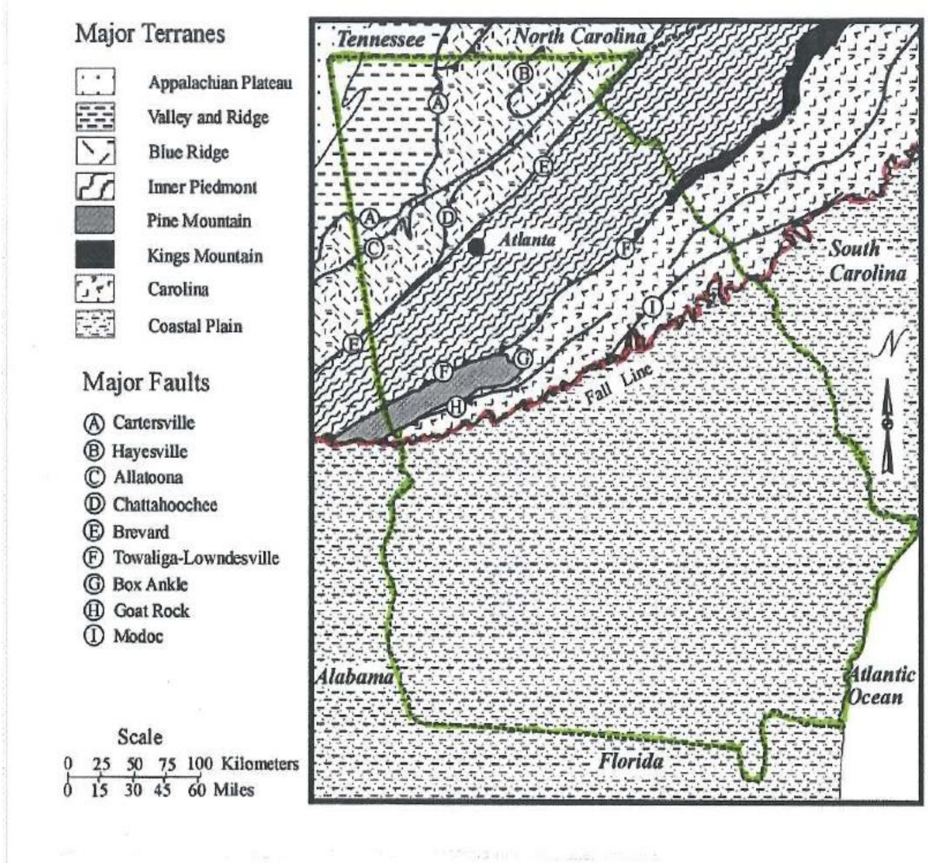

Figure 2.1

Geologic province map of Georgia. Red Line indicates Fall Line.

(modified from Cooker, 1999).

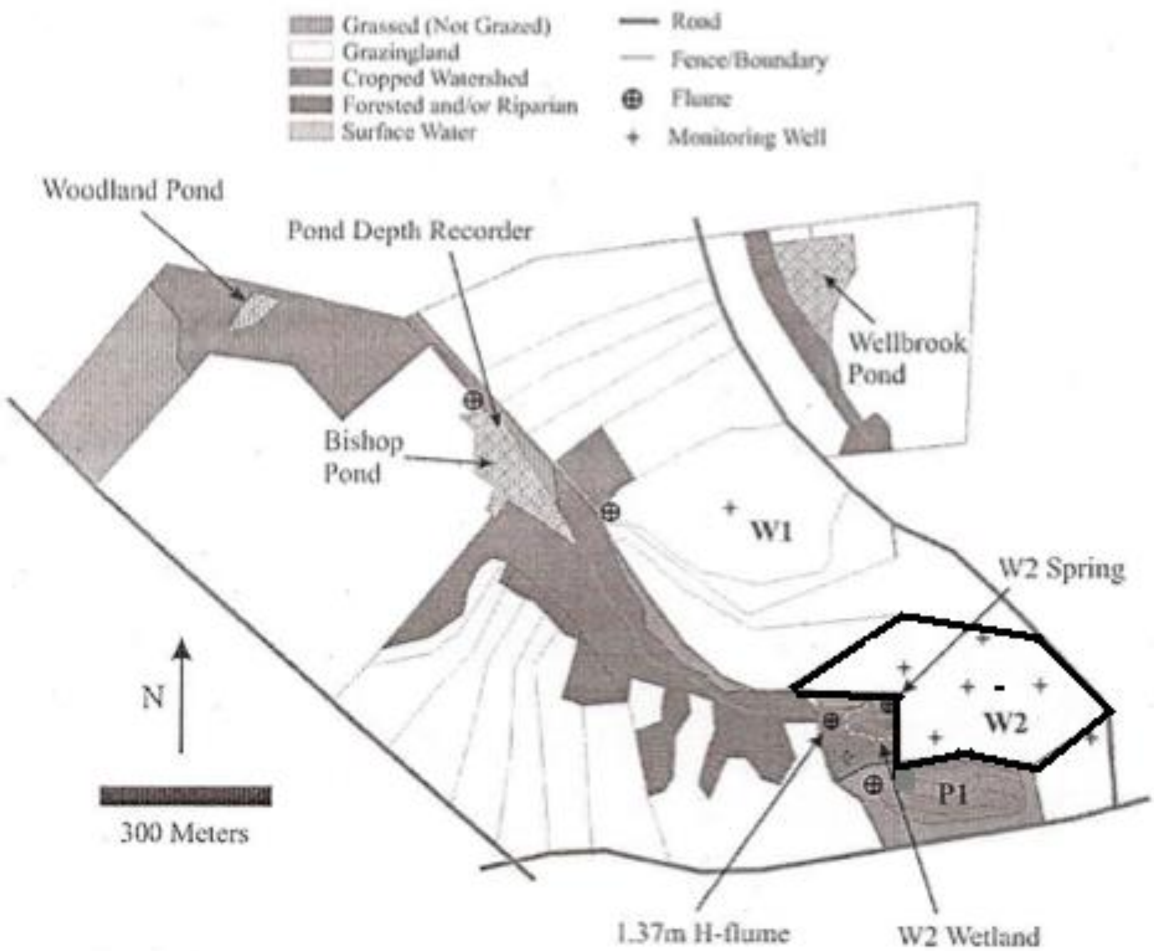

Figure 2.2

Map of USDA farm site in Watkinsville, GA. Showing Watersheds 1 and 2 as well as the EPA wells. Site of investigation is located in Watershed 2 (W2), which is the boldly outlined section upon the map (USDA ARS-JPC; Price, 2010).

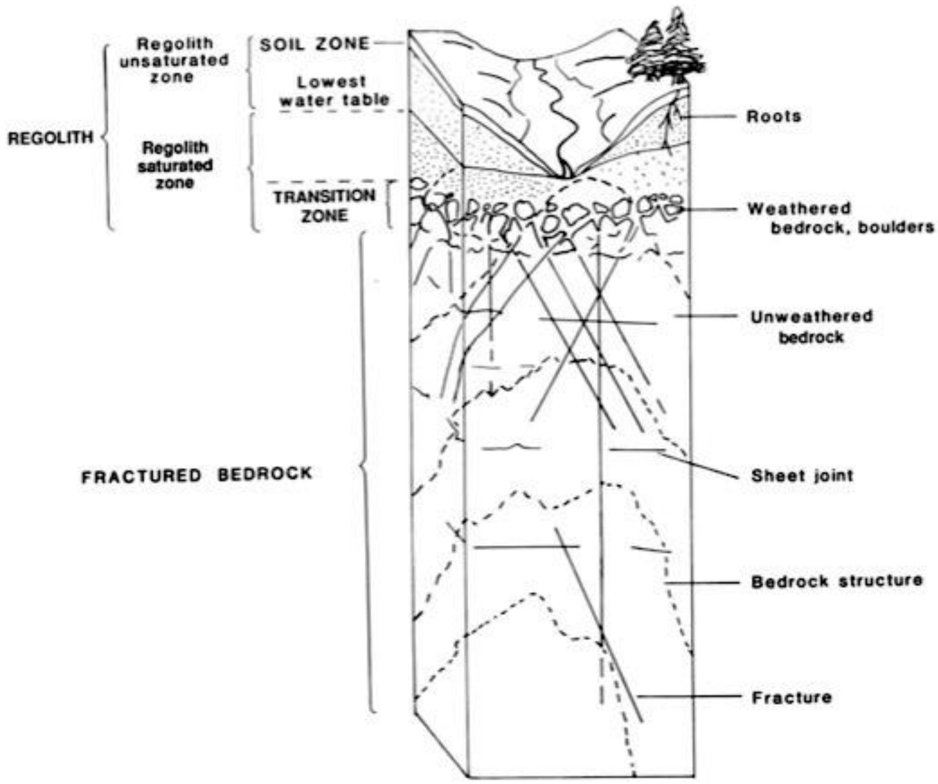

Figure 2.3

Diagram of a 4-component system of changing profile with depth in the Inner Piedmont showing a 2-layer system (Heath, 1980;Harned and Danial, 1989; LeGrand, 2004).

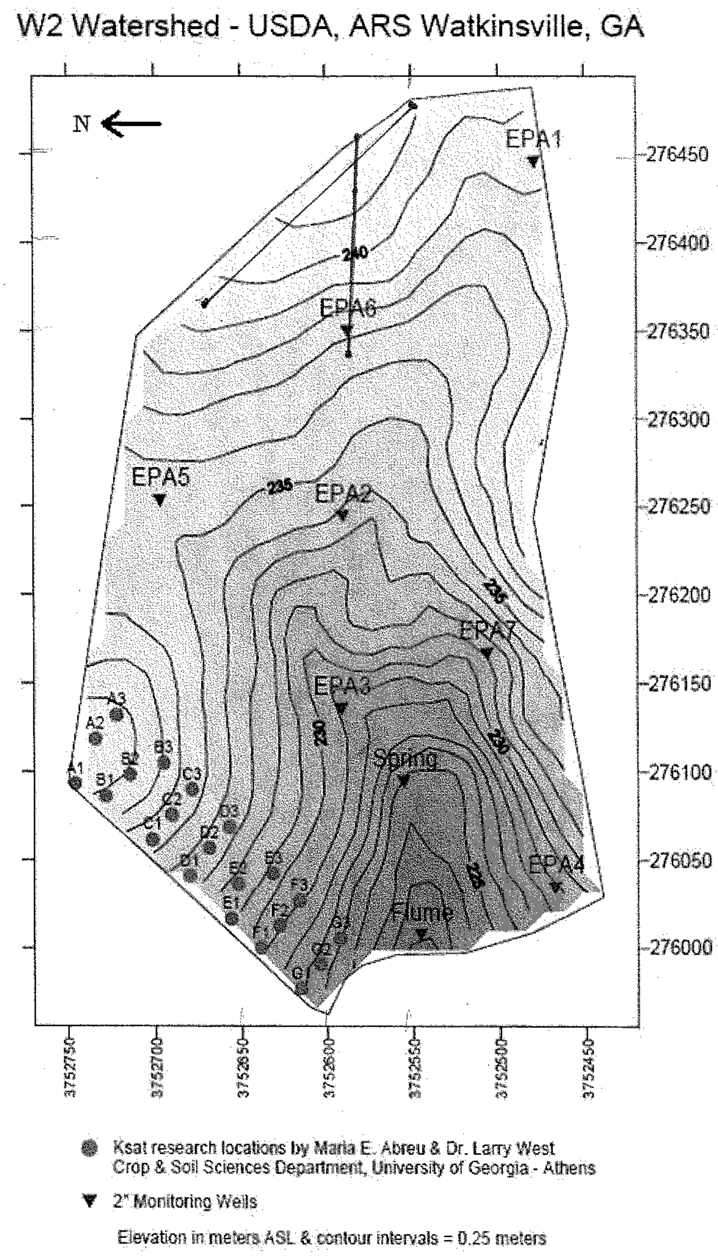

Figure 2.4

Elevation map of W2 showing locations of EPA monitoring wells and soil research stations.. Contour interval is .025m Positions of Line A (Southeast-Northwest) and Line Z (East-West) in watershed #2 are represented by lines intersecting at a high angle (modified from Price, 2010).

Recording Parameters	Line A (Nov 4, 2011; Nov 9, 2011)	Line Z (May 7-9, 2007)
Seismic Source	Sledgehammer	Sledgehammer
Geophones	4.5 Hz	30 Hz
Sampling rate	0.002 s	0.002s
Number of samples	500	500
Geophone Spacing	1 m	1 m
Source Offset	1 m	1 m
High-cut Filter	250 Hz	500 Hz
Low-Cut Filter	4 Hz	4 HZ

Table 2.1

Recording parameters for Line A and Line Z

CHAPTER 3

SHEAR WAVE MODELS

Data Processing and Parameters

There are three main steps to processing MASW data. The first step involves the acquisition of data as discussed in Chapter 2. After the data are collected, they are converted into the Winseis (Seg-Y) format. At this stage, ringing traces due to instrument and traffic noise are removed from the seismic records. Figure 3.1 shows an example of bad traces that are deleted. Next, the data are converted into the Surfseis format and the recording parameters entered (See table 2.1 in Chapter 2).

The data are next used to create overtone records. Overtone records are plots of phase velocity vs. frequency; fundamental and higher-mode surface waves appear as continuous curves. Figure 3.2 shows a generated overtone record with multiple modes. The fundamental mode is identified as the curve, generally starting at frequencies below 10 Hz, with the lowest phase velocity for a given frequency.

After review of the overtone records, it was determined that the seismic records required editing prior to the dispersion curve picks. Back-end mutes (mutes designed to eliminate energy after the surface waves) were required to improve the quality of the plots by removing the background noise. Figure 3.3 shows the unmuted and back-end muted seismic records for station 65. The reduction in noise improves the clarity of the image so that the modes are made more visible in the overtone record *(Figure 3.4).* The next step was to remove body waves and higher-mode surface waves that arrive before the fundamental surface waves using front-end mutes (Ivanov et al., 2005). The first 100 records for line A showed strong interference from higher modes. For some of the records, removal of the body waves and higher modes was not possible without removing a significant portion of the fundamental mode. In these cases, no mutes were applied. Figure 3.5 shows a comparison of the seismic records for station 65 for unmuted, back-end muted, and front-end muted processing. Figure 3.6 shows the corresponding overtone record after a front-end mute was applied. In general, there will be some overlap in travel time for higher modes and lower frequencies of the fundamental mode. Therefore, although muting often makes the fundamental mode easier to observe at higher frequencies, the removal of higher modes sometimes results in the distortion of the fundamental mode at lower frequencies (*Figure 3.6*)

The final part of the process is the inversion of the picks. Inversion parameters are summarized in Table 3.1. The inversions were repeated until the root-mean-square (RMS) misfit between the observed and computed phase velocities fell below a target value. The dispersion curves were inverted to create 1D (velocity as a function of depth) models *(Figure 3.7)*, which then were combined to create pseudo-2D (depth and location) models *(Figure 3.8)*. In some cases, the fundamental mode could not be separated and those stations were not included in this study. Surfseis will interpolate across these areas of missing data.

Line Z

Figure 3.8 shows the 2D shear wave velocity model for Line Z. This line is at a high angle to Line A (Figure 2.4) with a max depth image of 11 m. It has a shallower depth of penetration than Line A due to the use of 30 HZ geophones. Line Z runs east to west from the top of the ridge and passes through wells EPA6, EPA2, and EPA3. Depth to bedrock (as defined by shear-wave velocities exceeding 600 m/s) based upon bedrock exposures and comparison with Line A, is about 4 m from stations 1001-1020, 9m from station 1020 to about 1080, and then is not observable in the rest of the model. (Note, however, that higher-resolution models derived using half-spreads indicate that bedrock reaches the surface near station 1001; see Chapter 4). Low-velocity anomalies, (shear-wave velocities <200 m/s), underlie stations 1020-1035 at a depth of 2 meters. A sharp increase in depth to bedrock occurs at station 25 from 2 m depth to 8 m depth. A poorly resolved, relatively lower velocity zone occurs at depth of 7-9m at stations 1001-1020. Large areas of low velocities exist in the western part of the line as well. From stations 1100-1140, low velocity zones are observed at depths of 0-2 meters and again at 7-9 meters. Alternative models are discussed in Chapter 4.

Line A

Most of the extracted curves were in the 10-30 Hz frequency range and 250-600 m/s phase velocity range. Figure 3.9 shows the 2D shear wave velocity model for Line A. Exposures of gneissic bedrock at station 1001 of Line Z and 10 m north of station 1001 on line A, show that the depth to bedrock is very shallow at the top of the ridge. High shear wave velocities at shallow depths are interpreted to represent more competent and less weathered rock materials. Based on the correlation of bedrock exposures with velocity models derived from the half-spreads for Line Z (see Chapter 4), shear-wave velocities exceeding 600 m/s are interpreted as relatively unweathered bedrock. For Line A, the bedrock depth ranges from 6m to 13 m. A zone of lower velocities at depths of 10-14 m extends from station 1025 - 1055 and from stations 1100-1123. Two features associated with higher velocities appear from stations 1055-1065 at depths of 4-12m and from 1123-1140 at depths of 7-12m. Figure 3.10 shows the dispersion curves and 1D shear wave velocity model associated with a low velocity zone. The dispersion curves over the corresponding range in frequency (15-25 Hz) for the lower velocity zone show lower phase velocities than the curves found in higher velocity zones. In Figure 3.10B there is a clear jump from higher velocity at 10m to a lower velocity and back to a much higher velocity at depth 13m. The corresponding part of the dispersion curve (between 15-25 Hz) is less steep than the curve below 15 Hz. This may be a product of processing, because the slopes of curves under 15 Hz may be distorted by the loss of fundamental mode energy during the process of muting, as noted earlier.

Dispersion curve records for stations 1001-1090 show poor resolution of the fundamental mode. O'Neill and Matsuoka (2005) have shown higher mode interferences may be due to the very shallow depth to bedrock. Exposures of bedrock at the surface are found at the beginning of Line A and Line Z. For stations 1001-1100, 28 records were removed from analysis due to poor data quality. For stations 1025-1055, 11 records were removed, thus the resolution of that section on the 2D model may in fact be an artifact from interpolation. The most reliable frequency range for picking dispersion curves was between 10 and 30 Hz. Phase velocities for frequencies less than 10 Hz contained possible distortions due to muting; therefore picks in that frequency range were checked for consistency from record to record. Picks at frequencies higher than 30 Hz were more susceptible to contamination by higher modes. Alternative models are discussed in Chapter 4.

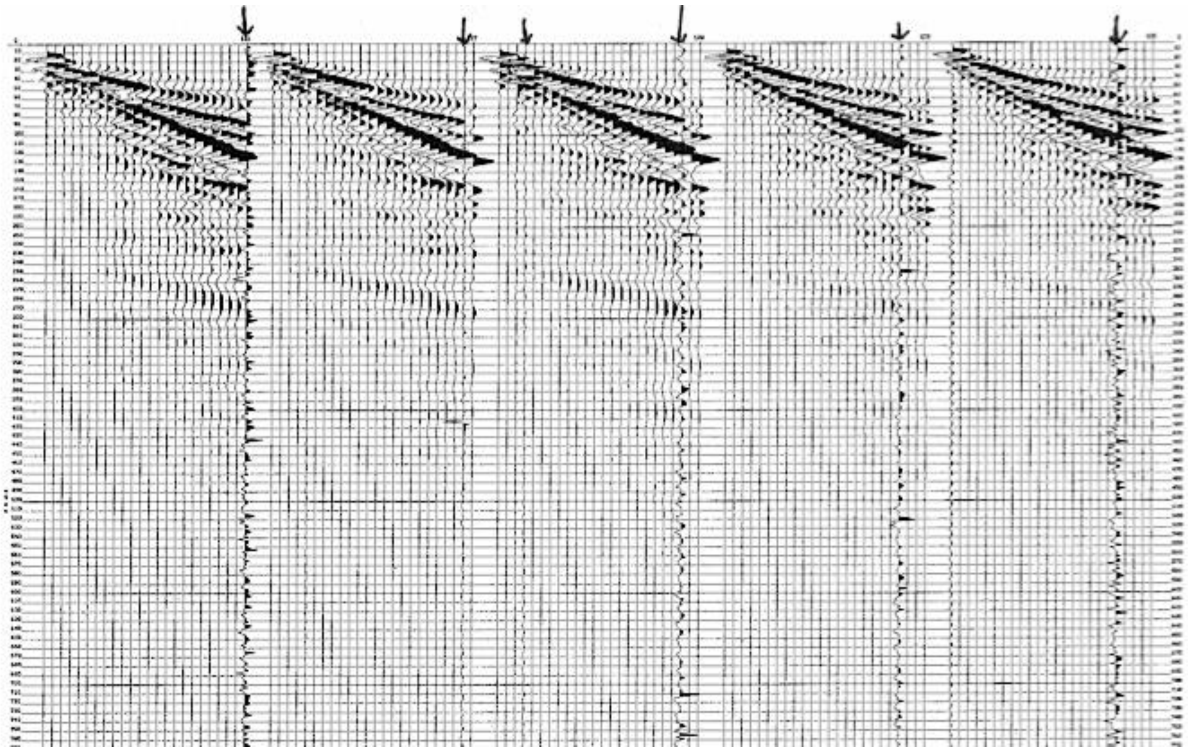

Figure 3.1

Seismic records for 5 stations along Line A. Arrows indicate the bad traces that were removed prior conversion into the Surfseis format. Bad traces were removed from all 166 seismic records.

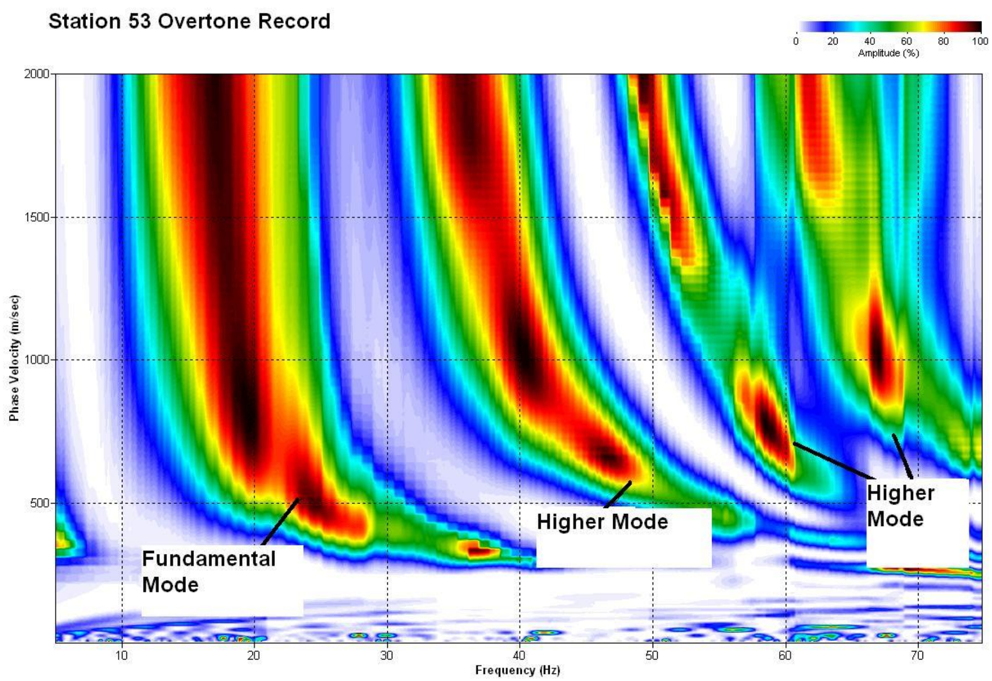

Figure 3.2

Overtone image showing plot of Phase Velocity (y-axis) vs. Frequency (x-axis) and an amplitude scale for station 1053 Multiple modes exist in the image with the fundamental mode found in the 15-40 Hz frequency range. Higher energy modes exist at higher frequencies and phase velocities.

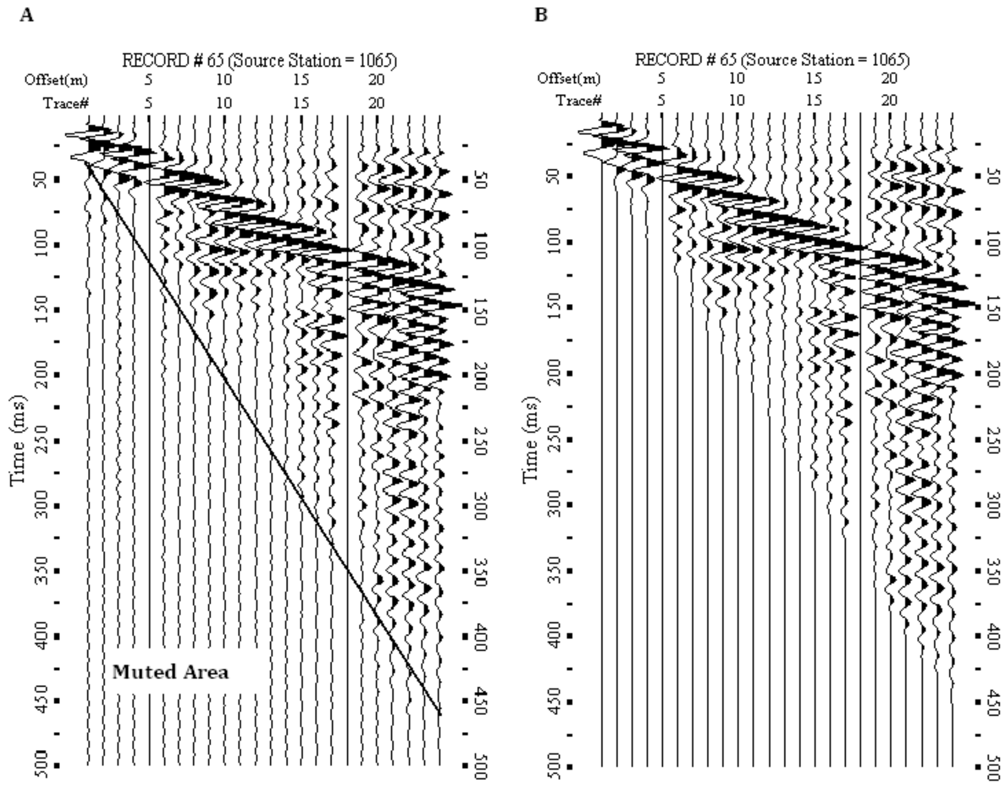

Figure 3.3

Seismic Records for Line A station 1065 A) unmuted seismic record B) Back-end muted seismic record. The line on record A shows where the beginning of the mute was applied, removing all energy below that line.

A.

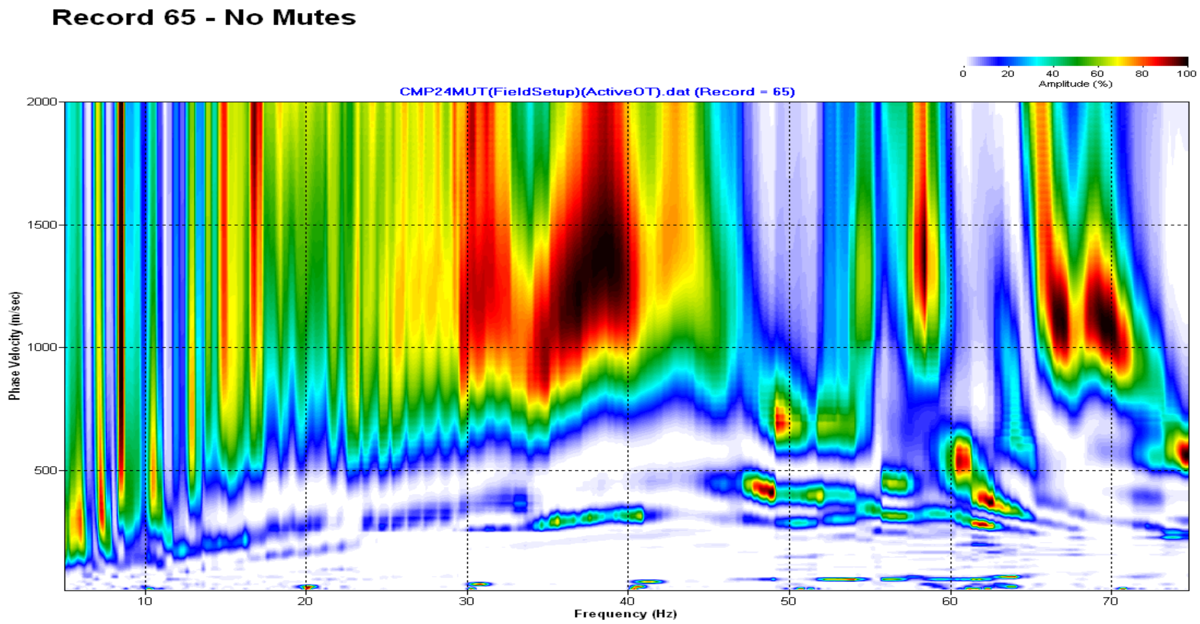

B.

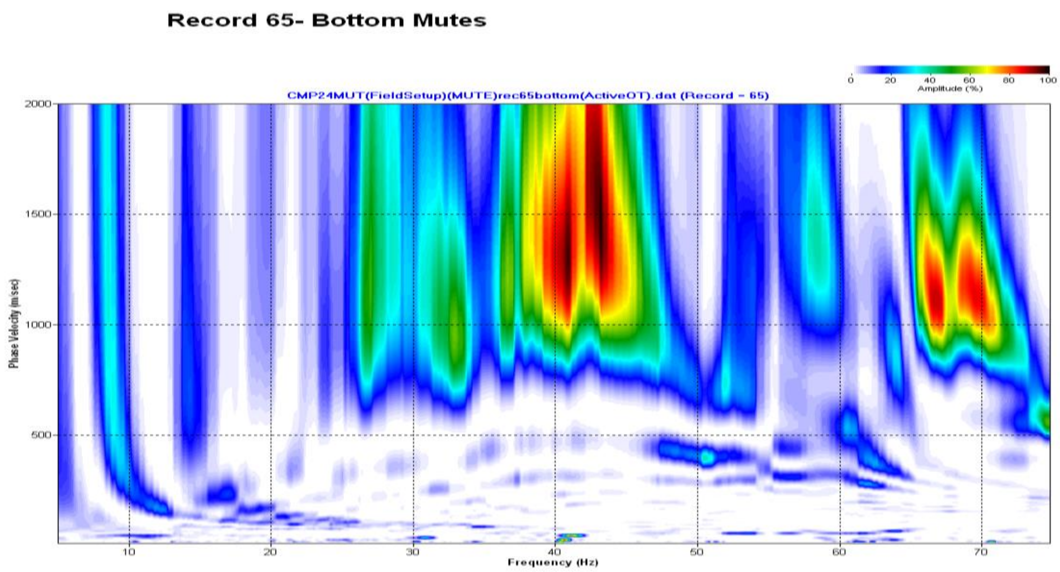

Figure 3.4

Overtone images for Line A station 1065. A) Unmuted record B) Back-end muted record. Note the improved image resolution due to removal of noise.

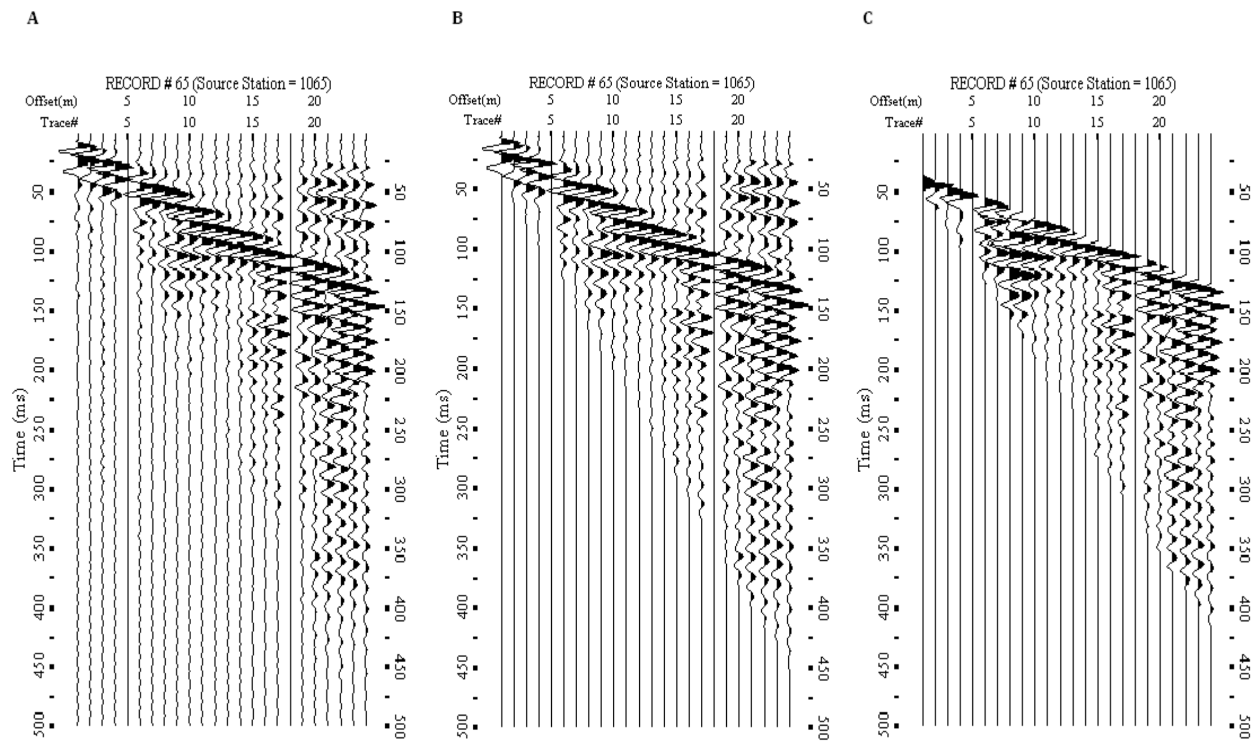

Figure 3.5

Seismic records for Line A station 1065 A) Unmuted B) Bottom mute applied to remove noise C) Top mute applied to remove body waves and higher mode energy.

Record 65- Top and Bottom Mutes

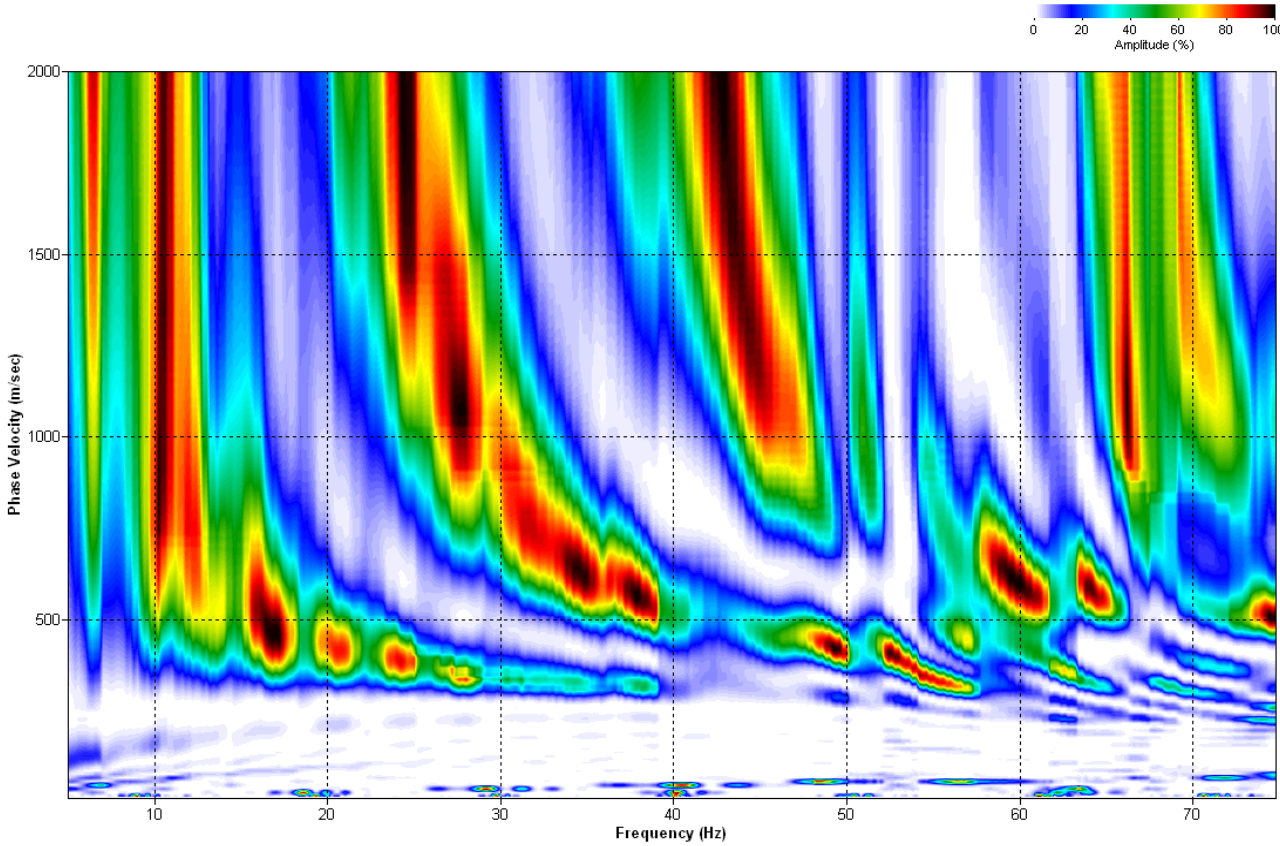

Figure 3.6

Generated overtone image for station 1065 after front-end and back-end mutes were applied to the seismic record. Improved image resolution separates the fundamental mode (10-40 Hz) from the higher modes.

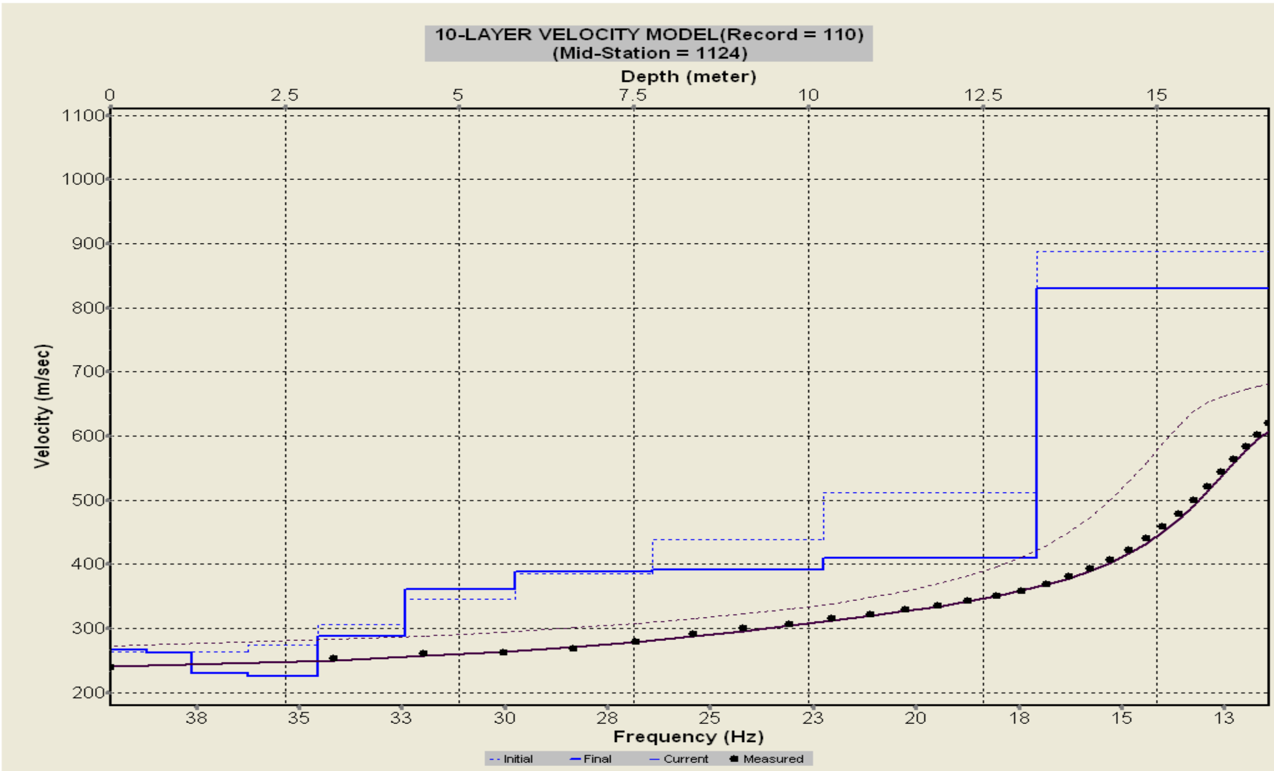

Figure 3.7

1-D shear wave velocity model after inversion for station 1110. This plot shows both shear-wave velocity as a function of depth and phase velocity as a function of frequency. Dashed blue curve: the initial velocity model. Solid blue curve: the final velocity model. Dashed black curve: Phase velocity as a function of frequency for the initial model. Solid black curve: phase velocity for the final model. Dots: dispersion curve picks.

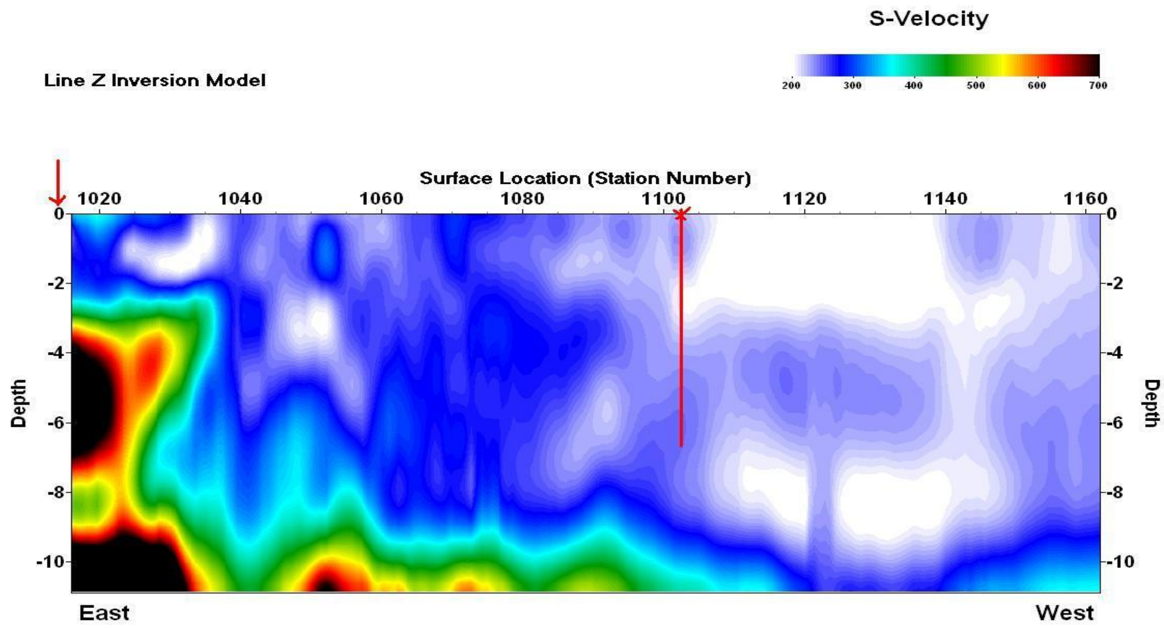

Figure 3.8

Inversion Model for Line Z (2D) showing depth and station location. Red arrow to the left of the image shows the intersection with Line A. The red line located between stations 1102 and 1105 shows the location of well EPA6 and extends to a depth of 7m. Due to lateral averaging of the velocity models there is a poor correlation between the borehole from the well and the model. Depth and station spacing are in meters.

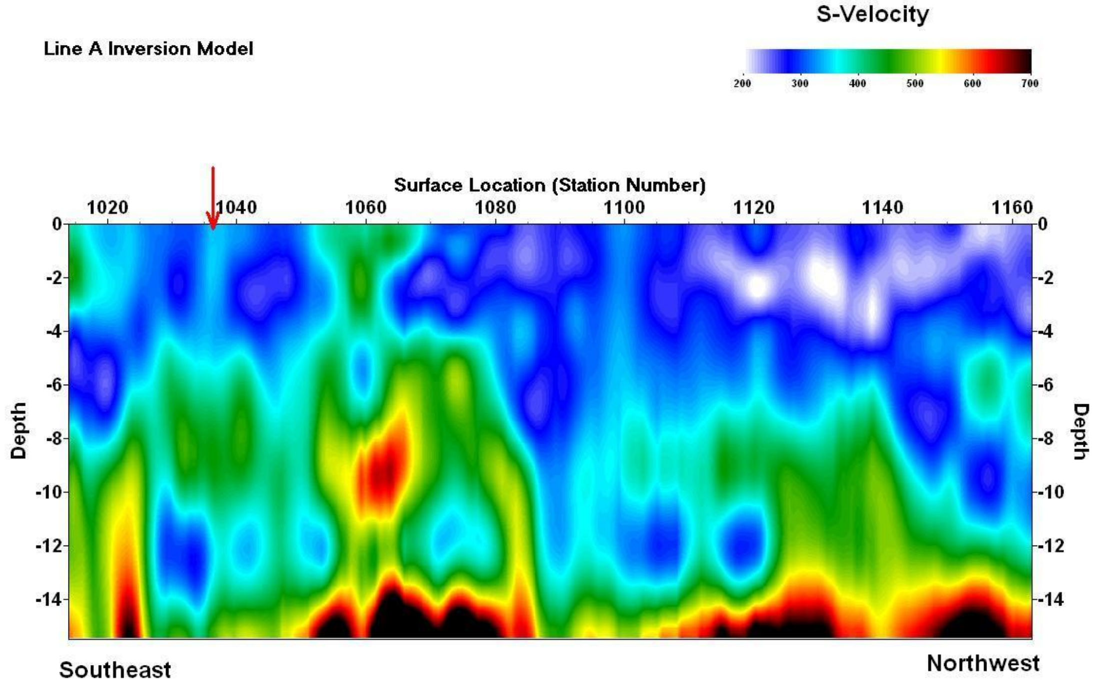

Figure 3.9

Inversion model (2-D) for Line A, showing depth and location. The red arrow shows the point of intersection with Line Z. Velocities exceeding 600 m/s are interpreted as relatively unweathered bedrock. Values associated with 550m/s are interpreted to be the transition zone. Note that the transition zone mimics the bedrock topography. Increase in chemical weathering is reflected by the lower s-velocities of saprolite (200-500 m/s). Depth and station spacing are in meters.

A.

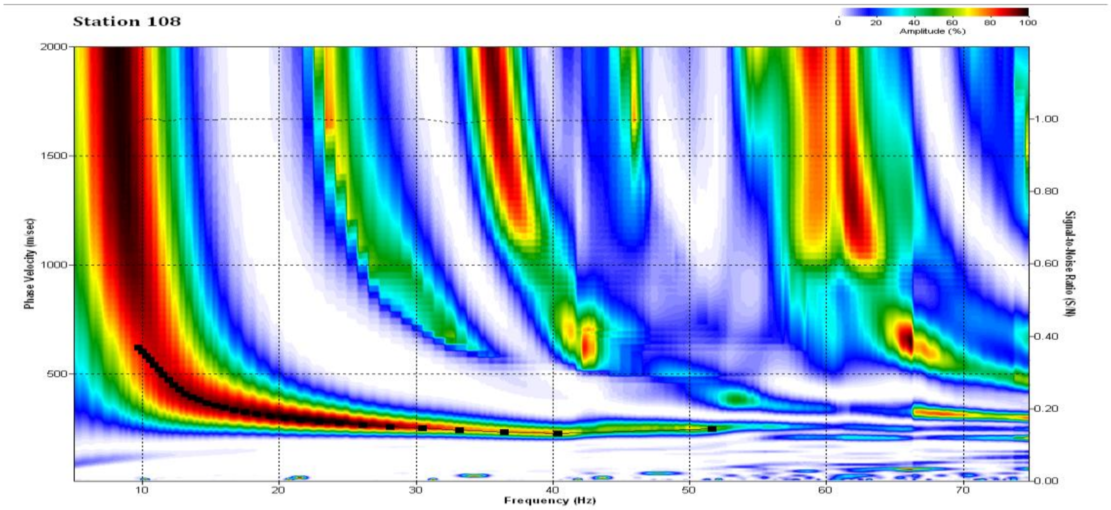

B.

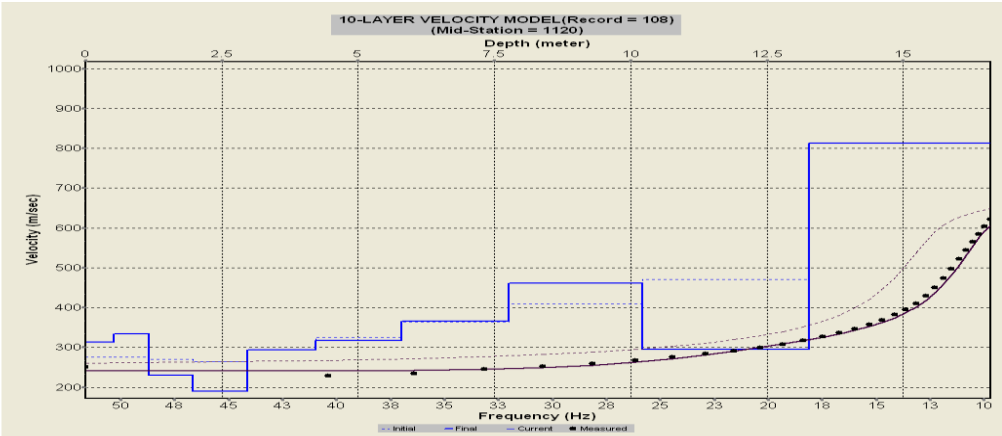

Figure 3.10

A) Dispersion curve picks and B) 1D Shear-wave velocity model across the low velocity zone associated with station 1108.

Inversion Parameters	
Poisson’s Ratio	0.4
Density	2.0g/cc
Number of Layers	10
Maximum Iterations	5
Target RMSE (in phase velocity)	5 m/s

Table 3.1 Inversion Parameters

CHAPTER 4

ALTERNATIVE MODELS

Alternative models were generated for Lines A and Z using variations in processing and inversion parameters to improve resolution. These models are discussed below in detail.

Half-Spread Analysis

The analyses were repeated using “half-spreads” (12 contiguous traces for each field record, rather than the original 24 traces) to improve lateral resolution of structure. This decreased the resolution widths from approximately 12 to 6 meters but also decreased the maximum depth of penetration by the same amount. Half spread models were generated using traces 3-14, 7-18, and 13-24. Inversion parameters for half spreads are found in Table 4.1. Restricting the dispersion curve picks to frequencies greater than 15 Hz avoided the distortion of phase velocities generated at low frequencies by mutes designed to suppress higher modes. In picking dispersion curves for Line A, it was found that stations 1030-1097 could not be included because the fundamental mode was not observable. The discussion of the half spread inversion models therefore focuses on the northern part of Line A, specifically stations 1098-1150.

Near Half-Spreads

Near half-spreads (traces 3-14) were used to create new overtone images. A frequency range of 25 to 50 Hz was selected as the optimum window for Line A and 10-25 Hz for Line Z. Figure 4.1 shows the near half-spread inversion model and a full spread model for Line A. In Figure 4.2, the two models are replotted to include only the range of uninterrupted coverage between stations 1099 and 1150. Stations 1120-1130 show an increase in resolution of the anomaly associated with the low shear wave velocity (200 m/s). The improved lateral resolution indicates that this anomaly extends from 2-4 m depth. This structure is not fully resolved on the full-spread model.

Figure 4.3 shows the comparison of the near half spread model with the full spread model for Line Z. In contrast with Line A, all but 5 stations were used in the inversion. Only bottom mutes were needed to remove the excess noise. Even with 30 Hz geophones, the optimum window was found to be at a lower frequency. This situation is not ideal, but is still possible to acquire lower frequencies than the geophones used. The depth of penetration decreased to around 7 meters. The comparison of the images is restricted to the first 8m. The lateral resolution is improved in the half spread. The key result for this model is the correlation of shear-wave velocities greater than 600 m/s with exposures of bedrock near the eastern end (Station 1001) of the profile. The low velocity zone (200 m/s) at 2 m depth between stations 1040 and 1150 thickens from 2 m in the east to 3 m in the west. From station 1055 to 1070, a structure associated with a shear wave velocity of 450 m/s is shown at depth 2-5 m. This structure is not resolved on the full spread model. Only by utilizing the half spread, was this structure resolved at a very shallow depth.

Middle Half-Spreads

The analysis was repeated using traces 7 to 18. For Line A, dispersion curves were not attainable for stations 1040-1098 and were not included in the final inversion model. Figure 4.4 shows the velocity models for Line A for the middle half-spread and full-spread analysis**.** A zone is marked off showing the area of missing data. This area was ignored for the discussion. In the first 40 stations, velocities exceeding 600 m (indicating bedrock) are observable at 8 m depth on the half spread model. The full spread model shows the bedrock to be at depth 12m. The increased lateral resolution implies higher velocities (> 450 m/s) are near the surface (1-4 m depth) at stations 1001-1020 and stations 1055-1065. Lower velocities (200 m/s to 450) are found at the same depths from station 1065-1160.

Again, the two models are replotted to include only the range of uninterrupted coverage between stations 1099 and 1150 (Figure 4.5). Figure 4.5 shows the depth of penetration to be slightly greater than the near traces and extends to about 7 m. Half-spreads for stations 1099-1150 on line A, show the same structures seen in the full spread model. The low velocity structures are once again highlighted in the half spread model. The half-spread model also provides greater detail of the low velocity zone (200 m/s) located at depth 2 m at station 1099 and extending to station 1130. This is where it dips down to a depth of 5 m, but stays relatively the same thickness of 2m.

Results for inversion of the middle half-spreads for Line Z are shown in Figure 4.6. Depth of penetration is around 7m. Some phase velocities for frequencies below 30 HZ were processed as part of the fundamental mode and increased the depth of penetration slightly. As shown in Figure 4.3, velocities in the near surface (1-4m) at stations 1001-1025 exceed 600 m/s, which correlates with exposed bedrock. West of these stations, the surface velocities decrease abruptly. Higher velocities (>450 m/s) drop to a depth of 5m then to 8 m at station 1040-1100. No velocities associated with bedrock are seen west of station 1100. A low velocity zone of 200 m/s is observed to follow the topography of the bedrock. The thickness of this layer varies from 1m to 4 m. A weak correlation can be made with the near half spreads at station 1060-1075. The structure associated with higher velocities is not as evident, but still exists.

Far Half-Spreads

The inversions were repeated using traces 13 - 24. This spread was highly sensitive to the choice of muting parameters. Muting removed body waves without difficulty and isolated the surface waves more effectively than with the near and middle half spreads. Lateral resolution was increased, but lower frequencies were lost. For Line A, a model spanning the entire profile could not be generated because the fundamental mode was not observed in records for stations 1001-1098. Figure 4.7 shows the comparison of the full and far half-spread velocity models for stations 1099-1150.

Similar to the half spread models of figures 4.2 and 4.5, a low velocity zone extends laterally at depth 2m. Though lateral resolution differs on each half-spread, lower velocities are consistently represented on each model. This low velocity zone (200 m/s) appears to be broken into 2 zones, unlike the previous half spread models. Zone one extends from stations 1099-1130 to a depth of 5 m. Zone 2 extends from station 1130 at depth 2 m to station 1150 at a depth of 8 m. The low velocity zone follows the same pattern as the higher velocities of the bedrock.

Far-spread models for Line Z are shown in Figure 4.8. A low velocity zone of 200m/s follows the bedrock topography to a depth of 7-9 m near the west end of the profile. Structures with velocities of 350 m/s are found between stations 1060-1090 at a depth of 2-4m, directly above the low velocity zone. These structures disappear at station 1100 where another low velocity zone is observed from the surface to a depth of 4 m. From stations 1100-1150, at depths of 4-7m, velocities of 350 m/s to 400 m/s are observed and have an elliptical appearance. High velocities associated with bedrock are only seen in the eastern portion of Line Z from stations 1001-1100. High velocities (>600 m/s, interpreted as bedrock as noted earlier) are seen at depths

1-4 m for the first 25 stations. This is consistent with models derived for the mid and near half spreads.

The high velocities drop to a depth of 6m from stations 1025-1035, and then drop to a depth of 9m from stations 1050-1100. A velocity layer of 550m/s, less than a meter thick, runs along the top of the bedrock in all images. This is all consistent with the previous half spread models. Figures 4.9A and 4.9B show summary figures for a comparison of full spreads with all half spreads for each line.

Effect of Number of Iterations

Variations in the inversion parameters also affected the resolution of the final model. The inversions were run until the RMSE (Root-Mean-Square- Error) between the observed phase velocities and velocities predicted by the model dropped below a specified value, or the specified maximum number of iterations was completed. For good quality dispersion curves the RMSE is met before the maximum number of iterations can run. For the purpose of this study, we selected a RMSE of 5 m/s, and changed the number of iterations for 3 trials of 4, 5, and 12. The models are as follows:

Line A

Figure 4.10 shows a comparison of 4,5, and 12 iterations for Line A. The image with the smallest number of iterations has less definition of the velocity gradient. The resolution of the low velocity zone at stations 1115 to 1160 (at depths of 9- 12 m) improves as the number of iterations is increased. However, increasing the number of iterations can also introduce spurious detail into the models. Depth to bedrock (velocity > 600 m/s) did not change. The low velocity anomaly at station 140 is much more sharply imaged in the 12-iteration model than in the 5-iteration model. The changes between 4 and 5 iterations are very subtle. Structures are correlated between all three models. The bedrock topography is undulating and is imaged at a depth range of 12-14.5m.

Line Z

Figure 4.11 shows a comparison of 5 and 12 iterations for Line Z. The increase in iterations increased the sharpness and details of the 2D velocity model. The structure at Station 1060 has a more defined velocity change and shape. Increasing the number of iterations to 12 improves the resolution of the final model so that the low velocity zone can be defined. The best resolved feature is at station 1-25 at depth 8-10m. The velocity gradient is defined at 450 m/s to 550 m/s. The resolution of this structure improved with an increase of iterations. The depth to bedrock (2-4 m; note that the half spreads indicate a shallower depth) does not change, but the image of the bedrock surface is enhanced. The low velocity zone follows the topography of the higher velocity zone and also deceases in depth to 12m.

Number of Model Layers

10-layer models are the default setting within Surfseis. A default setting of variable thickness assumes the layers become thicker with depth and can change the outcome of the inversion model. Changing the number of layers can increase or decrease the detail found in the 2D model. In all inversion models, Poisson's ratio is assigned a value of 0.4 and density of 2.0 g/cc (Park et al., 1999; KGS Surfseis manual, 2010) (see table 3.1 in Chapter 3) for each layer.

Figure 4.12 shows a comparison of Line A for a 10-layer and a 5-layer model. The structures at depth 5-9 m from stations 1-100 are better defined in the 10-layer model. The low velocity zone is better observed as well in the 10-layer model. This is consistent with the idea that more layers provide better resolution of an image. The depth of penetration increased to 16 m for the 5-layer model, but at a cost of lateral resolution. Pinnacles at stations 20 and 60 are associated with higher velocities in the 5-layer model.

A.

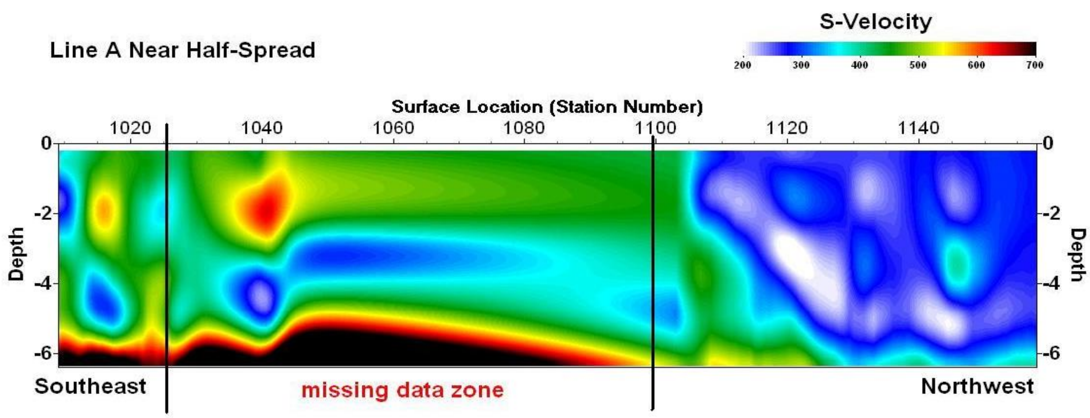

B.

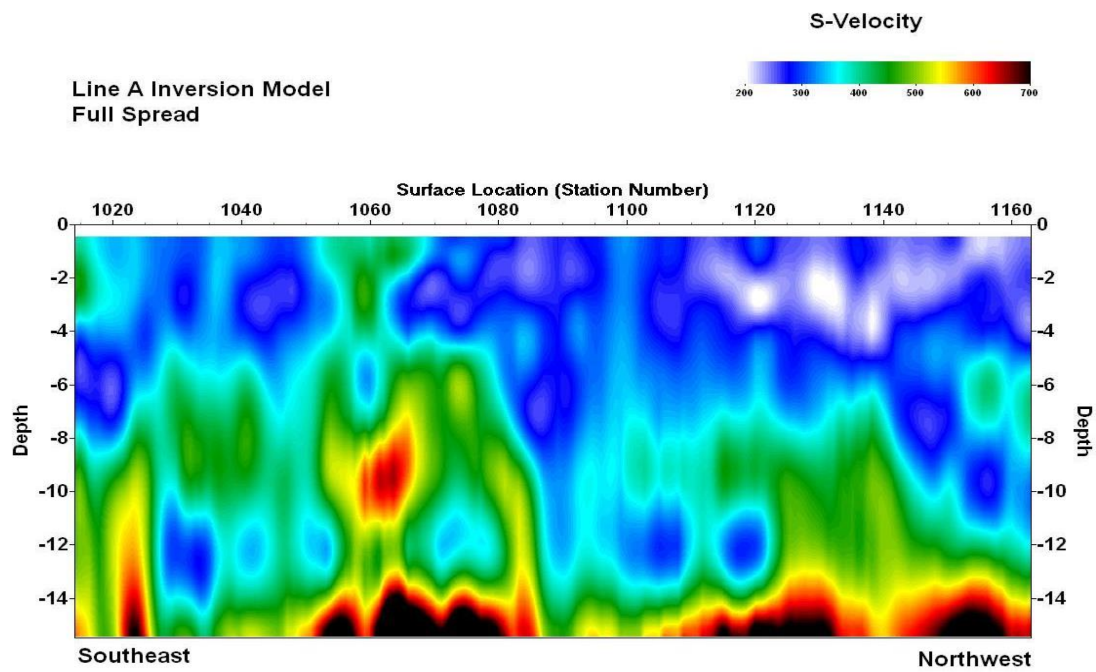

Figure 4.1

Shear-wave velocity models derived for Line A. A) Velocity model derived from near half-spread (traces 1-14) for Line A. Depth of penetration is 6m B) Inversion model for Line A using all 24 traces. Depth of penetration 15m.The half-spreads did not generate clear images of the fundamental mode for stations 1030-1097. Velocities shown over this range of stations (labeled as “missing data zone” on A) are interpolated between stations 1029 and 1098. Depth and station spacing are in meters.

A.

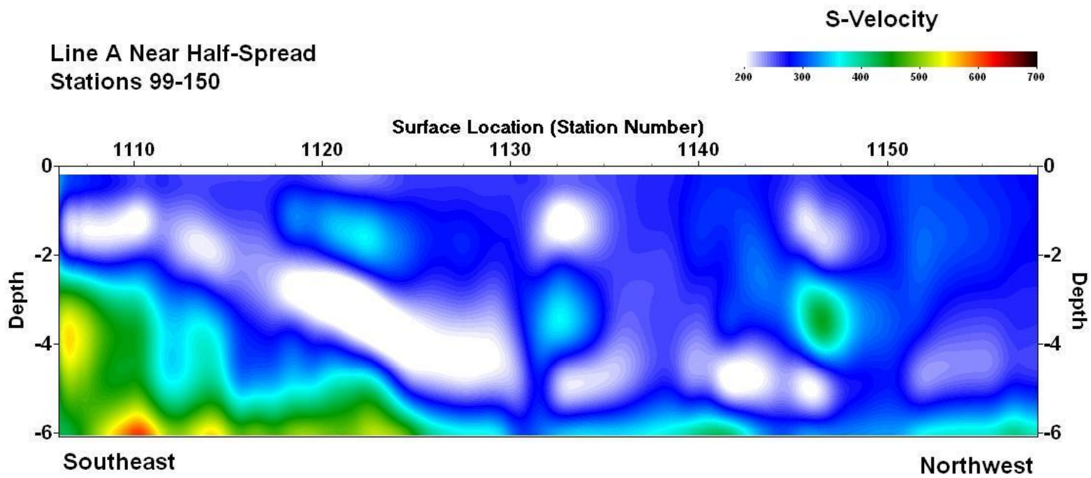

B.

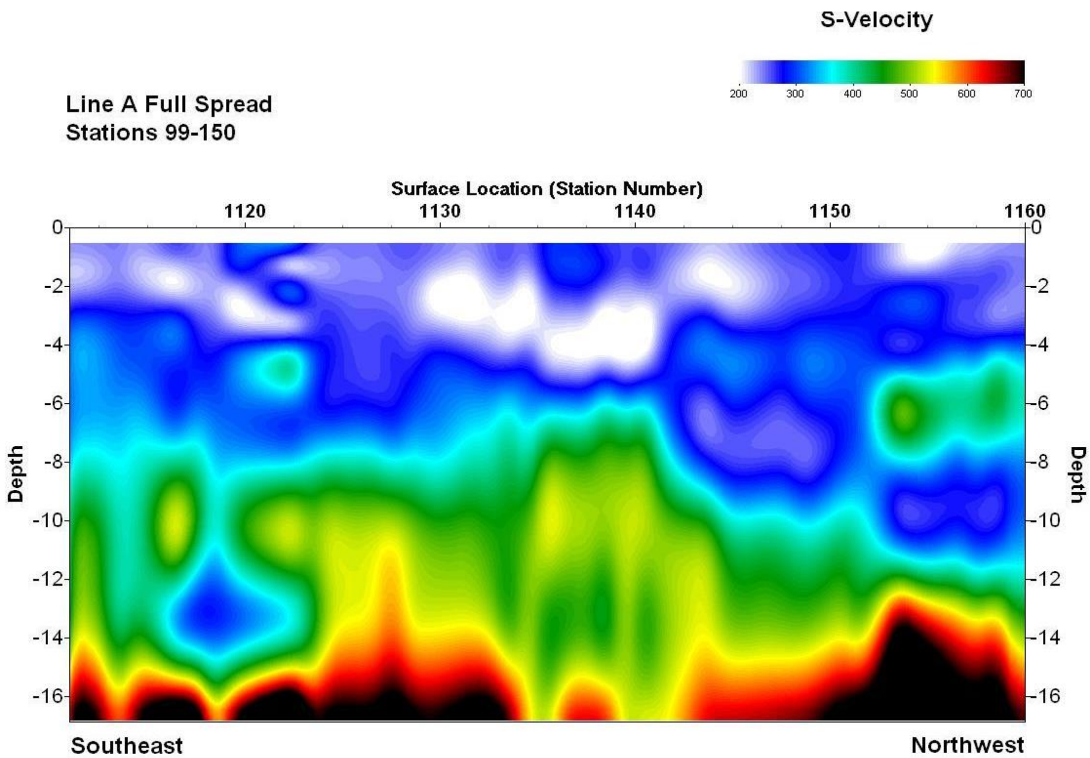

Figure 4.2

Shear-wave velocity models for Line A replotted to show only the results for stations 1099-1150. A) Models derived from near half-spread gathers (traces 1-14). B) Models derived from full-spread gathers (traces 1-24). Depth and station spacing are in meters.

A.

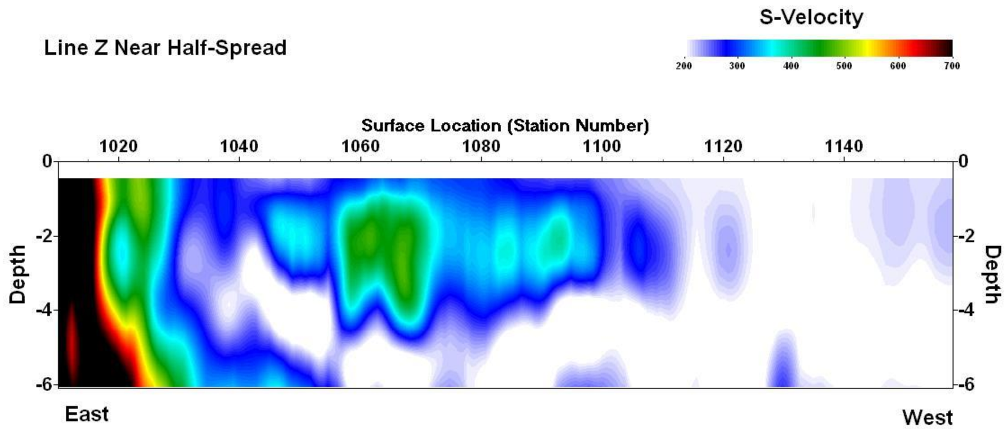

B.

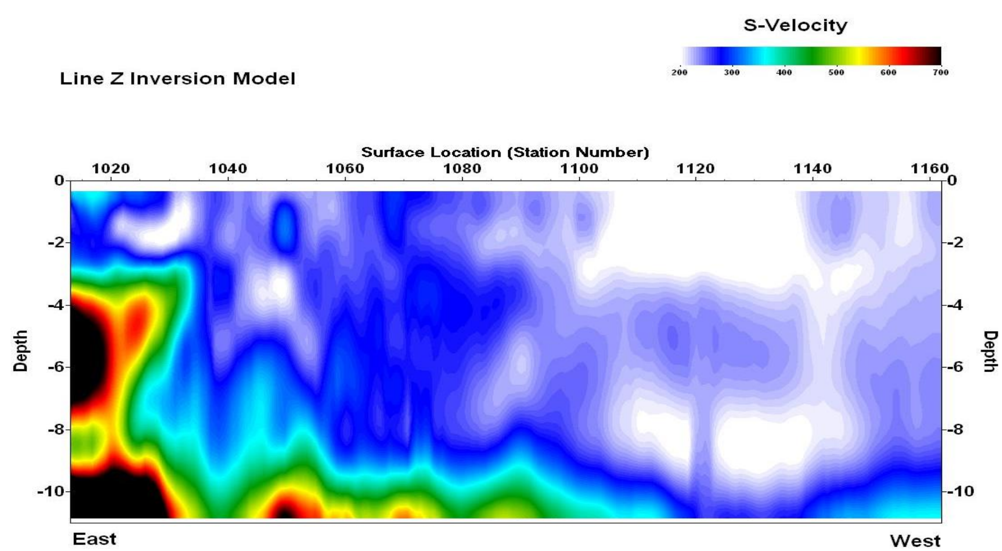

Figure 4.3

Shear-wave velocity models derived for Line Z. A). Models derived for near half-spread (traces 1-14). Velocities greater than 600 m/s correlate with exposures of bedrock at the eastern end of the profile. B) Models derived for full-spread (traces 1-24). Depth and station spacing are in meters.

A.

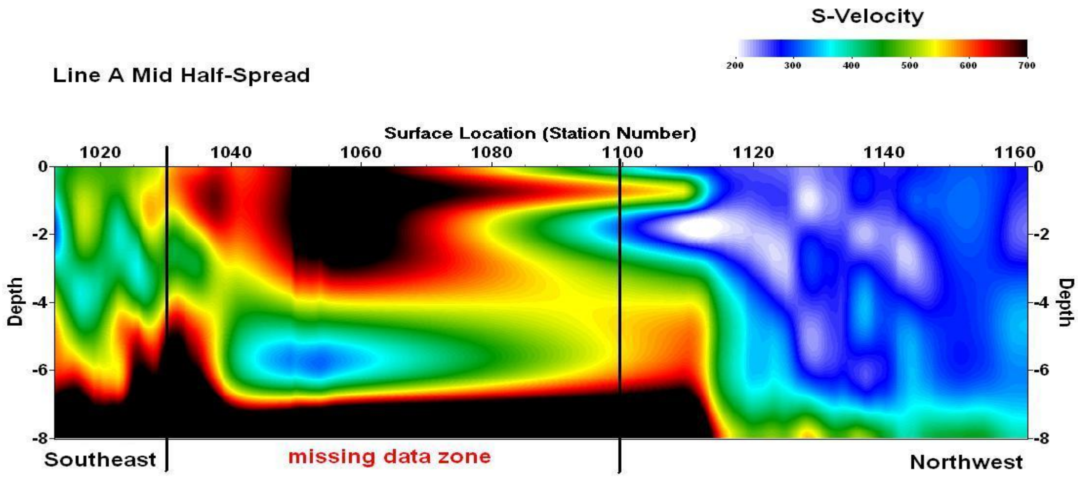

B.

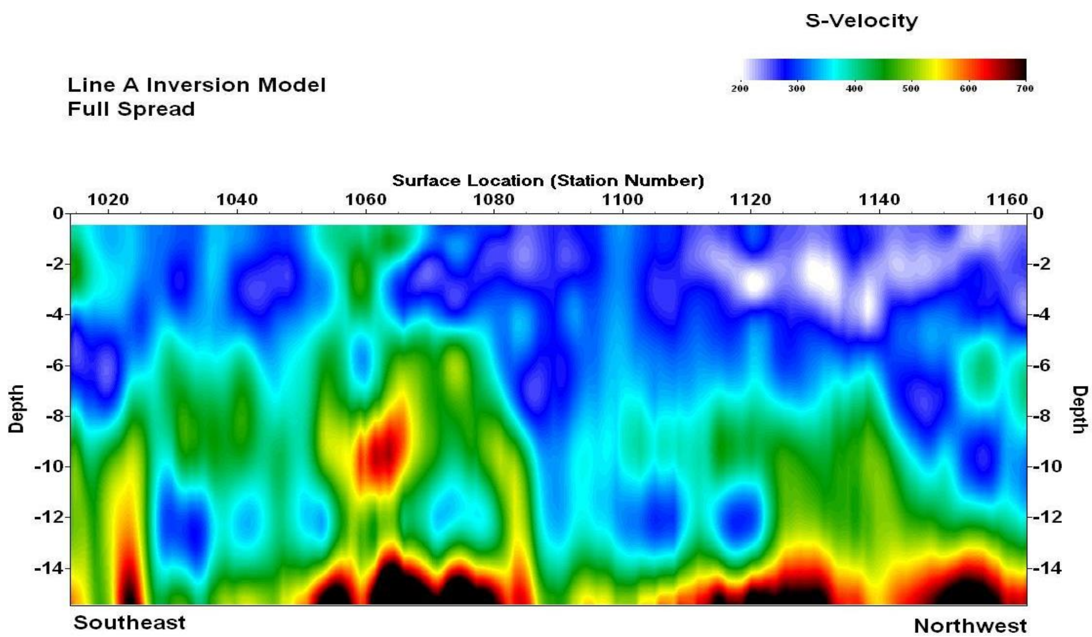

Figure 4.4

Shear-wave velocity models derived for Line A.

A.) Velocity models derived for middle half-spreads (traces 7-18) for Line A. As in Figure 4.1, the half spreads did not generate clear images of the fundamental mode for stations 30-97; velocities over this range are interpolated. B.) Inversion model for Line A using all 24 traces. Depth and station spacing are in meters.

A.

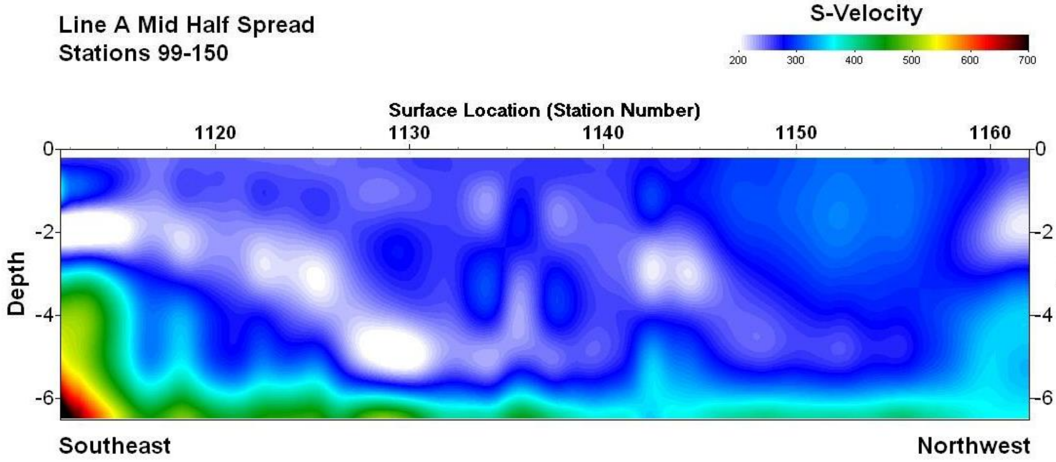

B.

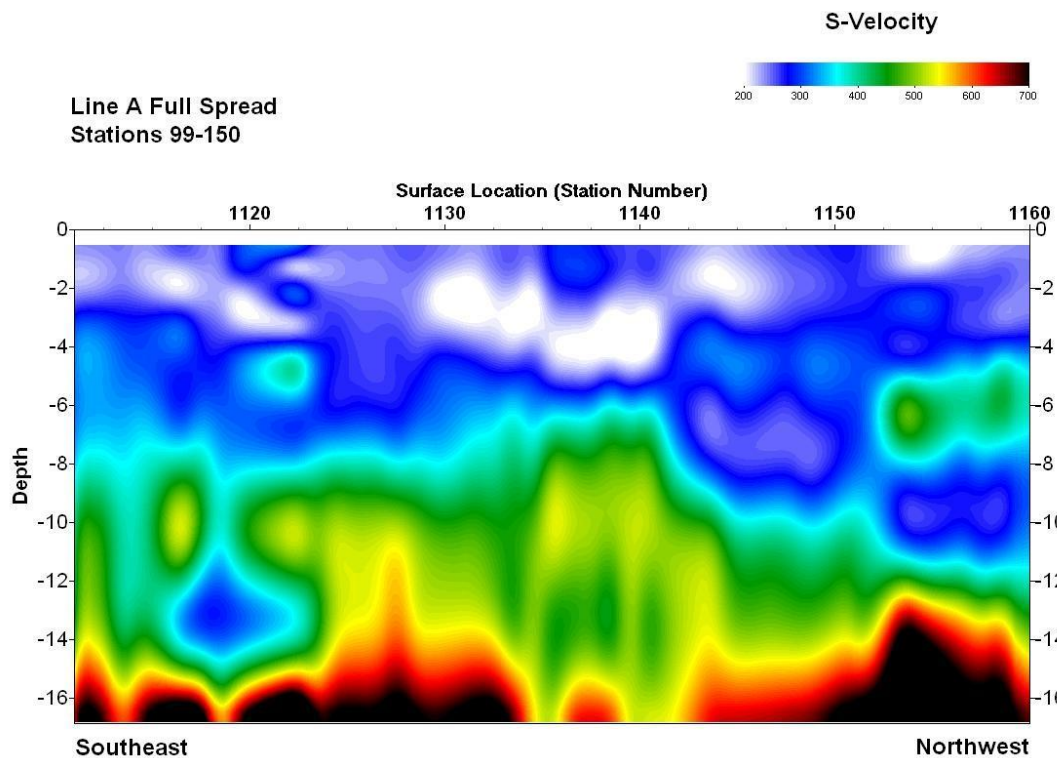

Figure 4.5

Shear-wave velocity models for Line A replotted to show only the results for stations 1099-1150. A.) Velocity models for middle half-spreads (traces 7-18). B.) Velocity models for full spread. Depth and station spacing are in meters.

A.

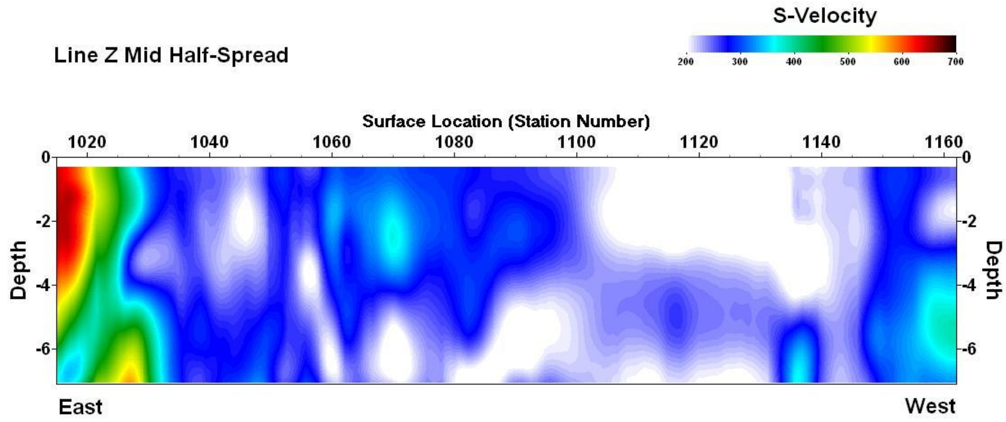

B.

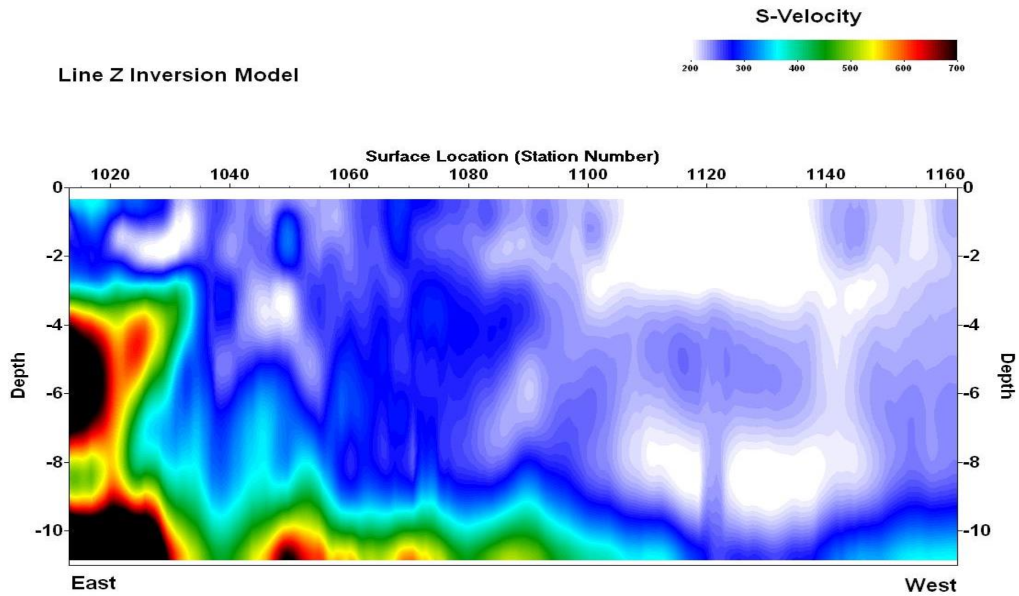

Figure 4.6

Shear-wave velocity models derived for Line Z.

A) Line Z middle half spread (traces7-18) B) Line Z full spread. Depth and station spacing are in meters.

A.

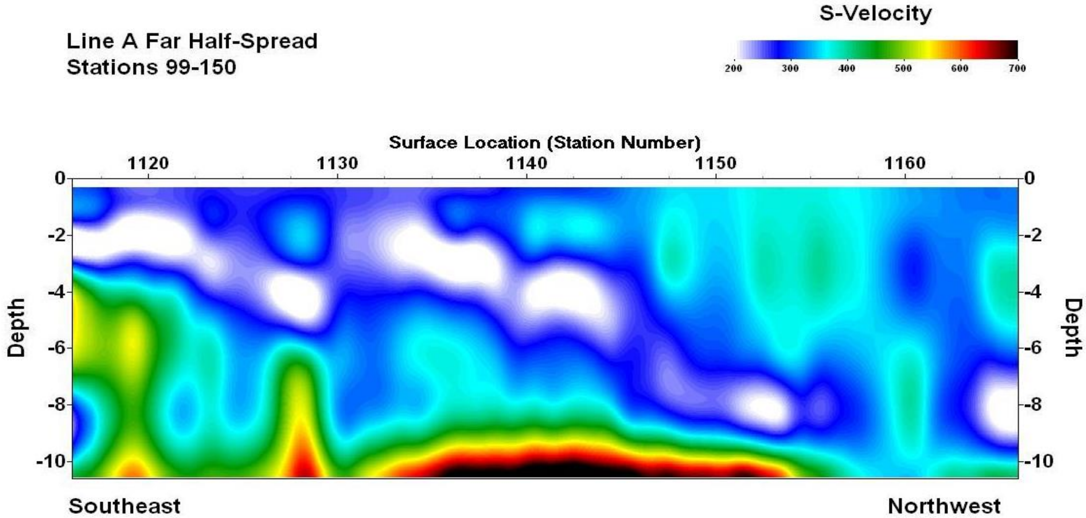

B.

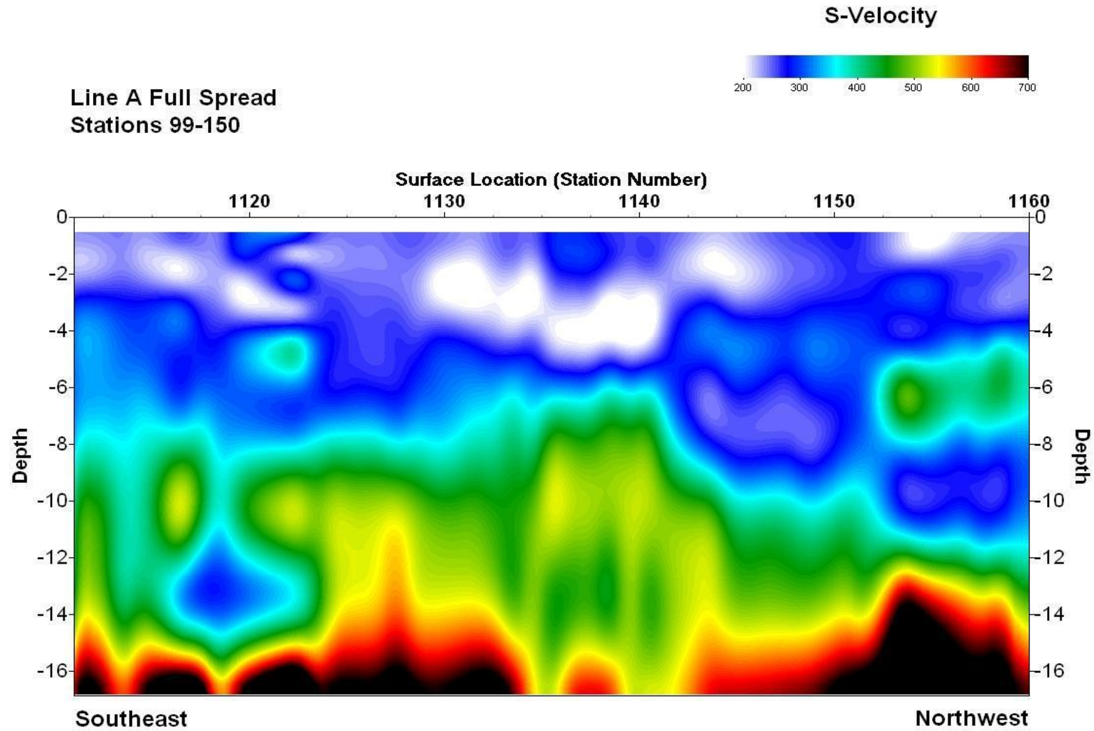

Figure 4.7

Shear-wave velocity models derived for Line A, stations 1099-1150.

A.) Velocity models derived from far half-spread (traces 13-24). B.) Velocity models derived from full-spread. Depth and station spacing are in meters.

A.

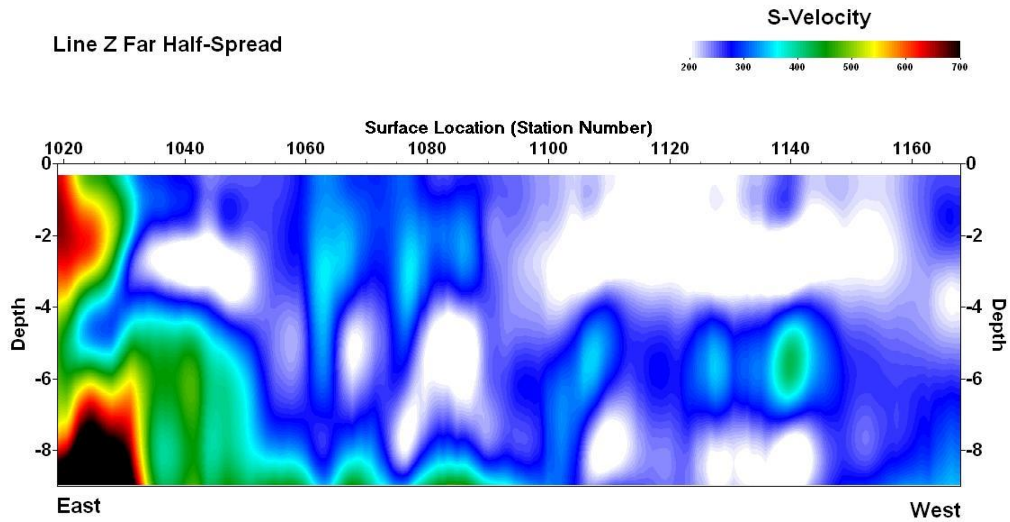

B.

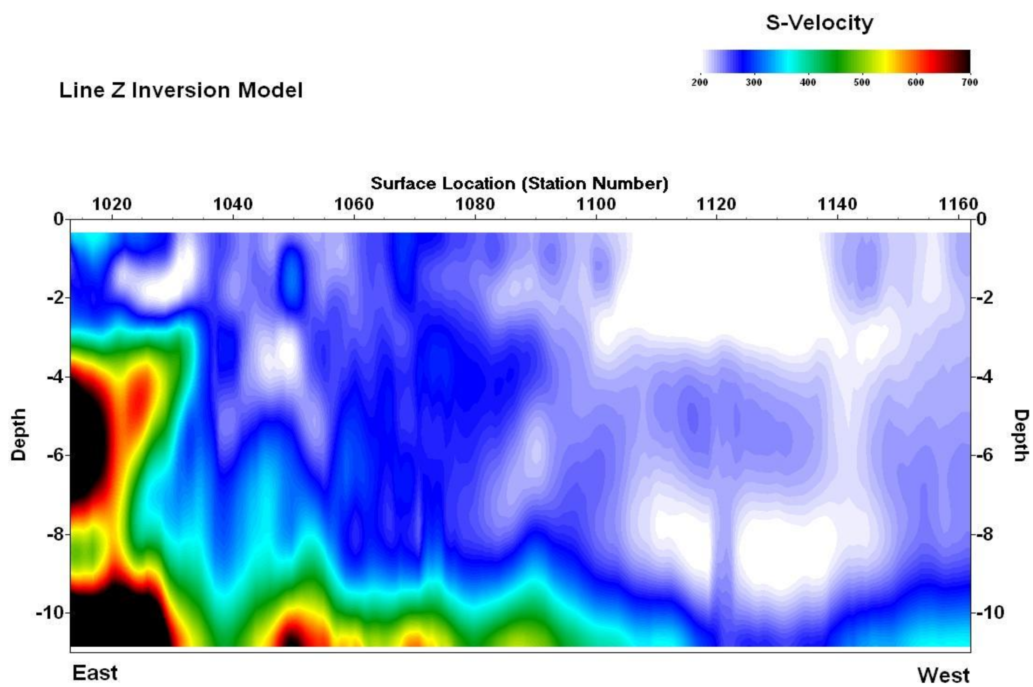

Figure 4.8

Shear-wave velocity models derived for Line Z.

A) Velocity models for far half-spreads (traces 13-24) B) Velocity models for full spreads. Depth and station spacing are in meters.

A.

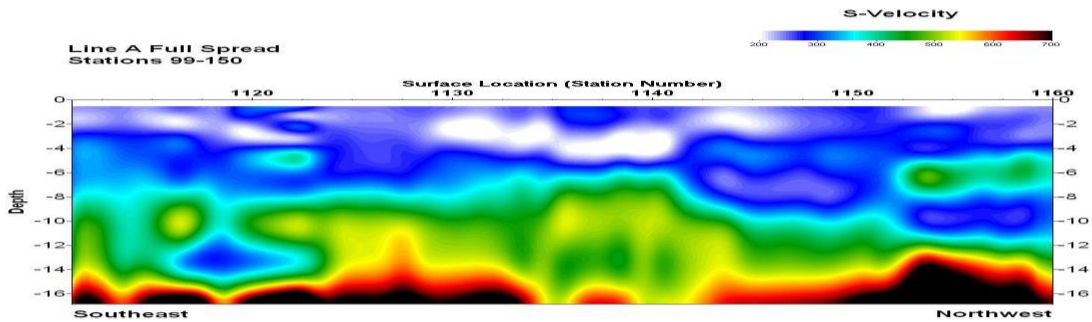

B.

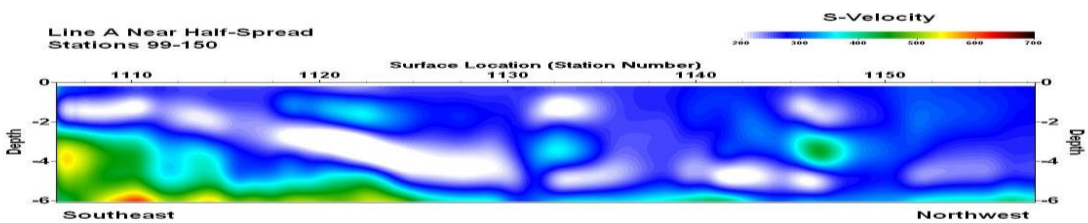

C.

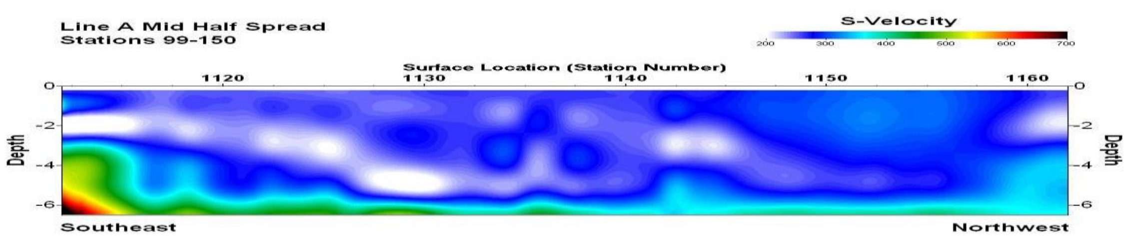

D.

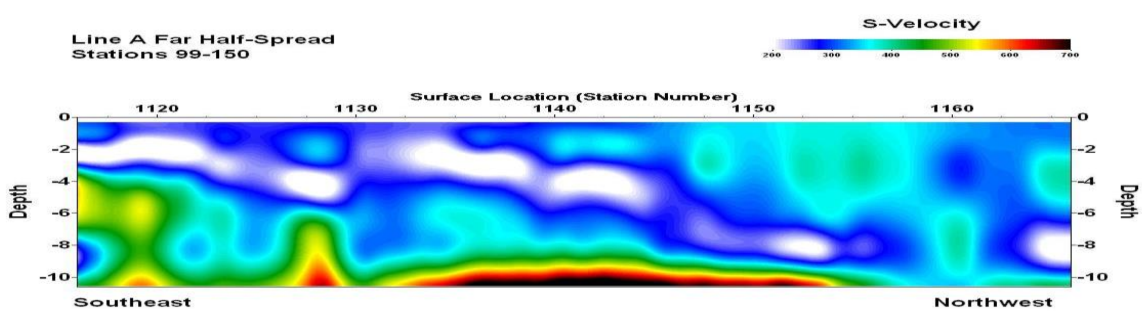

Figure 4.9 A

Comparison of Line A, stations 1099-1150 A) Full Spread B) Near Half-Spread C) Mid Half-Spread and D) Far Half-Spread. Depth and station spacing are in meters.

A.

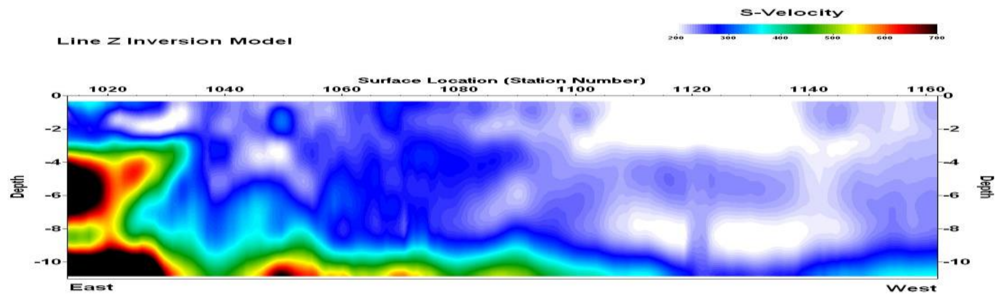

B.

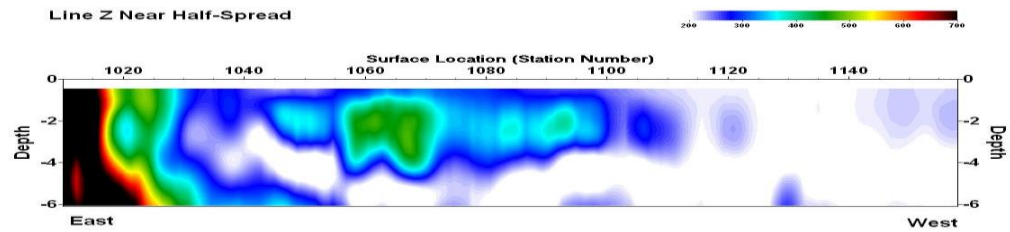

C.

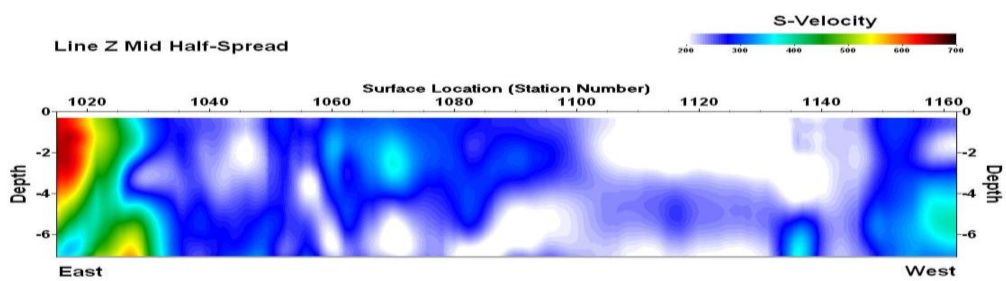

D.

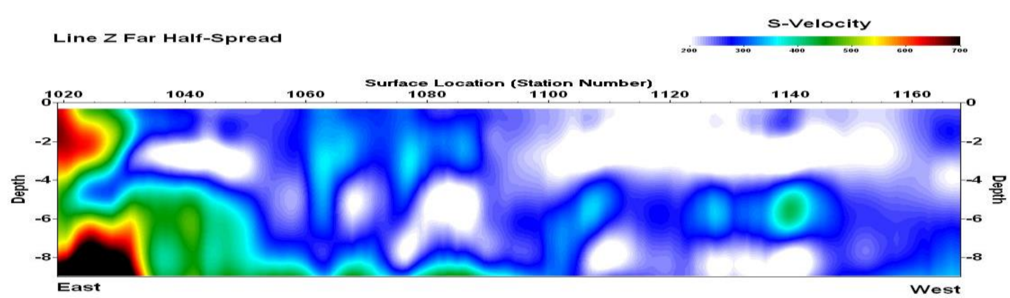

Figure 4.9B Comparison for Line Z A) Full Spread B) Near Half-Spread C) Mid Half-Spread D) Far Half Spread. Depth and station spacing are in meters.

A.

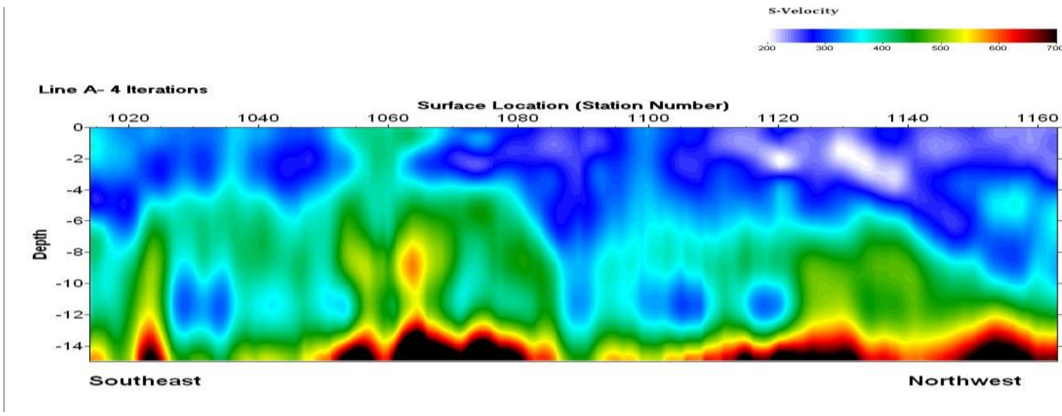

B.

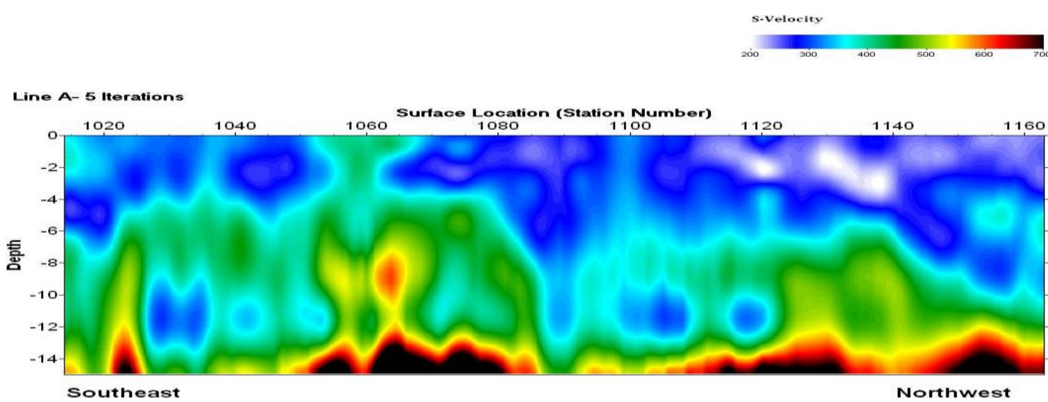

C.

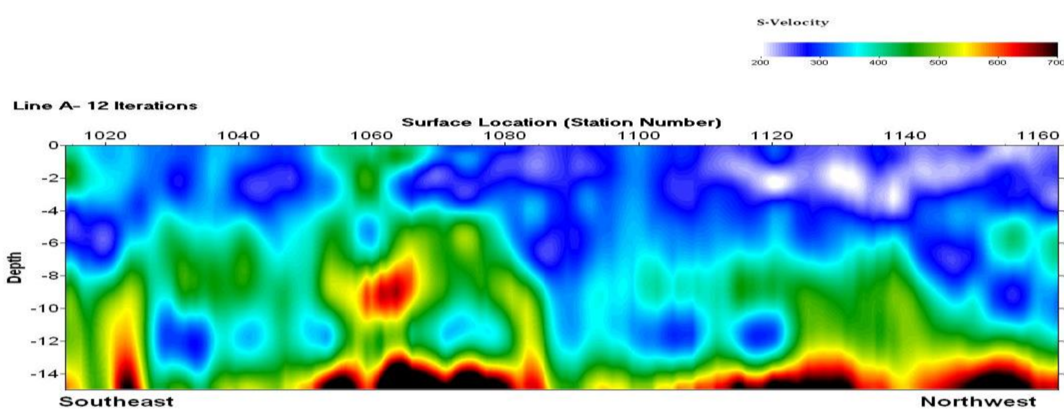

Figure 4.10

Shear-wave velocity models for Line A, derived using different numbers of iterations.

A) 4 Iterations B) 5 Iterations C) 12 Iterations. Depth and station spacing are in meters.

A.

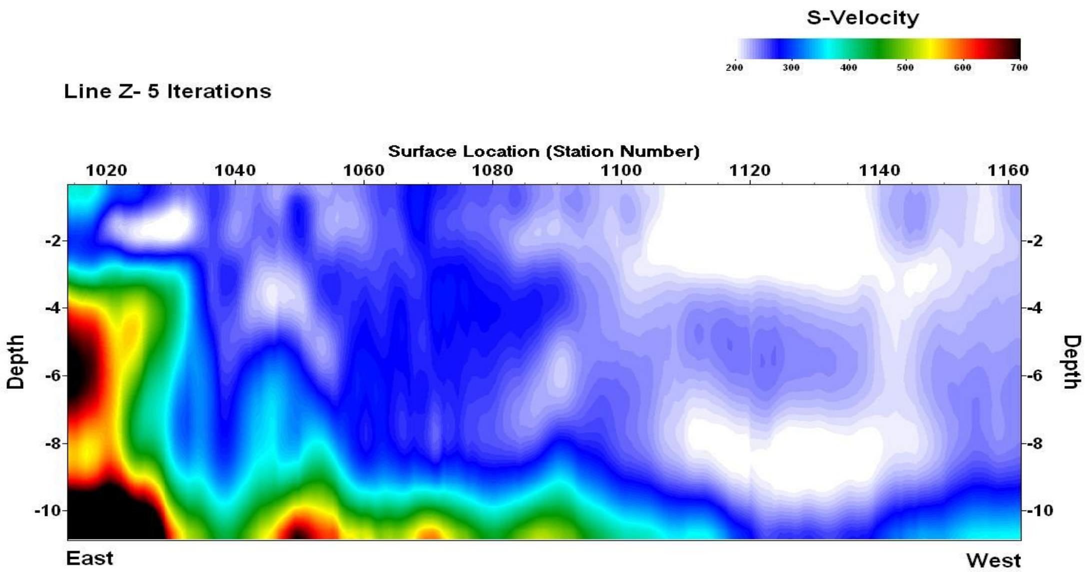

B.

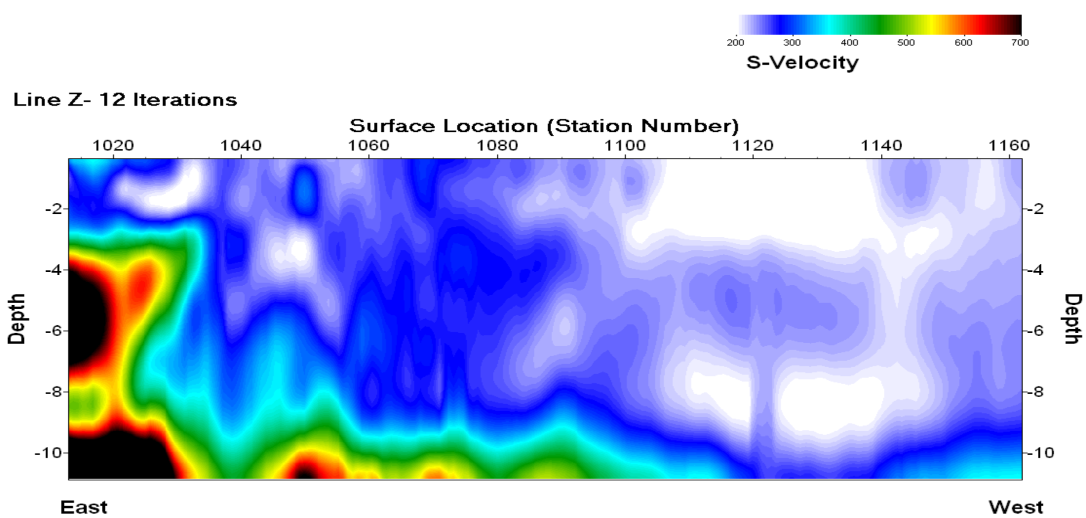

Figure 4.11

Shear-wave velocity models for Line Z, derived using different numbers of iterations.

A) 5 Iterations B) 12 Iterations. Depth and station spacing are in meters.

A.

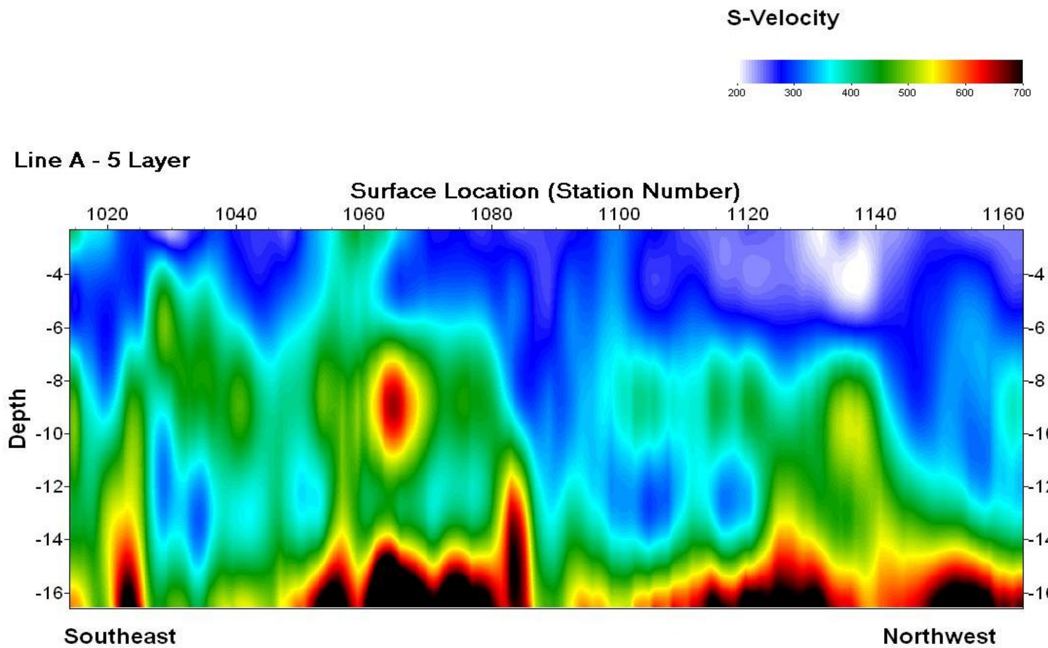

B.

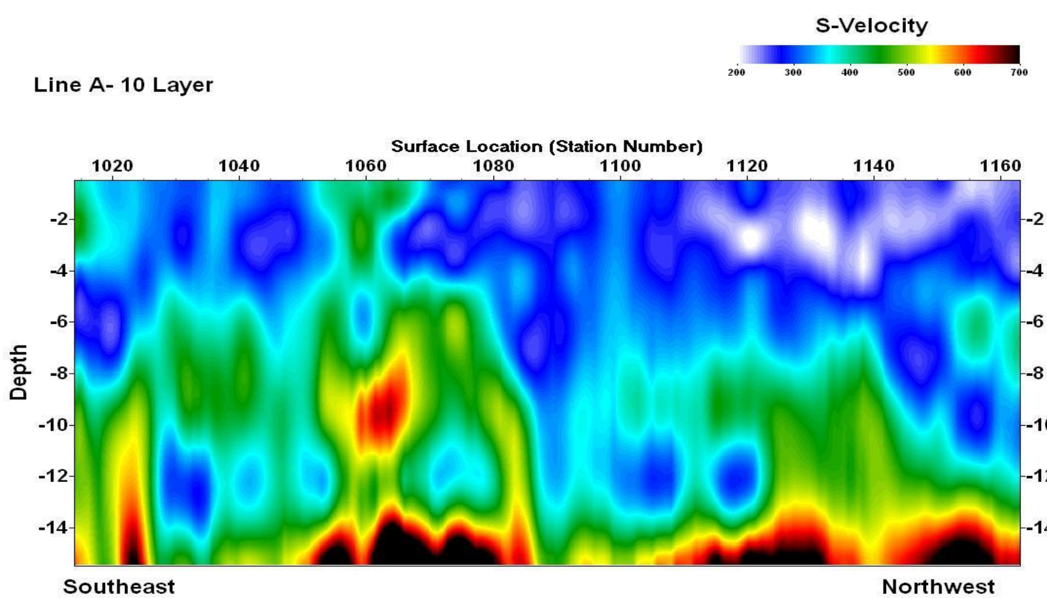

Figure 4.12

Shear-wave velocity models for Line A, for different numbers of layers. Number of iterations for both models was 12. A) 5-layer model B) 10-layer model. Depth and station spacing are in meters.

Half Spread Traces	RMSE Factor	Iterations	Optimum Frequency Window, Hz (Line A)	Optimum Frequency Window, Hz (Line Z)
3-14	5	12	35-50 and 20-50	20-35
7-18	5	12	35-50 and 20-40	15-30
13-24	5	12	20-40	15-30

Table 4.1

Inversion Parameters for Half Spread Analysis

CHAPTER 5

DISCUSSIONS AND INTERPRETATIONS

Processing Issues

Processing parameters are unique to every situation. Separation of the fundamental mode from higher modes is critical for deriving accurate models of the subsurface. Utilizing processing parameters to enhance the fundamental mode allows for receiver spreads to remain small during acquisition. Smaller recording spreads improve lateral resolution but decrease the maximum depth of penetration.

Small changes in dispersion-curve picks can have a large influence on the outcome of the inversion model. Front-end mutes designed to suppress P waves and higher-mode surface waves can distort the dispersion curve for the fundamental mode. Phase velocities can be shifted toward higher values (Figures *5.1 and 5.2*)**.** The distortion generally occurs at the lower frequencies and seems to have little effect at frequencies greater than 15-20 Hz. An alternative is to work with the unmuted gathers, and to use picks for lower frequencies only, below the frequency range affected by higher modes. The loss of higher frequency information, however, sacrifices resolution.

The bulk of the mode contamination occurs at the higher frequencies. This makes picking of the optimum frequency range very important. The optimum range in frequency for phase velocity picks showed little to no continuity for the first 100 stations on Line A. In many cases, even with mutes applied, the fundamental mode could not be isolated due to the dominant secondary mode (Figure 5.3).

LINE Z

The profile extends from the top of the ridge (east) downslope to the bottom of the ridge (west). As noted earlier, one of the key results from this profile is the correlation of S-wave velocities exceeding 600 m/s at the surface of half-spread models with exposures of bedrock near the eastern end of the profile. On the more poorly resolved full-spread model, depth to bedrock increases stepwise along the profile. From station 1001- 1030 the depth to bedrock is 4m, from stations 1030-1090 depth to bedrock is about 9 m, and from station 1090-1150 the bedrock is beneath the depth of penetration.

A low velocity zone in the half-spread images (Figure 4.3A) begins at station 1040 at depth of 2m and extends west to the end of the profile, slightly increasing to a depth of 7m and increasing to a thickness of around 5m. Based on comparison with Well EPA6 , this is inferred to be a sandy saprolite layer within a clay-rich saprolite This well shows lenses of sandy saprolite surrounded by a clay rich saprolite at depths of about 4.5 m. This low velocity zone is overlain by higher velocities (350 m/s -450 m/s) interpreted to be associated with more rigid clay-rich saprolite. This zone is seen in every model downslope, but not to the resolution as seen in the near half-spread model. S-Velocities (*Figure 3.8)* that best match well EPA6 are found around stations 1090. Due to lateral averaging in the inversion process, the correlation of well EPA 6 and the S-velocities in Figure 3.8 do not match.

The sharp drop in the high shear wave velocity at station 1030 may represent the edge of active weathering. The variations in weathering reflect that the bedrock is more resistant at the top of the ridge and undergoes more physical than chemical weathering. Saprolite is found at stations 1001- 1030 at a depth of 2m. Figure 4.11 shows the sudden decrease in S-velocity associated with an increase in chemical weathering of the bedrock downslope at station 1035.

Using the half spread models provided information on the lateral continuity of the low velocity zone, as well as variations in bedrock depth. The weathering of the bedrock occurred at a faster rate downslope than at the top of the ridge. This is shown as a thick layer of chemically altered clay rich saprolite. As the water moves downslope, the partially weathered bedrock becomes more clay rich and alters the saprolite. The water movement allows the chemical alteration of the formation of clays and sands. The increased weathering of the saprolite decreases the coherence of the bedrock and increased transport of material through the system (Dixon et al., 2009)

The interpretation of shear-wave velocities in terms of lithologies is summarized in Table 5.1. Bedrock had the highest velocities and sand rich saprolite had the lowest. Saprolite shear-wave velocities were intermediate between the high and low range. The lowest velocity zone was associated with a less dense material, such as sand saprolite. The variations in clay-rich and sand-rich saprolite, was a result of the spatial composition of the bedrock.

LINE A

Based on the half-spread results for Line Z, shear-wave velocities exceeding 600 m/s are interpreted as relatively unweathered bedrock. For Line A, these high velocities where observed at depths of 10- 14.5 m. at stations 1099-1150. Portions of bedrock are also located at depths 6-9m at stations 1055-1065 Major features are consistent from model to model, demonstrating the stability of the inversion process. A continuous low velocity zone (<200 m/s) was found at depth 1- 3m and at stations 1110- 1150. This low velocity was also observed on Line Z. Using Well EPA6 along Line Z as ground truth, these low velocities are interpreted as a sand-rich lens of saprolite. Low velocity anomalies with slightly higher velocity occur across the profile at a depth of 10 – 12 m. These low velocity anomalies are found at stations 1030-1050 and 1080-1120.

These anomalies have a velocity of 300 m/s overlain by material with a velocity of 400-500 m/s. Based on Well EPA6, this material is all saprolite with varying degrees of weathering with the variation in velocity attributed to the degree of chemical and mechanical weathering of the bedrock. The higher velocity saprolite (400-500 m/s) contains more clay as a result of chemical alteration of the regolith. A higher velocity zone of 550 m/s mimics the bedrock topography and is inferred to be the transition zone comprised of more mechanically weathered than chemically altered bedrock, which maintains the higher velocities..

A large velocity high is imaged at stations 1055-1070 and at depth range of 6-10 m. The high velocity range 550 m/s – 650 m/s reflects a portion of less (chemically) weathered bedrock above saprolite. Lower velocities associated with saprolite (350-400 m/s) are seen down the flanks of this structure. For Line A, the 12- iteration model is the best representation of the survey. Keeping in mind that the models derived using all 24 traces have a resolution width of 12 m, the jagged appearance of this image suggests that the undulation of the bedrock topography across the profile may be a reflection of the variable weathering of the bedrock related to fracturing. These lower velocity anomalies are correlated in all models of line A and may indicate fractures within the bedrock. The saprolite layer is thickest above the fractures within the bedrock.

The low velocity zone in the northern part of the profile (stations 1100-1150) is best resolved by the far half-spread model. It shows this very low velocity zone (200m/s) with a thickness of about 1 m extending from depths of 2 m to 8m. The zone is inferred to be composed of less rigid sandy saprolite. Well EPA6, which is found on Line Z, provides a tie to the sandy saprolite lens. The sandy saprolite lens is found at a depth range of 1-4m. The transition from clay to sand saprolite is a result of either more intense chemical weathering or variation in the composition of the parent rock.

A.

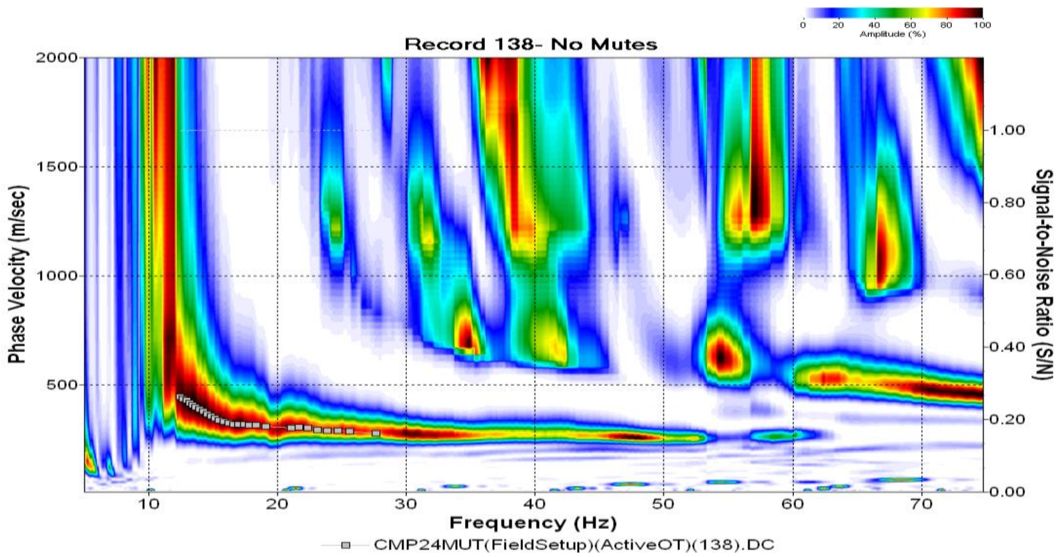

B.

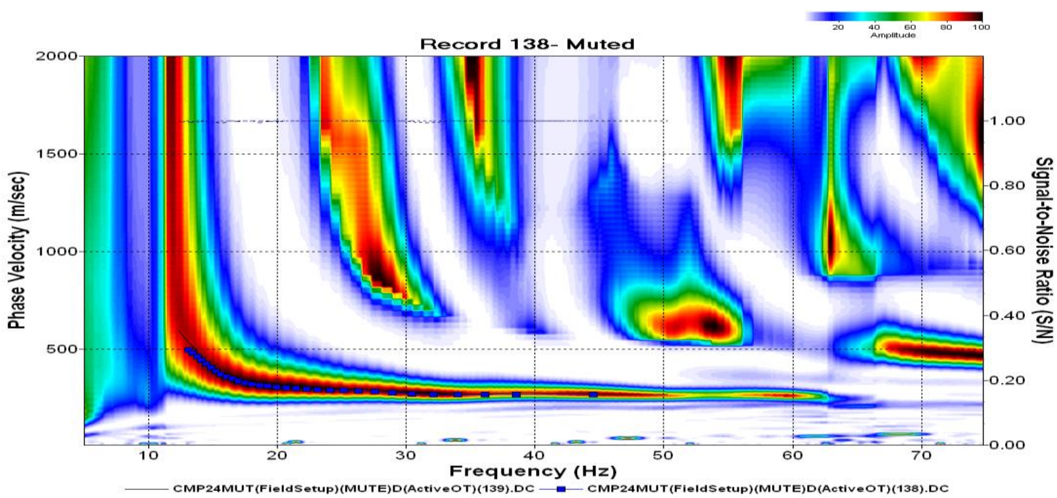

Figure 5.1

Overtone records (Line A, station 1138) with dispersion curve picks. A) No mutes applied to seismic record B) Back and front-end mutes applied to seismic record. The lower frequency portion of the dispersion curve (frequencies less than 15 Hz) for the fundamental mode has become slightly distorted after muting, shifting the picked curve from below 500m/s to just above 500 m/s for the phase velocity.

A

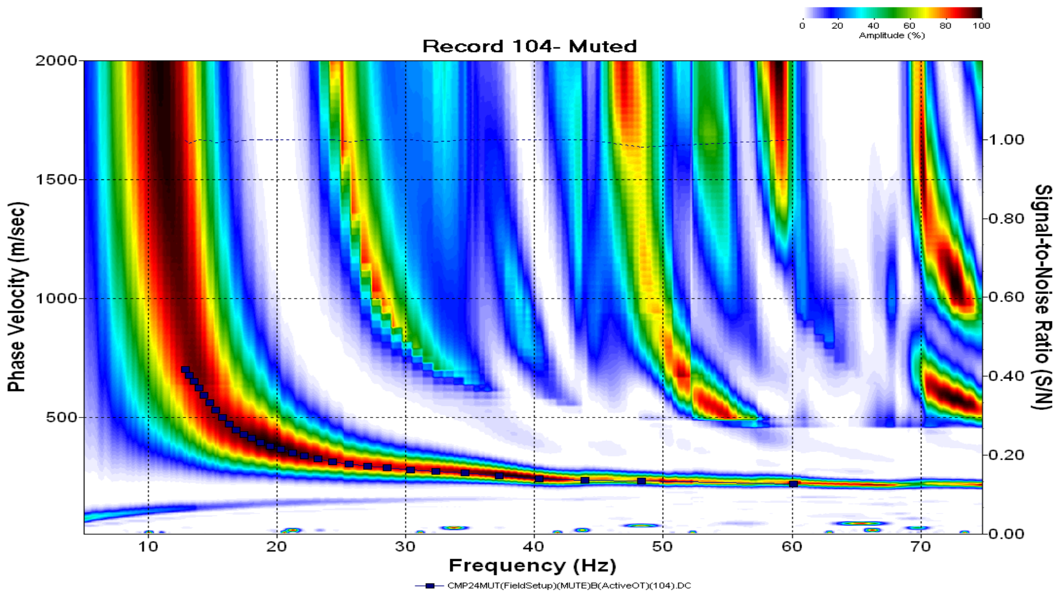

B.

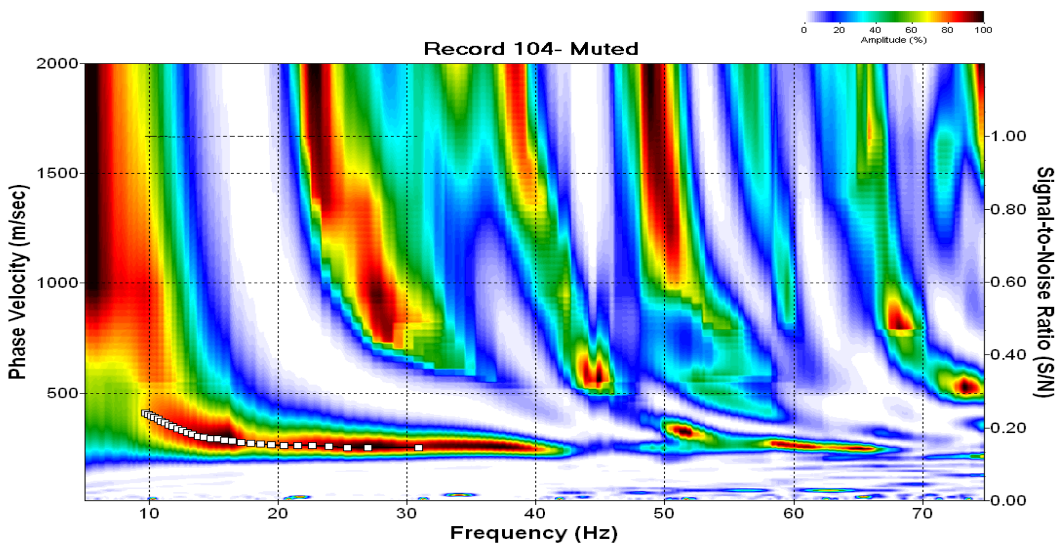

Figure 5.2

Overtone records (Line A, station 1104) with dispersion curve picks. A) Deep mutes applied to seismic record. B) Conservative mutes applied to seismic record. Loss of part of fundamental mode in A distorts the curve drastically in the lower frequency range of 10-18 Hz and shifts the curve to higher phase velocities.

A.

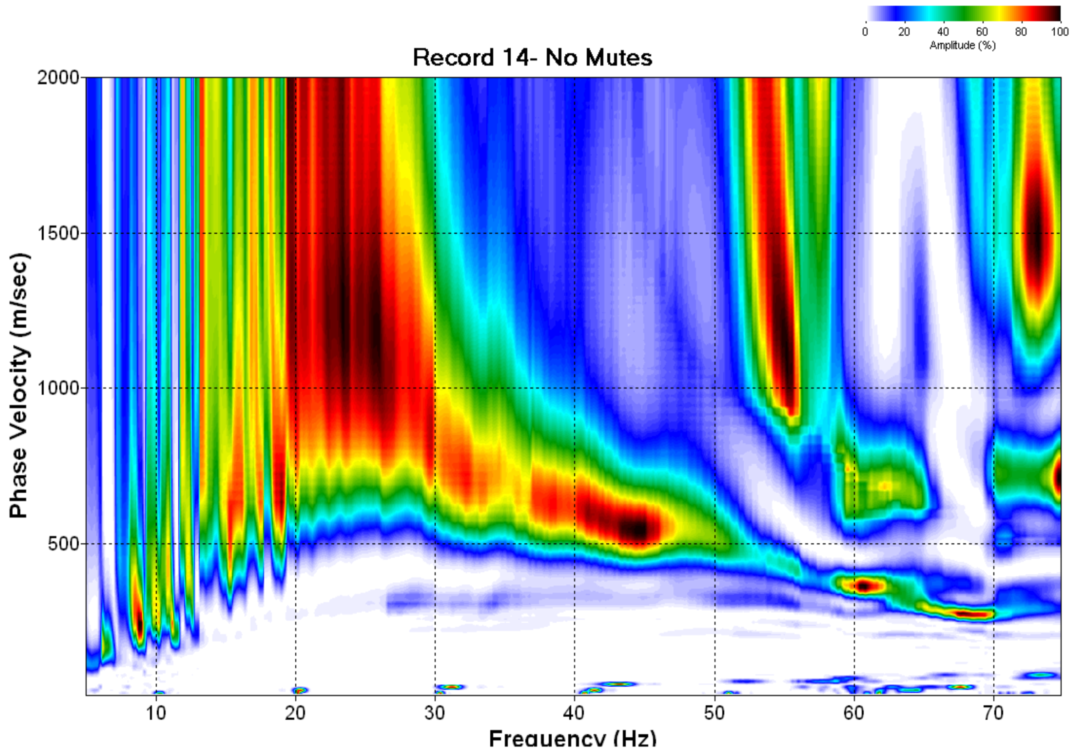
0 20 40 60 80 100
Amplitude (%)
Record 14- No Mutes
Phase Velocity (m/sec)
2000
1500
1000
500
10 20 30 40 50 60 70
Frequency (Hz)

B.

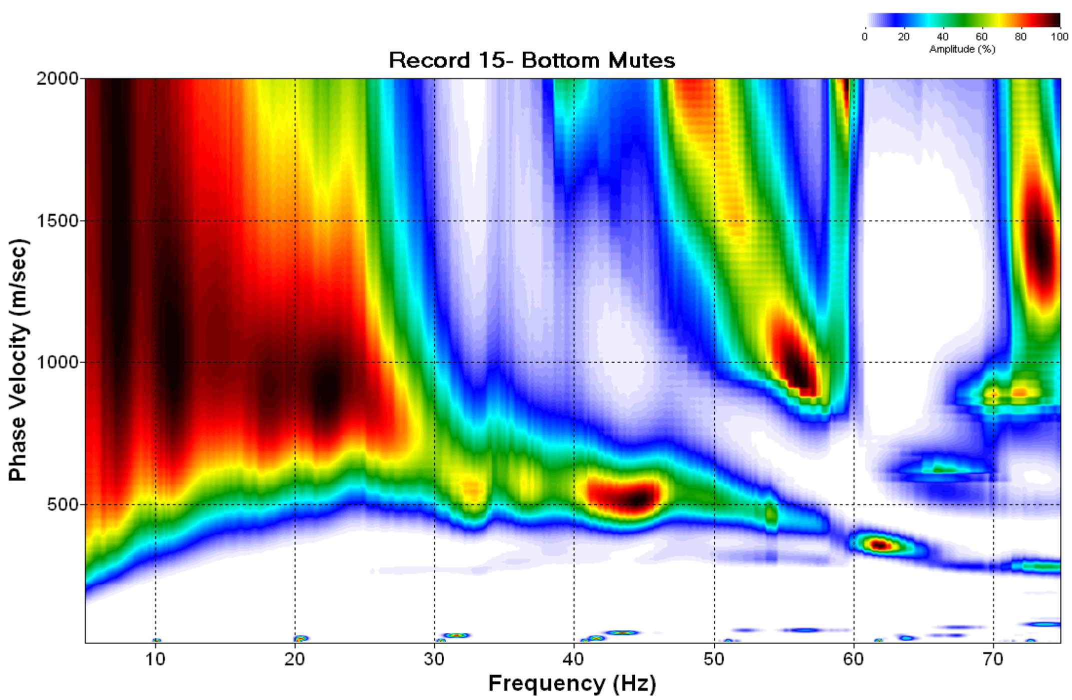
0 20 40 60 80 100
Amplitude (%)
Record 15- Bottom Mutes
Phase Velocity (m/sec)
2000
1500
1000
500
10 20 30 40 50 60 70
Frequency (Hz)

C.

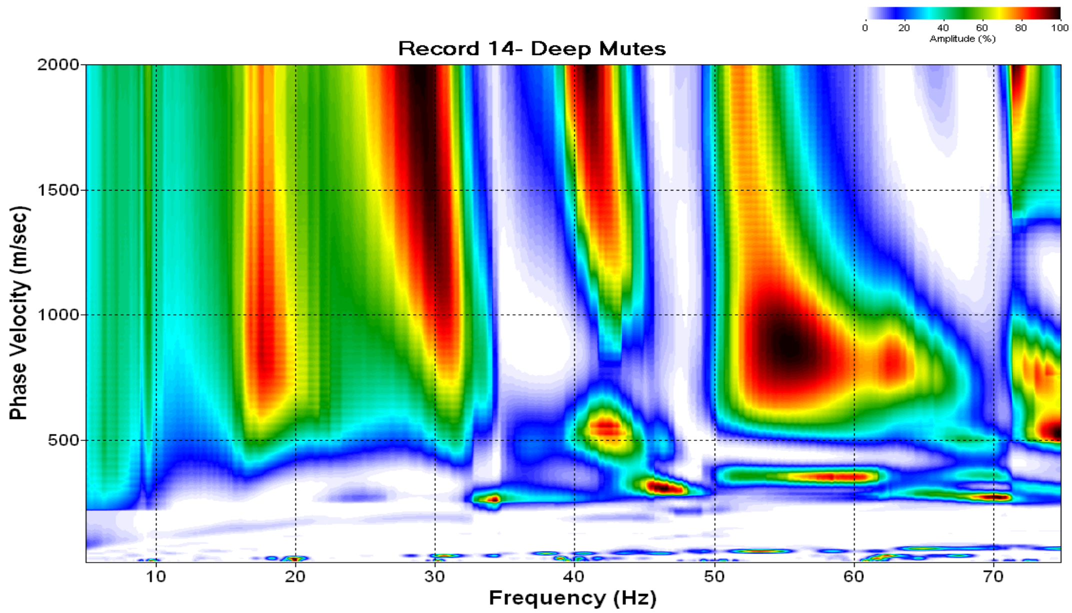

Figure 5.3

Overtone records (Line A, station 1014). A) Original record with no mutes B) with back-end mutes C) with back-end and front-end mutes applied. The fundamental curve could not be isolated due to the overlap in travel time with higher mode energy. By removing the higher modes, the fundamental mode was also removed.

S-Wave Velocity	**Material**
200 m/s- 250 m/s	Sandy saprolite (no clay), unconsolidated material
250 m/s – 400 m/s	Saprolite (clay), unconsolidated material
400 m/s – 550 m/s	Saprolite and highly weathered bedrock
550 m/s- 600 m/s	Transition zone, minimally weathered bedrock
> 600 m/s	Fresh, un-weathered bedrock

Table 5.1

Table representing S-wave velocities and their interpreted corresponding lithologies.

CHAPTER 6

CONCLUSIONS

Multi-channel analysis of surface waves (MASW) was used to provide constraints on hydrologic parameters in the Inner Piedmont. This method successfully mapped bedrock topography and identified the transition zone. The surface wave data were acquired along 2 profiles in Watershed 2: a 400-m, E-W profile recorded in 2007 using 30-Hz geophones, and a 170-m, NW-SE profile recorded in 2011 using 4.5-Hz geophones. Maximum depth of penetration was 12 m for the 2007 profile and 15 m for the 2011 profile. Lateral resolution of subsurface structure was improved by analyzing subsets of 12 contiguous traces. Models were similar for inversions carried out using the near 12, middle 12, and far 12 traces, demonstrating the stability of the inversion process.

Interpretations of shear-wave velocities were constrained by Well EPA6 and outcrops of bedrock along the E-W profile. Velocities of 200-250 m/s found at a depth of 2-3 m along both survey lines are interpreted as sandy saprolite. Velocities from 250-400 m/s are interpreted as more clay-rich saprolite. Based on a comparison of velocity models derived from near-half-spread gathers with outcrops on the eastern end of the 2007 profile, velocities exceeding 600 m/s are interpreted as relatively unweathered bedrock (gneiss). Velocities between 400 and 550 m/s are interpreted as less weathered saprolite and highly degraded bedrock. Thus, as expected, shear-wave velocity is inversely related to intensity of weathering. Velocities of 550-600 m/s are interpreted as a transition zone directly overlying bedrock. This material is less degraded than saprolite and consists largely of fragmented bedrock. Compared with saprolite, chemical

weathering is not as complete, and thus pore spaces are not filled with clay. Shear-wave velocities within the transition zone are higher than those within the overlying saprolite, because the effect of open pore space is more than offset by the less complete chemical alteration.
The MASW method was not able to resolve details within the soil column due to its shallow depth (< 1m).

As noted in the Introduction, the transition zone plays an important role in controlling groundwater flow in the Inner Piedmont. The transition zone mimics the bedrock topography and maintains a Vs velocity between clay rich saprolite and that of unweathered bedrock. The present study suggests that seismic surface waves can provide useful constraints on the depth to the transition zone and its thickness. Combined experiments that incorporate other geophysical methods such as P-wave tomography and electrical resistivity would most likely improve those constraints.

REFERENCES

Abreu, M.E., 2005, Permeability Estimates for soils in the Southern Piedmont of Georgia, Masters Thesis in Geology, University of Georgia.

Brown, L.T., Boore, D.M. and K.H. Stokoe, II, 1999, "Comparison of shear-wave velocity profiles from SASW and downhole seismic tests at a strong-motion site", *Proceedings, 12th World Conference on Earthquake Engineering,* Auckland, New Zealand.

Callaghan, C.L., 1997, Design and Testing of a PVC Plug for Installation of TDR Rods at Depth, Masters Thesis in Geology, University of Georgia.

Cooker, M.D, 1999, Geochemical mapping in Georgia, USA: a tool for environmental studies, geologic mapping, and mineral exploration, Journal of Geochemical Exploration, v.67(i.1-3), 345-360.

Dixon, J.L., Heimsath, A.M., and Amundson, R., 2009, The critical role of climate and saprolite weathering in landscape evolution, Earth Surface Processes and Landforms,v. 34 (11), pp. 1507-1521.

Endale DM, Fisher, DS, Steiner JL. 2006. Hydrology of a Zero-Order Southern Piedmont Watershed Through 45 Years of Changing Agricultural Land Use. Part 1. Monthly and Seasonal Rainfall-Runoff Relationships: Journal of Hydrogeology 316, 1-12.

Feild, J.B. and Dowd, J.F. 2001, Piedmont Hydrology: Implications for Contaminated Sites. *In* Proceedings of the 2001 Georgia Water Resources Conference March 26-27, 2001, Athens, GA, University of Georgia, pp. 578-581.

Fetter, C.W., 1994, Applied Hydrogeology, 3rd ed.: Macmillan College Publishing, Inc., New York.

Gonthier, G.J., Conceptual Model of Ground-Water Flow in Fractured Crystalline Rock- A Case Study Based on Constant-Discharge Tests at U.S. Air Force Plant 6, Marietta, Georgia, 2003, *In* Proceedings of the 2009 Georgia Water Resources Conference April 27-29, 2009, Athens, GA, University of Georgia.

Harned, D.A. and Daniel III, C.C. 1989. The Transition Zone Between Bedrock and Regolith: Conduit for Contamination? In Ground Water in the Piedmont, *In* Proceedings conference on GROUND WATER in the Piedmont of the Eastern United States October 16-18, 1989, Clemson, S.C, Clemson University, pp. 336-348.

Hatcher, R.D., Jr., 1989. Tectonic Synthesis of the U.S. Appalachians. The Geology of North America: The Appalachian-Quachita Orogen in the United States: Geological Society of North America, v. F-2, p. 511-535.

Hatcher, R.D., Jr, 2010, The Appalachian orogeny: A brief summary, *in* Tollo, R.P., Batholomew, M.J., Hibbard, J.P., and Karabinos, P.M., eds., From Rodinia to Pangea: The Lithotectonic Record of the Appalachian Region: Geological Society of America Memoir 206 p 1-19.

Heath, R.C., 1980, Basic Elements of Ground-Water Hydrology with Reference to Conditions in North Carolina, U.S. Geological Survey Water-Resources Open-File Report 80-44, 86 p.

Higgens, M.W., Atkins, R.L., Crawford, T.J., Crawford III, R.F., Brooks, R., and Cook, R.B., 1988, The Structure, Stratigraphy, and Evolution of the Southern Most Part of the Appalachian Orogen: U.S. Geological Survey Professional Paper 1475, 173 p.

Ivanov, J. , Park C.B., Miller, R.D., and Xia, J., 2001, Modal Separation Before Dispersion Curve Extraction by MASW Method, *In* Proceedings of SAGEEP 2001, Denver, Colorado, SSM-3.

Ivanov, J., Park, C.B., Miller, R.D., and Xia, J. 2005, Analyzing and Filtering Surface-Wave Energy by Muting Shot Gathers, Journal of Environmental and Engineering Geophysics, v. 10, 3: pp. 307-322.

Kansas Geological Survey, 2010, SurfSeis Manual, Software for Multi Channel Analysis of Surface Waves, Lawrencevlle, Kansas (http://www.kgs.ku.edu/software/surfseis/index.html).

Khalifa, M., and Hawman, R.B. 2007, Unpublished Data.

LeGrand HE. 1989. A Conceptual Model of Ground Water Settings in the Piedmont Region In Ground Water in the Piedmont, *In* Proceedings conference on GROUND WATER in the Piedmont of the Eastern United States October 16-18, 1989, Clemson, S.C., Clemson University, pp. 317-327.

LeGrand, H.E., 2004, A master conceptual model for hydro- geological site characterization in the Piedmont and Mountain region of North Carolina, A guidance manual: North Carolina Department of Environment and Natural Resources, Division of Water Quality, Groundwater Section, 50 p.

Lowrie, W., 1997, Fundamentals of Geophysics, Cambridge University Press, Cambridge, United Kingdom.

Miller, R.D., Xia, J., Park, C.B., and Ivanov, J., 2001, Shear wave velocity field to detect anomalies under asphalt: Proceedings of the 52nd Highway Geology Symposium, May 16, Baltimore, Maryland.

Nazerian , S., Stokoe II, K.H., and Hudson, W.R., 1983, Use of spectral analysis of surface waves method for determination of moduli and thicknesses of pavement systems, Transportation Research Record No. 930, 38-45.

Nelson AB. 1989. Hydraulic Relationship Between a Fractured Bedrock Aquifer and a Primary Stream, North Carolina Piedmont, *In* Proceedings conference on GROUNDWATER in the Piedmont of the Eastern United States October 16-18 1989, Clemson, S.C., Clemson University, pp.159-162.

O'Neill, A. and Matsuoka, T., 2005, Dominant Surface-wave Modes and Possible Inversion Pitfalls, Journal of Environmental and Engineering Geophysics, 10(2),
pp. 185-201.

Park, C.B., Miller, R.D., and Xia, J., 1997, Summary report on surface-wave project at Kansas Geological Survey (KGS): Kansas Geological Survey Open-file Report 97-80

Park, C.B., R.D. Miller, and J. Xia, 1999, Multichannel Analysis of Surface Waves: Geophysics, 64, 800-808.

Park, C.B., Miller, R.D., and Miura, H., 2002, Optimum Field Parameters of an MASW Survey, *In* Proceedings of the SEG-Japan 2002, Tokyo, Japan.

Park, C.B., R.D. Miller, J. Xia, and J. Ivanov, 2007, Multichannel analysis of surface waves (MASW) - active and passive methods: The Leading Edge, 26, 60-64.

Price, B.M., 2010, Recharge and Baseflow of a First Order Stream in the Piedmont, Master's Thesis in Geology, University of Georgia.

Railsback LB, Bouker PA, Feeney TP, Goddard EA, Hall AS, Jackson BP, McClain AA, Orsega MC, Rafter MA, Webster JW. 1996. A survey of the major-element geochemistry of Georgia groundwater. Southeastern Geol 36: 99-122.

Schumak BBG, Neil J.; Smith, Jimmy N., 1989. Fracture Trace Analysies and Other Investigative Techniques for Determination of Conductive Zones in Rock at a Chemical Manufacturing Facility in the Piedmont, *In* Proceedings of a Conference on GROUND WATER in the Piedmont of the Eastern United States Oct 16-18 1989, Clemson, S.C., Clemson University, pp.349-358.

Shearer, P. M., 1999, *Introduction to Seismology* (p. 260). Cambridge, U.K.; New York: Cambridge Univeristy Press.

Stewart, J.W., 1962 Water -yielding potential of weathered crystalline rocks at the Georgia Nuclear Laboratory: U.S. Geological Survey Professional Paper 450-B, 2 p.

Stewart, J.W., Callahan, J.T., and Carter, R.F., 1964, Geologic and hydrologic investigation at the site of the Georgia Nuclear Laboratory, Dawson County, Georgia: U.S. Geological Survey Bulletin 1133-F, 90 p.

Stokoe II, K. H., Wright, G. W., James, A. B., and Jose, M. R., 1994, Characterization of geotechnical sites by SASW method, in Geophysical characterization of sites, ISSMFE Technical Committee #10, edited by R. D. Woods, Oxford Publishers, New Delhi.

Stormer, J. C., Whitney, J. A., and Hess, J. R. (1980) In Geological, Geochemical, and Geophysical Studies of the Elberton Batholith, Eastern Georgia, J. C. Stormer and J. A. Whitney (eds.), Guidebook 19, Georgia Dept. Nat. Resources, 10-30.

Washington, J.W., Endale, D.M., Samarkina, L.P., Chappell, K.E., 2004, Kinetic Control of Oxidation State at Thermodynamically Buffered Potentials in Subsurface Waters, Geochimica et Cosmochimica Acta 68: 4831-4842.

Washington, J.W., Thomas, R.C., Endale, D.M., Schroer, K.L., Samarkina, L.P., 2006 Groundwater N Speciation and Redox Control of Organic N Mineralization by O 2 Reduction to H 2 O 2, Geochimica et Cosmochimica Acta 70: 3533-3548.

Yoon, S. and Rix, G., 2009, Near-Field Effects on Array-Based Surface Wave Methods with Active Sources. Journal of Geotechnical and Geoenvironmental Enginering, 135(3), 399–406.

APPENDIX A

EPA WELL BORE HOLE DATA

Figures A1-A10 show the borehole data from the EPA for wells 6 and 7 that were drilled in Watershed #2 in February 2000. These figures provide details about the lithologies found at these sites.

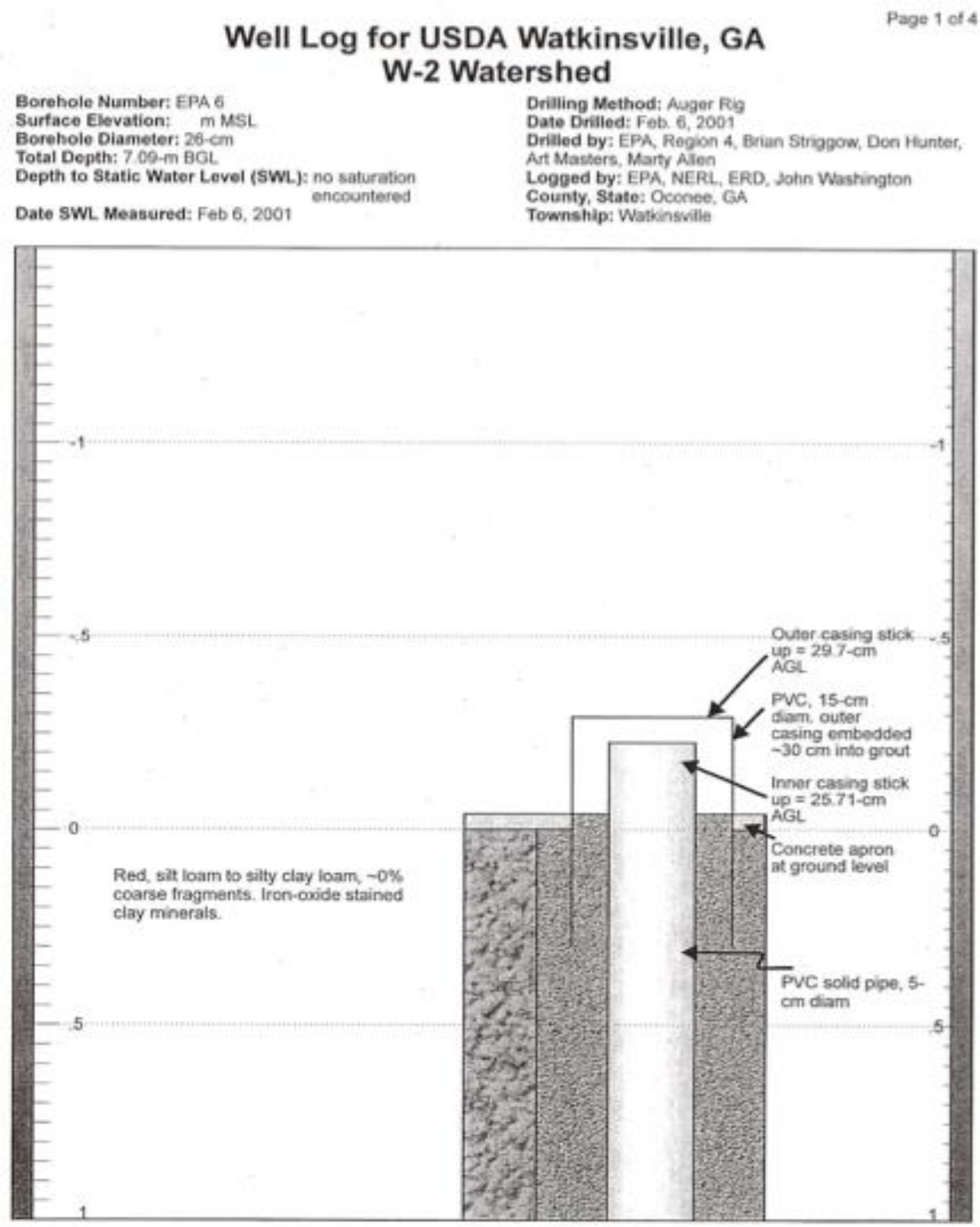

Figure A1-Well EPA6 drilled core from surface (0m) to 1m. Material in the core is comprised of silt loam to silty clay loam.

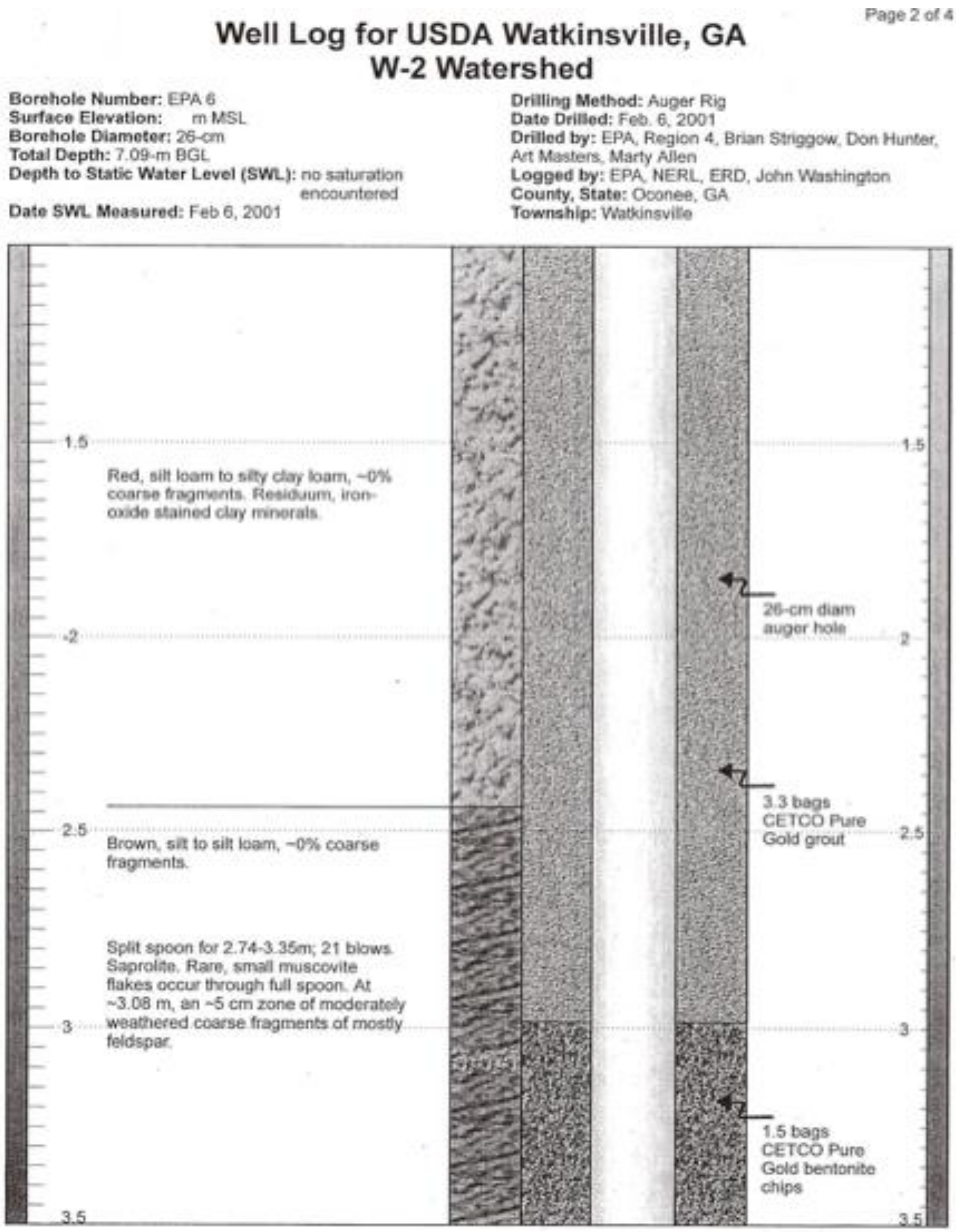

Figure A2- Well EPA 6 from 1m to 3.5 m depth. Material is comprised of red and brown silt loam to silty clay loam, saprolite, and some moderately weathered coarse feldspar fragments.

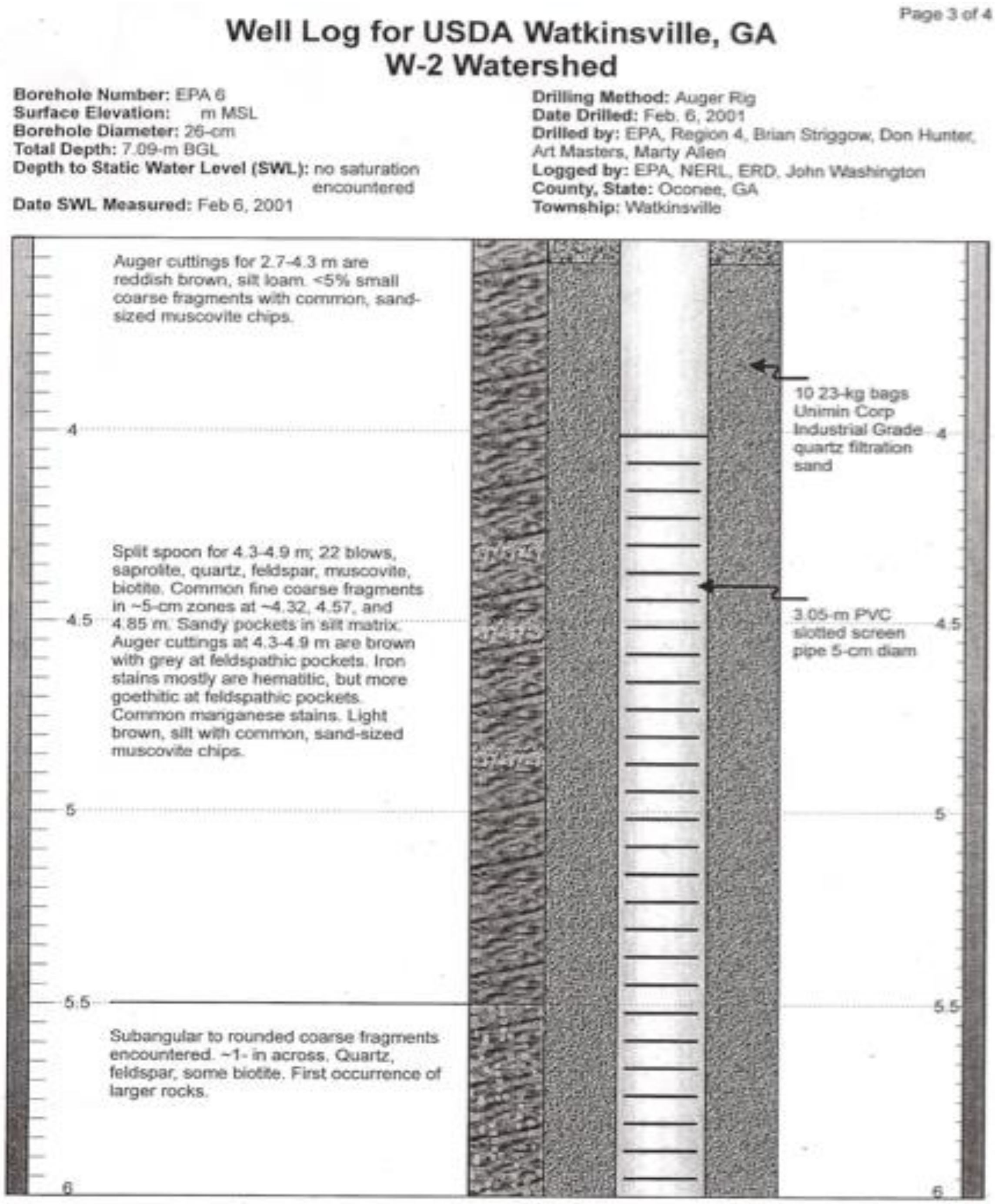

A3- Well EPA 6 from 3.5 m to 6 m depth. Material is comprised of reddish/brown silt loam and saprolite with an appearance of larger rock fragments at 5.5m.

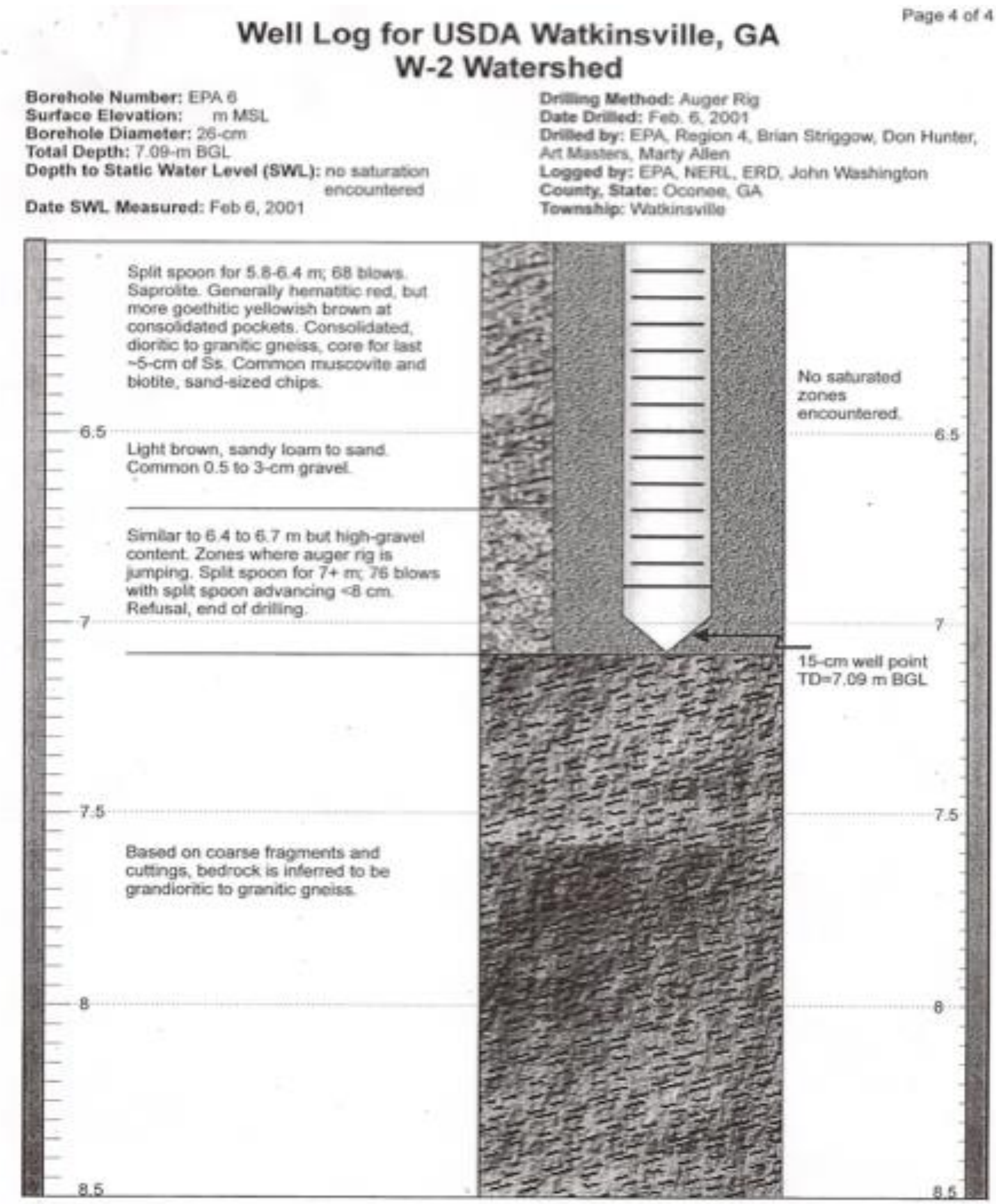

A4- Well EPA 6 from 6 m to a final depth of 7.09 m at which point the drill met with bedrock. This section is comprised of saprolite with fragments of gravel overlying the bedrock (granodioritic to granitic gneiss).

Well Log for USDA Watkinsville, GA
W-2 Watershed

page 1 of 6

Borehole Number: EPA 7
Surface Elevation: m MSL
Borehole Diameter: 26 cm
Total Depth: 11.9 m BGL
Depth to Static Water Level (SWL): 6.21 m BGL
Date SWL Measured: Feb 6, 2001

Drilling Method: Auger Rig
Date Drilled: Feb 6 - Feb 7 2001
Drilled by: EPA, Region 4, Brian Striggow, Don Hunter, Art Masters, Marty Allen
Logged by: EPA, NERL, ERD, John Washington
County, State: Oconee, GA
Township: Watkinsville

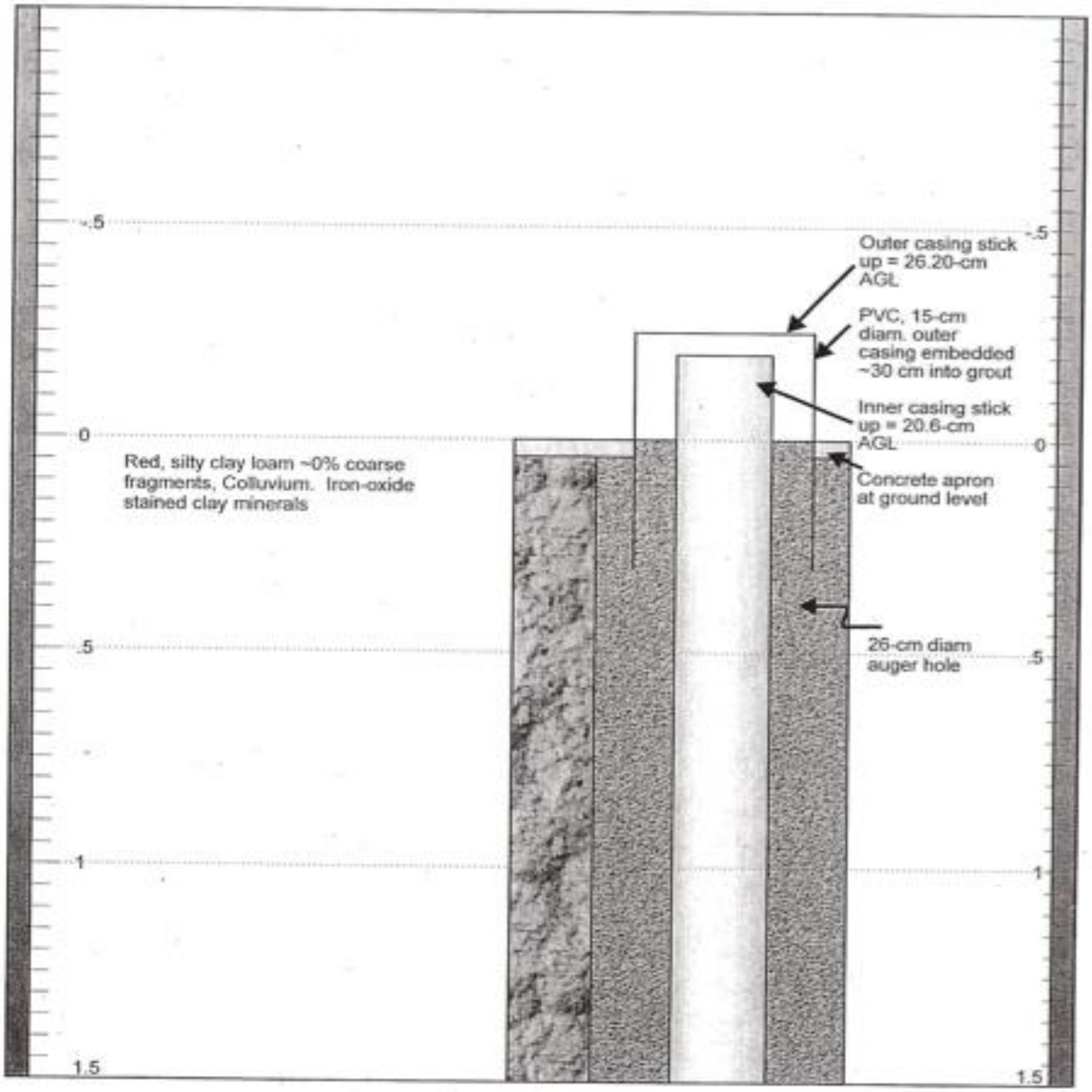

A5- Well EPA 7 from surface (0m) to depth of 1.5m. Material is comprised of red silt clay loam.

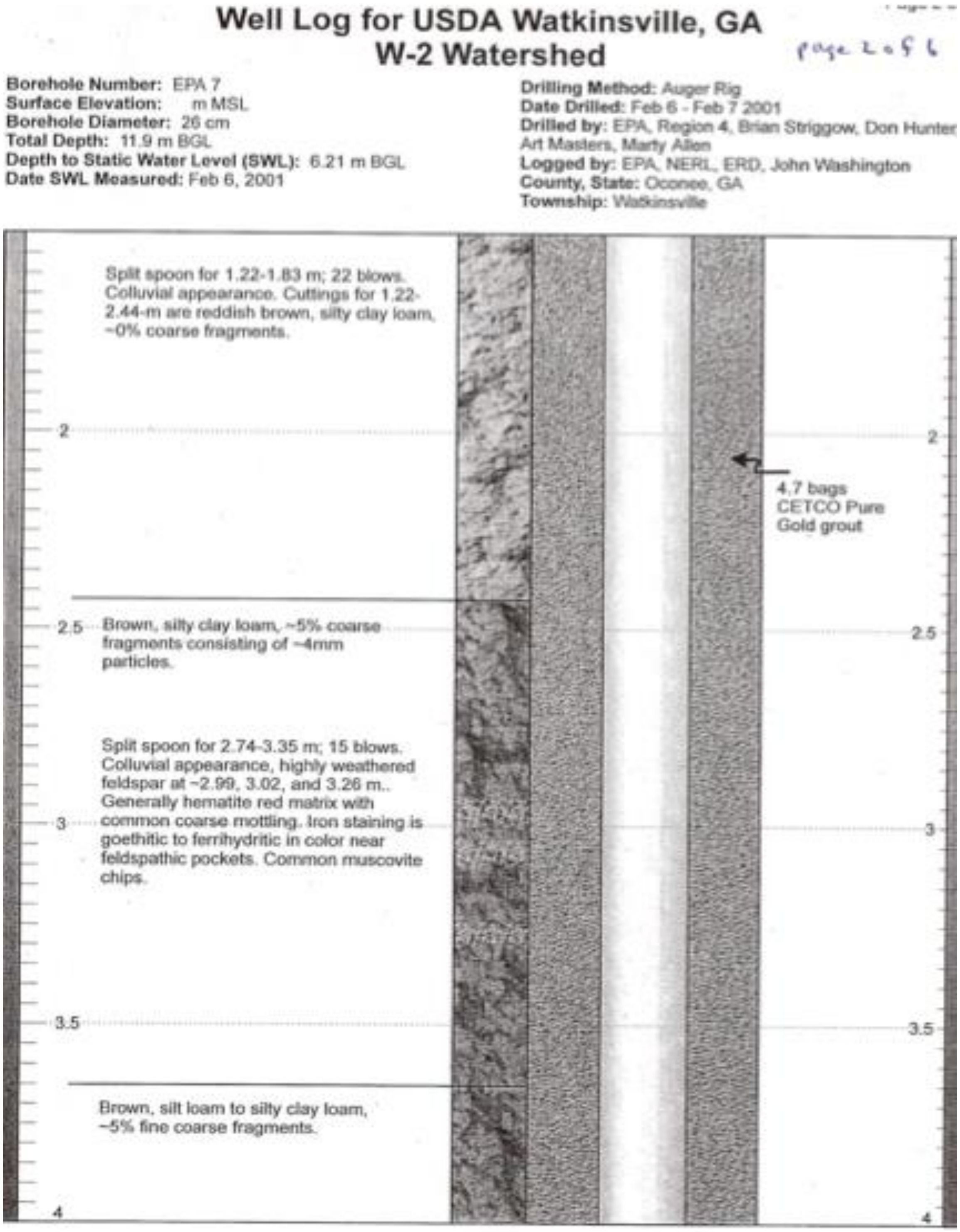

A6- Well EPA 7 from 1.5 m to 4 m depth. Material is comprised of red/brown silty clay loam, with highly weathered mineral fragments.

Well Log for USDA Watkinsville, GA
W-2 Watershed

page 3 of 6

Borehole Number: EPA 7
Surface Elevation: m MSL
Borehole Diameter: 26 cm
Total Depth: 11.9 m BGL
Depth to Static Water Level (SWL): 6.21 m BGL
Date SWL Measured: Feb 6, 2001

Drilling Method: Auger Rig
Date Drilled: Feb 6 - Feb 7 2001
Drilled by: EPA, Region 4, Brian Striggow, Don Hunter, Art Masters, Marty Allen
Logged by: EPA, NERL, ERD, John Washington
County, State: Oconee, GA
Township: Watkinsville

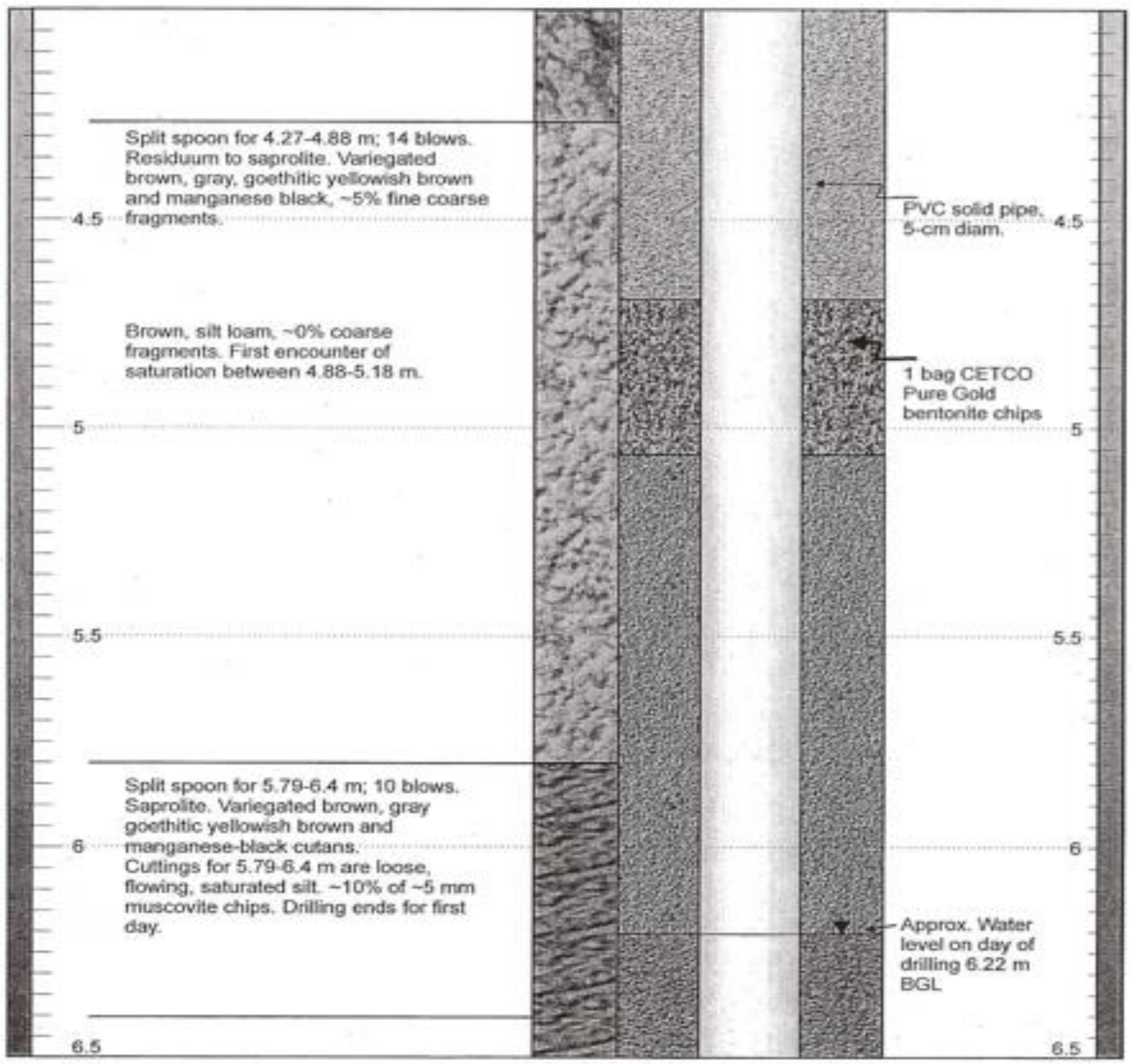

A7-Well EPA 7 from 4m to 6.5 m. Material is comprised of soils with highly weathered minerals, saprolite, and intermingled with brown silt loam. This well found saturation at 4.88m, within the saprolite.

Well Log for USDA Watkinsville, GA
W-2 Watershed

page 4 of 6

Borehole Number: EPA 7
Surface Elevation: m MSL
Borehole Diameter: 26 cm
Total Depth: 11.9 m BGL
Depth to Static Water Level (SWL): 6.21 m BGL
Date SWL Measured: Feb 6, 2001

Drilling Method: Auger Rig
Date Drilled: Feb 6 - Feb 7 2001
Drilled by: EPA, Region 4, Brian Striggow, Don Hunter, Art Masters, Marty Allen
Logged by: EPA, NERL, ERD, John Washington
County, State: Oconee, GA
Township: Watkinsville

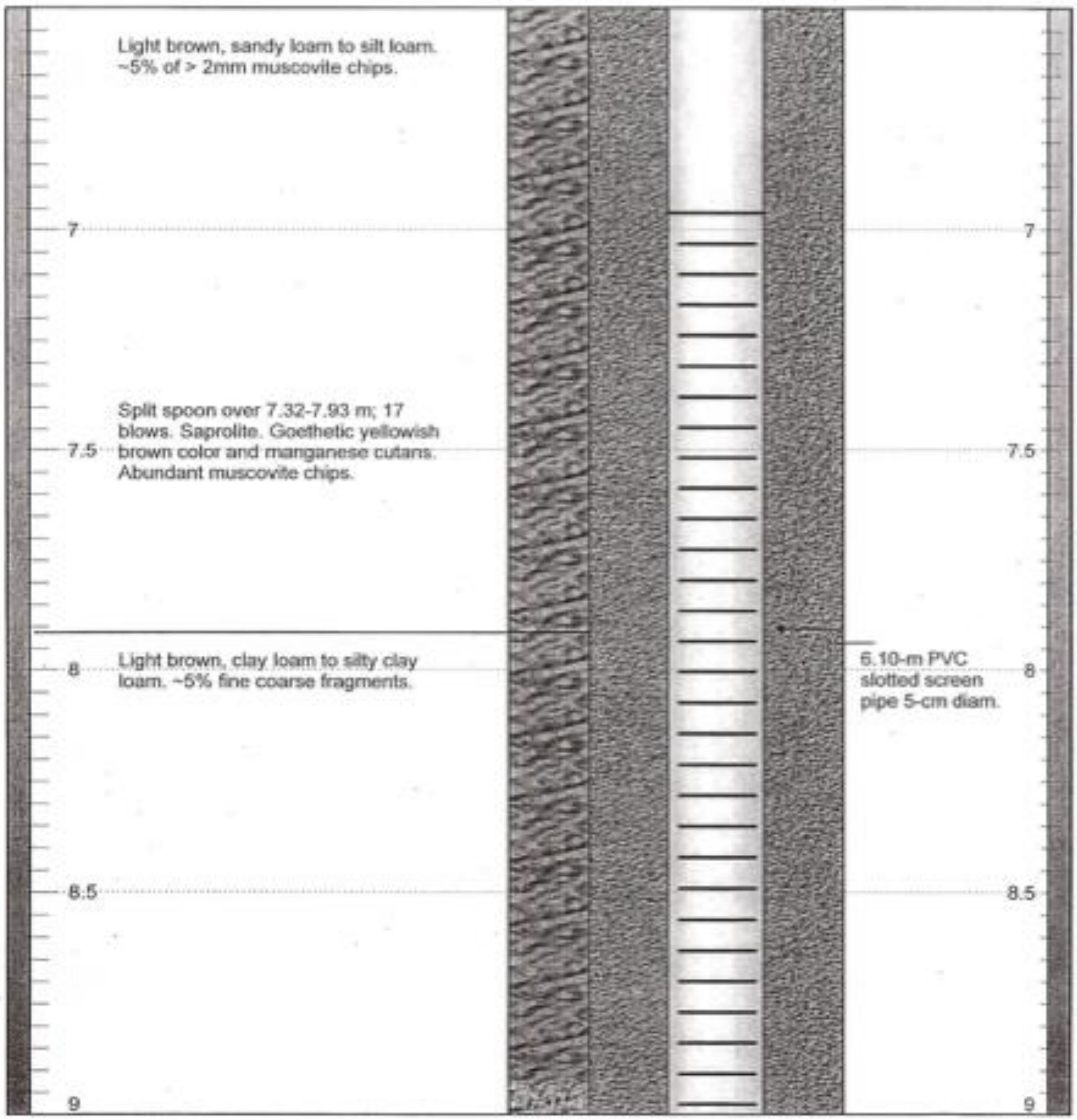

A8- Well EPA7 from 6.5 m to 9 m depth. Material is comprised of saprolite with highly weathered minerals overlying brown clay loam to silty clay loam.

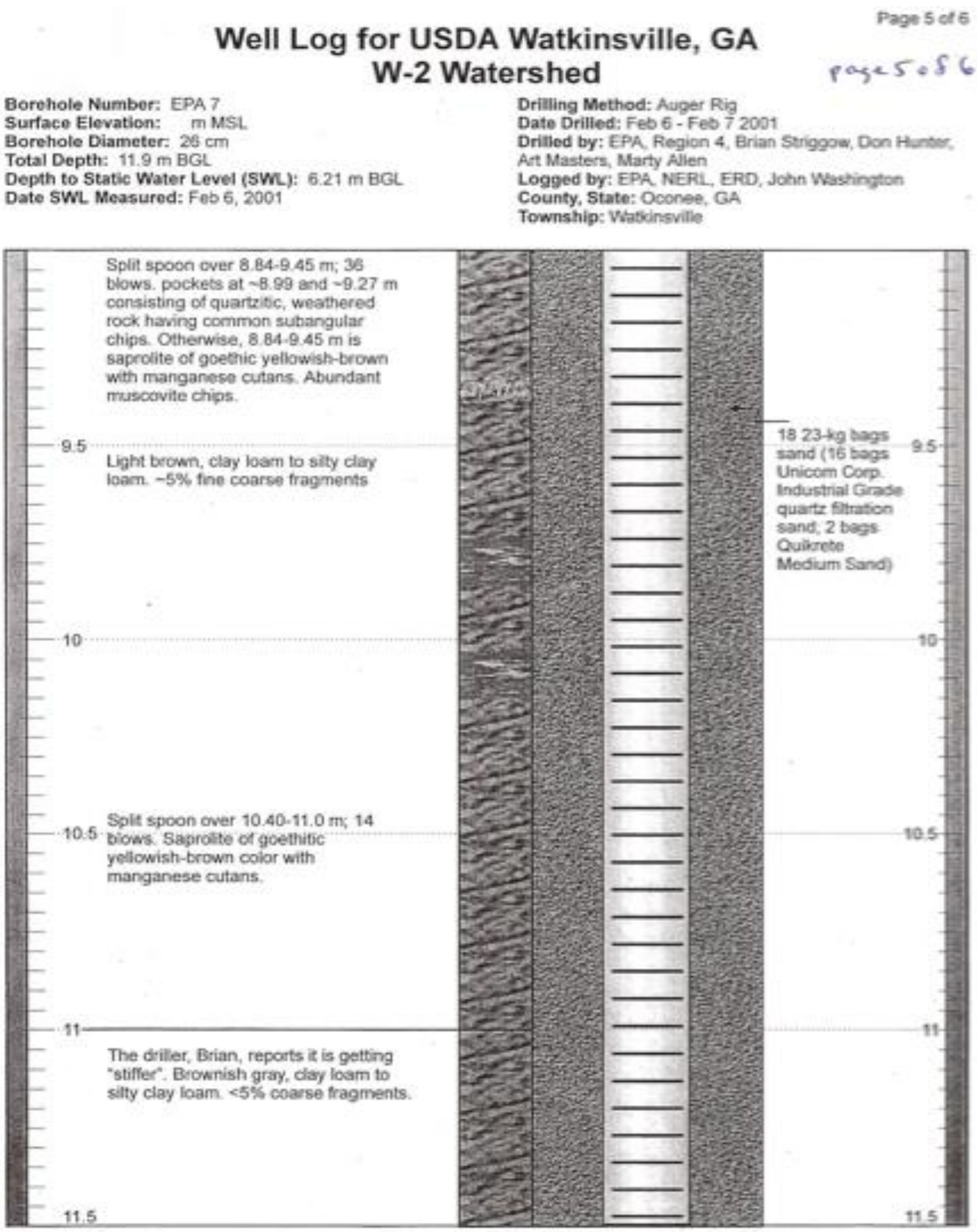

A9-Well EPA 7 from 9m to 11.5 m depth. Material is comprised of intermingled layers of saprolite and brown silt loam with coarser fragments appearing at 11 m.

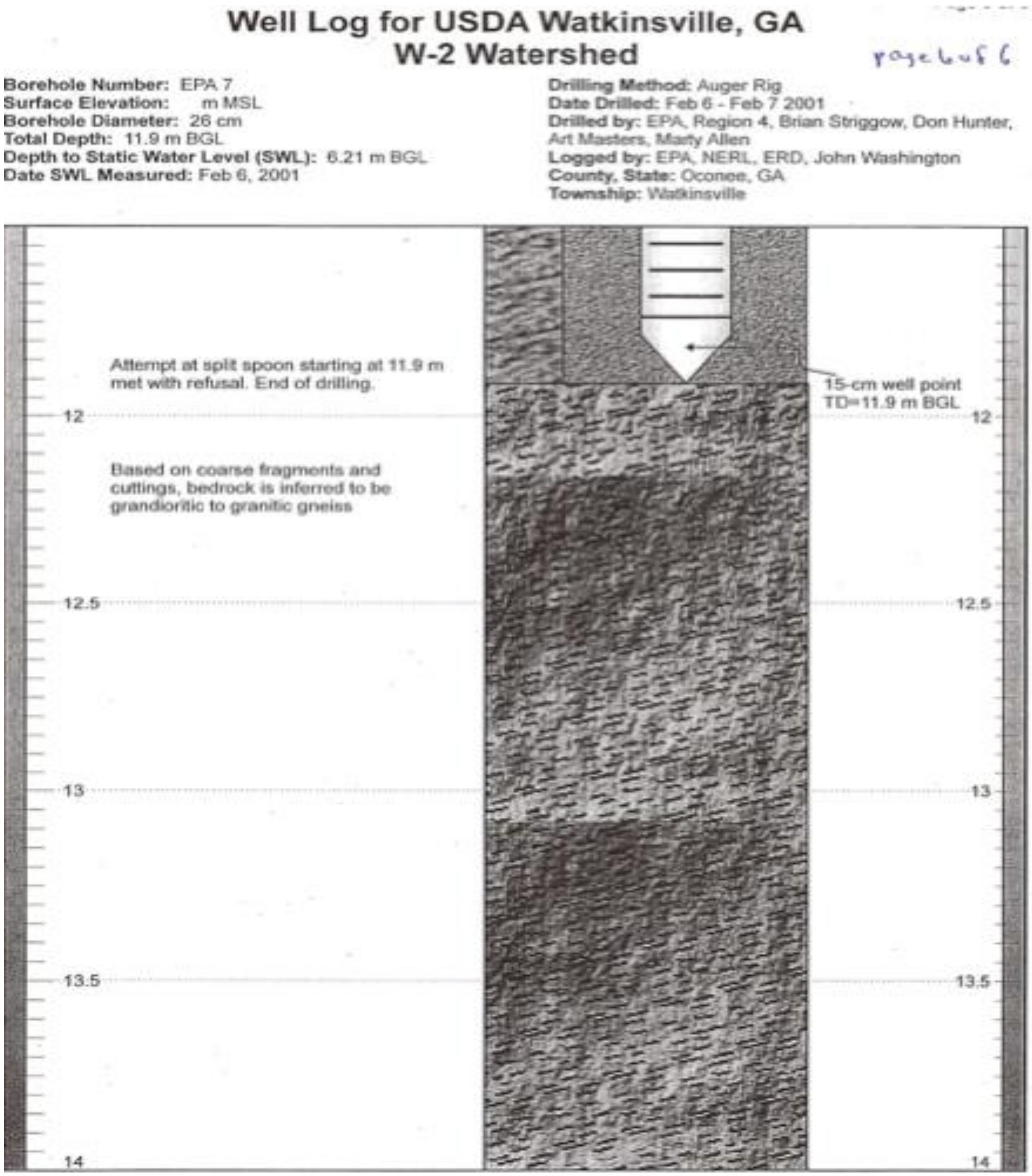

A10- Well EPA 7 from11.5 to 12m depth. Drill meets with resistance of bedrock (granodioritic to granitic gneiss) .